Cusped hyperbolic 3-manifolds with a compact totally geodesic boundary

by

Hasitha Anuradha Ekanayake

Bachelor of the Science of Engineering, University of Moratuwa , 2015

Submitted to the Graduate Faculty of

the Dietrich School of Arts and Sciences in partial fulfillment

of the requirements for the degree of

Doctor of Philosophy

University of Pittsburgh

2023

UNIVERSITY OF PITTSBURGH

DIETRICH SCHOOL OF ARTS AND SCIENCES

This dissertation was presented

by

Hasitha Anuradha Ekanayake

It was defended on

July 26th 2023

and approved by

Jason DeBlois, University of Pittsburgh

Bruno Martelli, University of Pisa

Paul Gartside, University of Pittsburgh

Carl Wang-Erickson, University of Pittsburgh

Cusped hyperbolic 3-manifolds with a compact totally geodesic boundary

Hasitha Anuradha Ekanayake, PhD

University of Pittsburgh, 2023

This thesis is a study on the volumes of cusped hyperbolic 3-manifolds with a compact totally geodesic boundary. The class of such manifolds is denoted by $\mathcal{N}_{c,c}$. The main goal of the thesis is to identify the smallest member in this class. Author outlines a process that zeroes in on a manifold which was preidentified as a candidate for the smallest manifold in $\mathcal{N}_{c,c}$. Most of the computations are parameterized in terms of x_1 ; a quantity closely associated with the volumes of manifolds with geodesic boundary. Chapter 3 describes the construction of a lower bound for the volumes of manifolds in $\mathcal{N}_{c,c}$ in terms of their x_1 values. In chapter 4, the relation between the geometry of a manifold in $\mathcal{N}_{c,c}$ is leveraged to obtain a lower bound for its x_1 value. Results in those two chapters yield an interval of possible x_1 values for the smallest manifold in $\mathcal{N}_{c,c}$. The remainder of the thesis investigate this interval extensively.

Table of Contents

List of Tables

List of Figures

Acknowledgement

First and foremost I would like to thank my advisor Professor Jason DeBlois. I don't think my words can do justice for his incredible support throughout last five years. This thesis would not exist without his guidance. I'm really grateful to have someone as supportive and patient as him as my advisor.

I'm also thankful for my committee members Prof. Bruno Martelli, Prof. Paul Gartside and Prof. Carl Wang-Erickson for their support and guidance. Their comments and suggestions has helped me to improve the quality of this thesis immensely.

I would also like to thank Rahul, Sushmita, Thesath and Chanuka and my other friends and colleagues in the Math Department. Graduate school was highly challenging at times and I would not have survived those tough times without their friendship. I'm also thankful for other graduate students of my advisor; Priyadip, Mark, Tyler and Arshia for sharing their valuable insights.

I'm grateful for Dr. Pantaleon Perera for his immense support during the period in which I was a student in transition from Engineering to Mathematics.

My parents sacrificed a lot in their lives so that I could follow my dreams. I'm forever indebted to them and my sister for their unconditional love and unwavering support.

Finally, none of these would have been possible without the constant support of my wife, Lakshika. I'm incredibly fortunate to have her in my life. Her love and dedication are the reasons behind my success.

I dedicate this thesis to the loving memory of my grandmother, Mary Nona. Thank you Grandma for teaching me so many things in life and filling my childhood with fond memories.

1.0   Introduction

Determining the lowest volume examples in various classes of manifolds is an extensive project in the field of topology and geometry of hyperbolic manifolds with its roots dating at least to Thurston's notes written in 1979[1]. Thurston observed that the volume is a good measurement of topological complexity. (Chapter 6, [1])

Since then, various developments were made in the class of multi-cusped hyperbolic 3-manifolds. Note that a hyperbolic 3-manifold with a finite volume but non compact can be decomposed as the union of a compact part and finite collections of **'cusps'** each of which is homeomorphic to $T \times [0, \infty)$ where T is a 2-dimensional torus. Cao and Meyerhoff identified the smallest orientable hyperbolic manifolds with one cusp and the subsequent work of Gabai, Meyerhoff and Milley identified the Weeks manifold with volume ≈ 0.94 to be the smallest compact 3-manifold.

We turn our attention to the class of orientable hyperbolic 3-manifold with compact totally geodesic boundary. Kojima and Miyamoto identified the the smallest compact manifold in this class [2]. We feel a natural extension of this project would be to determine the smallest cusped manifold in this class. To phrase it precisely, our goal is to identify the lowest volume manifold in $\mathcal{N}_{c,c}$ where by $\mathcal{N}_{c,c}$ we denote the set of orientable hyperbolic 3-manifolds with non empty compact totally geodesic boundary and one cusp. Through out this thesis N denotes a manifold that belongs to $\mathcal{N}_{c,c}$.

Our candidate manifold can be found in a census of 3-manifolds with non empty totally geodesic boundary, built by Figerio, Martelli and Petronio [3]. The census contain 3-manifolds with totally geodesic boundary that admits an ideal triangulation up to 4 tetrahedra. The candidate that belongs to $\mathcal{N}_{c,c}$ has a volume ≈ 7.798 and admits a triangulation of 3 truncated tetrahedra; 1 compact and 2 non-compact. We denote this candidate manifold by N_0.

In this introductory chapter we briefly outline our strategy. In chapter 2 we review the basics of hyperbolic space and its isometry group and introduce hyperbolic manifolds with totally geodesic boundary. In 2.4 we introduce some of the commonly used terminology associated with these manifolds. Most of these were first introduced by Kojima and Miyamoto in [2]. A notion of particular importance is *return paths*. A return path is a geodesic arc in the manifold that is perpendicular to the geodesic boundary at both end points. The volume of a manifold with totally geodesic boundary is closely associated with its length of the shortest return path l_1. Most of our computations in succeeding chapters are parameterized in terms of $cosh(l_1)$ which is denoted by x_1. We also record few existing results in this chapter that set us up to begin the task of identifying the smallest manifold in $\mathcal{N}_{c,c}$.

Our work is divided into the next 5 chapters of this thesis. In chapter 3 we construct a lower volume bound for the manifolds in $\mathcal{N}_{c,c}$ in terms of their x_1 values. Our approach for this chapter is based on the work of Kojima and Miyamota in [2]. A main contribution for the volumes of compact manifolds they investigated is a collar of the boundary. As one increase the depth of such a collar, at some point it becomes non embedded inside the manifold. In [2] this self intersection of the collar of the boundary is handled by a solid of rotation around the shortest return path. Kojima and Miyamoto named this solid as a *Muffin*. This muffin around the shortest return path and the part of the collar of the boundary outside the muffin together bounds the volume of a compact hyperbolic manifold with compact totally geodesic boundary.

While their volume bound can also be applied for the manifolds in $\mathcal{N}_{c,c}$, its far from being sharp enough for our purposes. In order to construct an improved volume bound for manifolds in $\mathcal{N}_{c,c}$, another source of volume needs to be considered. This comes in the form of a cusp neighbourhood. We handle the intersections between these different sources of volumes by another solid of rotation around an arc that runs from the boundary to the cusp. We call this solid of rotation as a *Half ideal muffin*. Its construction is described in 3.3. We then estimate volumes of all the volume sources and muffins mentioned above by functions

of x_1. By taking their sum we obtain a lower bound for the volume of manifold. This process is outlined in 3.4.

Another class of objects that prominently features in our computations is right angled hexagons in the universal cover of a manifold. These hexagons have lifts of return paths as alternating sides. If such a hexagon consists of the lifts of ith, j^{th} and k^{th} shortest return paths, we call it as an (i, j, k) hexagon. Three alternating sides that are lifts of return paths as called as internal edges of this hexagon while other three edges (which lie on $\partial \tilde{N}$) are called as external. We get a first taste of these hexagons when estimating the volume of the cusp neighbourhood. We conclude chapter 3 by proving the following result which follows from the volume bound we constructed. A more precise statement can be found in theorem 1.

Theorem 1. *The smallest manifold in $\mathcal{N}_{c,c}$ has an x_1 value less than 1.2158 and a $(1, j, k)$ hexagon visible from the cusp for some $j, k \geq 1$.*

In chapter 4 we consider manifolds with x_1 values less than 1.2158. Now the question is how small x_1 of these manifolds can be ? It was proved in [2], compact manifolds with compact totally geodesic boundary has their x_1 values bounded below by 1.183. This is also valid for the manifolds in $\mathcal{N}_{c,c}$. The main goal of chapter 4 is to further improve this lower bound of x_1.

Our work in this chapter leverages the relation between the geometry of the manifold and the geometry of its boundary. In particular, our arguments build upon the dependence between the lengths of two geodesic arcs on the boundary of the manifold and how they relate to x_1. Let

$d_{11} =$ The length of the shortest non constant geodesic arc in ∂N with each end

point at a foot of the shortest return path

$d_{01} =$ The length of the shortest geodesic arc in ∂N between the foot of shortest

arc out of the cusp and a foot of the shortest return path on the boundary

First we have a simple explicit relationship between d_{11} and x_1 when the manifold has a $(1, 1, 1)$ hexagon in its universal cover. It was proved in [4] such a right angled hexagon exists when x_1 of the manifold is less than 1.215. (This will be increased to 1.23 in a forthcoming preprint of DeBlois and Shalen. [5]) A description of $(1, 1, 1)$ hexagons and this explicit relation between x_1 and d_{11} is given in 4.1.

Then we look to understand how d_{01} is related to x_1 value of the manifold. Hyperbolic trigonometry results proved in [6] provide a lower bound for d_{01} in terms of x_1. The majority of our work in this chapter is on finding an upper bound for the same distance d_{01} in terms of x_1.

Given a hyperbolic surface and a finite set of points on it, the machinery of *Centered Dual Decomposition* introduced in [7] by DeBlois describes a method of decomposing the surface such that the given set of points are the vertices of the decomposition. We apply this machinery to our context where the surface will be the boundary of our manifold and the finite set of points will be the feet of the shortest return path. Centered Dual Decomposition is described in section 4.2. Two cells in these decompositions are unions of cyclic polygons. In section 4.3 we provide a brief review of cyclic polygons and record some of the pertinent results proved in [7].

The remainder of the chapter 4 is focused on understanding the circumcircle radius of these $2-$cells. At first, our computations will be in terms of d_{11}. We first classify the possible $2-$cells in Centered Dual Decomposition based on the d_{11} value of the manifold. These are recorded in corollary 4.5.4. The different possibilities of $2-$cells listed in 4.5.4 is then analysed separately in sections 4.6, 4.7 and 4.8. For each such possibility we compute an upper bound for the circumcircle radii of $2-$cells in the decomposition. These bounds - which are initially functions of d_{11} - are then converted to functions of x_1 using the relation between d_{11} and x_1 provided by $(1, 1, 1)$ hexagons. These functions are in fact the upper bounds of d_{01} we were seeking, because an upper bound for all the circumcircle radii also bounds d_{01} by above.

Finally we compare these upper bounds of d_{01} with the lower bound of d_{01} provided by trigonometry in [6]. We observe that for all the x_1 values listed in corollary 4.5.4, the lower bound of d_{01} actually exceeds upper bound we computed using the centered dual decomposition. Hence no manifold in $\mathcal{N}_{c,c}$ can have an x_1 value in that range and in Theorem 2 we obtain the following lower bound for x_1 of a manifold in $\mathcal{N}_{c,c}$.

Theorem 2. *No manifold in $\mathcal{N}_{c,c}$ has an x_1 value less than 1.2081.*

Combining the Theorem 1 and 2, we see that the smallest manifold in $\mathcal{N}_{c,c}$ must have its x_1 value in the interval $[1.208, 1.2158]$. Furthermore its universal cover $\tilde{N}$ should have a $(1, j, k)$ hexagon visible from the cusp. Let's denote by $\mathcal{N}'_{c,c}$, the set of all manifolds in $\mathcal{N}_{c,c}$ that has its x_1 value in the above interval and contain a $(1, j, k)$ hexagon visible from the cusp in its universal cover. It's important to note that our candidate manifold N_0 has an x_1 value of 1.213 and $\tilde{N}_0$ has a $(1, 1, 1)$ hexagon visible from the cusp. Hence N_0 belongs to $\mathcal{N}'_{c,c}$

The main goal of chapter 5 is to determine the values j and k that does not make the volume of the manifold too big. We do so by reconstructing a volume estimation specifically for the manifolds in $\mathcal{N}'_{c,c}$. The key elements from our previous volume estimation from chapter 3 will remain the same here except for one change : The volume of the embedded cusp neighbourhood is now estimated using the $(1, j, k)$ hexagon in the universal cover. This new estimate restricts the range j and k can take without making the volume of the manifold bigger than that of N_0.

In Proposition 5.6 and 5.7 we apply the new estimation to the cases $j = 2$, $k = 2$ and $j = 1$, $k = 2$. In Propositions 5.8 and 5.9 and we prove its enough to consider only those two combinations of j and k. These four propositions together yield the main result of chapter 5, recorded in Corollary 5.4.2. We restate it below.

Theorem 3. *Let N be a manifold in $\mathcal{N}'_{c,c}$. If the volume of N does not exceed the volume of N_0 then one of the following is true.*

1. *$\tilde{N}$ has a $(1,1,1)$ hexagon visible from the cusp.*

2. *$\tilde{N}$ has a $(1,1,k)$ hexagon visible from the cusp for some $k > 1$. x_1 of N is between 1.208 and 1.2091 and the volume of N is greater than 7.782*

Chapter 6 and 7 are devoted to analyse the first case of the above theorem. Consider a manifold N in $\mathcal{N}_{c,c}$ which also has a $(1,1,1)$ hexagon visible from the cusp. Projection of external edges of this hexagon on to the boundary of the manifold forms a graph on the boundary with two vertices ; feet of the shortest return path. We denote this graph by G. We start chapter 6 with a discussion on complementary regions of this graph G on the boundary. In 6.1 and 6.2 we show there are only two different combinations of complementary regions of G. We list them below.

1. Two complementary regions both of which are hexagons
2. Three complementary regions ; a hexagon , an annulus and a rectangle.

The remainder of the thesis focus on analysing the first case listed above. Note that our candidate manifold N_0 also has two hexagonal complementary regions on its boundary, matching the description of case 1. The second case remains to be analysed at this point. We expect the method we used to analyse the first case to also work for the second, at least to some extent.

For a manifold N in $\mathcal{N}'_{c,c}$ that has two hexagonal complementary regions of G on its boundary, we identify a $2-$complex of N with a simple combinatorial description. We show that the manifold X obtained by thickening up this $2-$complex has a hyperbolic structure and $N - X$ is a disjoint union of the cusp of N and a solid torus. Put another way, N can be obtained from the interior of X by a **Dehn filling**. This is a well-studied operation in

the context of three-manifolds in which a solid torus is identified to a torus boundary component T of another three-manifold along its boundary which has the effect of "closing T off".

The manifold X constructed above has a totally geodesic boundary and two cusps. We recognise it to be another manifold in the Frigerio, Martelli and Petronio census [3], [8]. It is the unique member in their census that has two cusps and a genus $2-$surface as its boundary and admits a triangulation of four partially truncated tetrahedra. This is stated in theorem 3.

Theorem 4. *Let N be a manifold in $\mathcal{N}'_{c,c}$ that contains a $(1,1,1)$ hexagon visible from the cusp in its universal cover. If ∂N has two hexagonal complementary regions in G then N can be obtained by a Dehn filling of X, where X is the unique member of $\mathcal{M}_{2,2}$ where $\mathcal{M}_{g,k}$ is the class of $k-$ cusped hyperbolic $3-$ manifolds with totally geodesic boundary of genus g and admits a triangulation of $g+k$ partially truncated tetrahedra.*

With the above result, we shift our focus to the Dehn fillings of X. A Dehn filling of a manifold reduce its volume. The amount of the volume reduction depends on the length of the slope, along which the manifold was Dehn filled. The basic idea is when the length of the slope is large enough, volume of the manifold produced by the Dehn filling is going to exceed a certain threshold. We first used [9] to determine the minimum slope length required to guarantee a Dehn filling of X which has a volume greater than that of N_0. Then we classified all the slopes of a cusp in X that has a length smaller than this minimum slope length. We counted 89 such slopes and list them in the table 2.

If a Dehn filling of X produces a manifold which has a volume smaller than or equal to the volume of N_0 then it has to be filled along one of the slopes in table 2. Hence we need to determine whether Dehn filling along a given slope in table 2 produces a hyperbolic manifold and if so, what its volume is.

The 3$-$manifold software *SnapPy* [10] can be used to obtain this kind of information when

it comes to hyperbolic manifolds without a boundary. The issue here is X has a geodesic boundary and *SnapPy* can not take such a manifold as an input. To counter this, we construct a hyperbolic manifold without boundary; DX - The double of X along its boundary. Note that DX has a self isometry that is the reflection along the boundary of X. Let's denote this isometry by Ψ and the cusp of X we fill by T_1. Then the volume the Dehn filling of X along a slope γ in T_1 is equal to one half of the volume of the Dehn filling of DX along slopes γ in T_1 and $\Psi(\gamma)$ in $\Psi(T_1)$.

Chapter 7 explain the process of obtaining an ideal triangulation of DX that *SnapPy* can read. With this triangulation we can access the information of Dehn fillings of DX. In particular we can obtain the volume of a Dehn filling along a given slope. We then use this information to compute volumes of Dehn fillings of X along each slope given in table 2. Final analysis yield following results.

- 6 of the Dehn fillings in the table 2 are non hyperbolic.
- 6 of the Dehn fillings have the same volume as N_0
- All the remaining slopes in table 2 yield Dehn fillings with volumes bigger than the volume of N_0

The complete list of volumes for all the slopes listed in table 2 is given in table 5 The observations above, yield the final major result of this thesis ; Theorem 4.

Theorem 5. *Let N be a manifold in $\mathcal{N}'_{c,c}$ which satisfy the following conditions.*

1) N has a $(1,1,1)$ hexagon visible from the cusp

2) ∂N has two complementary components in G

where G is the graph on ∂N which has the feet of λ_1 as vertices and projections of external edges of the two $(1,1,1)$ hexagons as edges.

$$\text{Then volume of } N \geq \text{volume of } N_0$$

Furthermore if the volume of N is equal to the volume of N_0 then $N = N_0$

We summarise all of our results in chapters 3 - 7 in theorem 5.

Theorem 6. *If N is the least volume manifold in $\mathcal{N}_{c,c}$ then one of the following must be true.*

- $N = N_0$

- $\tilde{N}$ *has no* $(1,1,1)$ *hexagons visible from the cusp but has a* $(1,1,k)$ *hexagon visible from the cusp for some* $k > 1$. *Furthermore the volume of N is greater than* 7.782 *and* x_1 *of N is between* 1.208 *and* 1.2091

- $\tilde{N}$ *has* $(1,1,1)$ *hexagons. N has two complementary components of G in ∂N*

2.0 Background

2.1 Hyperbolic space

Hyperbolic $n-$ space is the unique $n-$dimensional complete, simply connected Riemannian manifold with sectional curvature -1. There are several models that can be used to define the hyperbolic $n-$ space. Most of our computations will be done in the Upper Half-Space model which is defined as

$$\mathbb{H}^n = \{\,(x_1,\ldots,x_n) \in \mathbb{R}^n \mid x_n > 0\}$$

equipped with the Riemannian metric tensor $< v, w >_p = \frac{v_1 w_1 + \ldots v_n w_n}{x_n^2}$

for $p = (x_1,\ldots,x_n) \in \mathbb{H}^n$ and $v = (v_1,\ldots,v_n), w = (w_1,\ldots,w_n) \in T_p\mathbb{H}^n$.

$\partial\mathbb{H}^n$, the boundary of $\mathbb{H}^n$ is defined to be $(\mathbb{R}^{n-1} \times \{0\}) \cup \infty$. Points in $\partial\partial\mathbb{H}^n$ are also called as 'ideal points' of $\partial\mathbb{H}^n$. It is given the topologized and is homeomorphic to S^{n-1}. The compactification of $\mathbb{H}^n$ is then $\overline{\mathbb{H}}^n = \mathbb{H}^n \cup \partial\mathbb{H}^n$.

A $k-$dimensional hyperbolic subspaces of $\mathbb{H}^n$ are intersections of Euclidean $k-$ planes and Euclidean $k-$ spheres that are orthogonal to $\mathbb{R}^{n-1} \times \{0\}$ with $\mathbb{H}^n$. A $1-$dimensional hyperbolic subspace is called as a geodesic line of $\mathbb{H}^n$. An $n-1$ dimensional hyperbolic subspace is called as a geodesic hyperplane of $\mathbb{H}^n$. A geodesic hyperplane H split $\mathbb{H}^n$ into two parts each of which is a component of $\mathbb{H}^n - H$. Let C be one such component. Then $\overline{C} = C \cup H$ is called as a half space bounded by H

In 3 dimensions, geodesic lines and hyperplanes of $\mathbb{H}^3$ are semicircles and semispheres that

10

are orthogonal to $\mathbb{R}^2 \times \{0\}$.

2.2 Isometries of the hyperbolic space

Non trivial isometries of $\mathbb{H}^n$ can be classfied into 3 types depending on their fixed points. An isometry is called as *elliptic* if it fixes a point in $\mathbb{H}^n$. A *parabolic* isometry fixes no points in $\mathbb{H}^n$ and has a unique fixed point in $\partial \mathbb{H}^n$. hyperbolic. An isometry that fixes no points in $\mathbb{H}^n$ and has exactly two fixed point in $\partial \mathbb{H}^n$ is called as *hyperbolic*. Any non trivial isometry of $\mathbb{H}^n$ belongs to one of these three types.

The group of orientation preserving isometries of $\mathbb{H}^3$ is isomorphic to $PSL(2, \mathbb{C})$. By identifying $\mathbb{R}^{n-1} \times \{0\}$ with $\mathbb{C}$, we can write $\partial \mathbb{H}^3$ as $\mathbb{C} \cup \infty$. Then $PSL(2, \mathbb{C})$ acts on $\partial \mathbb{H}^3$ by

$$\begin{pmatrix} a & b \\ c & d \end{pmatrix} \cdot z = \frac{az + b}{cz + d}$$

Any orientation preserving isometry of $\mathbb{H}^3$ is given by an extension of this action on $\partial \mathbb{H}^3$ by an element of $PSL(2, \mathbb{C})$.

2.3 Hyperbolic manifolds

A hyperbolic $n-$manifold (without a boundary) is an $n-$ dimensional Riemannian manifold that is locally isometric to an open set of $\mathbb{H}^n$. As mentioned above, $\mathbb{H}^n$ is the unique complete and simply connected hyperbolic $n-$manifold up to isometry. Any complete hyperbolic $n-$manifold is isometric to $\mathbb{H}^n/\Gamma$ for some subgroup Γ of isometries of $\mathbb{H}^n$ that is acting freely and properly discontinuously. Equivalently Γ is discrete and contains only parabolic

and hyperbolic isometries.

When Γ contains only parabolic transformations acting properly discontinuous and fixes $\infty \in \partial \mathbb{H}^n$, $\mathbb{H}^n/\Gamma$ is a very simple type of hyperbolic manifold called as a *cusp*. Any such a parabolic translation Φ is an extension of a Euclidean isometry ϕ on $\mathbb{R}^{n-1}$ acting freely and extended by $\Phi(x,t) = (\phi(x),t)$. Consider a group Γ' of Euclidean isometries acting freely on $\mathbb{R}^{n-1}$ and the of group of parabolic isometries Γ consists of their extensions. If $\mathbb{R}^{n-1}/\Gamma' = M$ then $\mathbb{H}^n/\Gamma$ is homeomorphic to $M \times (0,\infty)$. A subset $M \times [a,\infty)$ of a cusp is called as a *truncated cusp*. Orientation preserving Euclidean isometries acting freely on $\mathbb{R}^2$ are translations and hence a $3-$ dimensional cusp is homeomorphic to $T \times (0,\infty)$ where T is a $2-$ dimensional Euclidean torus. Then a truncated cusp takes the form $T \times [a,\infty)$.

In this thesis our focus will be on hyperbolic manifolds with totally geodesic boundary. A hyperbolic $n-$ manifold with totally geodesic boundary is a Riemannian $n-$ manifold and is locally isometric to an open set in a half space of $\mathbb{H}^n$. To be precise, each point x in a hyperbolic manifold with totally geodesic boundary has a neighbourhood U of x and an isometry ϕ from U to an open set of a half space H in $\mathbb{H}^n$ such that $\phi(U \cap \partial N) = \phi(U) \cap \partial H$.

Universal cover of a complete hyperbolic manifold with totally geodesic boundary is a convex subset of $\mathbb{H}^n$ which is the intersection of countably many half spaces which are bounded by disjoint geodesic hyperplanes.

2.4   Basic terminology and existing results

Some of the terminology introduced in [2] will be heavily used throughout this write-up and are stated below.

Definition 2.4.1. A **return path** of N is a geodesic arc in N such that its end points are

in ∂N and is perpendicular to ∂N at it's end points.

Kojima showed there are only finitely many return paths of bounded lengths which means return paths of N can be enumerated by $\lambda_1, \lambda_2, \ldots$ such that their lengths are increasing. We use the following notations.

Definition 2.4.2.

- l_i = length of λ_i
- $x_i = cosh(l_i)$
- d_{ij} = length of the shortest geodesic arc in ∂N joining an endpoint of λ_i to an endpoint of λ_j.

In particular , the length of the shortest return path is denoted by l_1 and $cosh(l_1)$ is denoted by x_1.

Definition 2.4.3. We denote by λ_0 , **the shortest arc out of the cusp** measurable with respect to a fixed cusp neighbourhood. By d_{0j} we denote the length of the shortest geodesic arc in ∂N joining the endpoint of λ_0 to the endpoint of λ_j on ∂N.

We start off the search for the smallest manifold in $\mathcal{N}_{c,c}$ by recording two propositions. First one is due to the work of Miyamoto in [11] and the latter was proved in [2].

Proposition 2.4.4. *Volume of a manifold $N \in \mathcal{N}_{c,c}$ exceeds the volume of N_0 if $\chi(\partial N) < -2$.*

Proposition 2.4.5. *If $\chi(\partial N) = -2$ then it's x_1 value has the the following lower bound.*

$$x_1 \geq \frac{3 + \sqrt{3}}{4} \approx 1.183$$

.

3.0   Volume Estimation

Let N be a manifold in $\mathcal{N}_{c,c}$. As stated in Proposition 2.4 we can assume $\chi(\partial N) = -2$. The goal of this chapter is to find a lower bound for the volume of N as a function of x_1.

There are two main sources that contribute to the volume of N.

- A collar of ∂N
- A cusp neighbourhood of N

To encompass more volume , we would like to make these components as large as possible. But after some point they will not be embedded in N (for an example if the height of the collar of ∂N exceeds $\frac{l_1}{2}$) or intersect each other. Figure 1 depicts these scenarios as viewed in $\tilde{N}$, the universal cover of N.
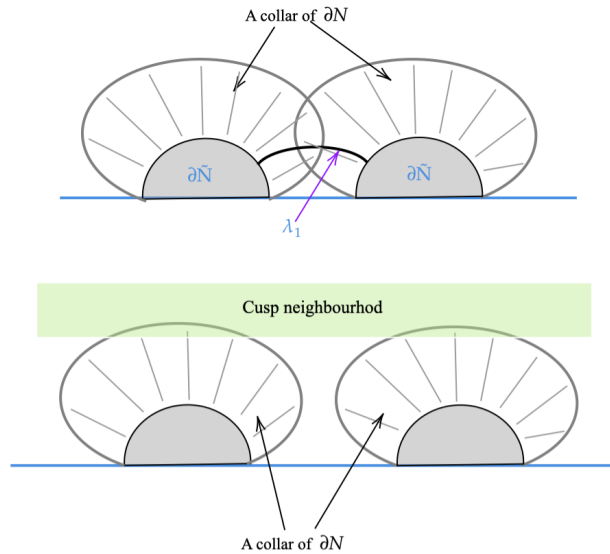
Figure 1: Volume sources may be non embedded or intersect each other

3.1 Muffins

The device used to handle these regions of overlaps is called as "Muffins". Kojima and Miyamoto showed in [2] a muffin like object - a hyperbolic solid of rotation can be embedded in N along the shortest return path λ_1. This allows the collar of remaining part of ∂N to have a greater height. Denote this muffin by M_{l_1}.
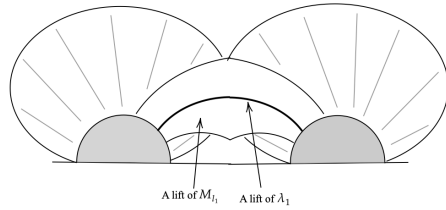
Figure 2: Muffin around the shortest return path

Below we give a brief description of M_{l_1}. Consider a right angled hexagon with alternating sides l_1 (see figure 3). M_{l_1} is obtained by rotating the shaded pentagon with four right angles about the side with length l_1.
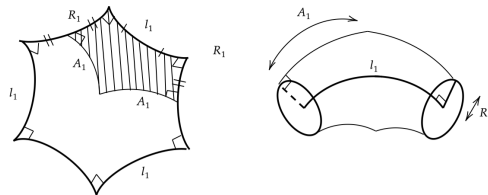
Figure 3: Construction of M_{l_1}

Using right angled hexagon R_1 can be written as a function of x_1.

$$R_1 = \sqrt{\frac{2x_1 - 1}{2(x_1 - 1)}}$$

15

Side altitude A_1 satisfies

$$cosh(2A_1) = \frac{4x_1 + 1}{3}$$

The intersection of M_{l_1} with the boundary is two disks with radius R_1 around each feet of λ_1. Now we consider a collar of the $\partial N-$ these two disks. The height of this new collar can be increased further than $l_1/2$ because the shortest return path is now entirely outside the collar now. The question is how much further the height can be increased before it run into itself again. M_{l_1} and this new collar is tangent to each other along the side altitude of M_{l_1}. Hence the height of the new collar can not exceed A_1 or else it will self overlap. But it may even not be possible to have a height of A_1. While the shortest return path does not intersect with this collar, it may entirely contain other return paths. The length such a return path can have is greater than or equal to l_2. So if we keep the height of the collar of the remaining part of ∂N to be $min\{A_1, \frac{l_2}{2}\}$ then its guaranteed to avoid self overlap.

But the length of the second shortest return path l_2 is not a function of l_1. Kojima and Miyamoto [2]) showed there exist two functions E and F such that $l_2 \geq min\{E_1, F_1\}$ where $E_1 = E(x_1)$ and $F_1 = F(x_1)$.

Then take the collar of the remaining part of ∂N to be

$$H_1 = max\left\{ min\left\{ \frac{E_1}{2}, \frac{F_1}{2}, A_1 \right\}, \frac{l_1}{2} \right\}$$

Below, we described the process used in [2] to find these two functions E_1 and F_1 that bounds l_2 by below.

3.2   Bounding l_2 by below - Functions E_1 and F_1

Suppose d_{12} ; the shortest distance between the end points of λ_1 and λ_2 on ∂N is attained

on a component Π_0 of $\partial \tilde{N}$. Let Π_1 and Π_2 be the components of $\partial \tilde{N}$ that contains the other end points of the corresponding lifts of λ_1 and λ_2. Finally, let the length of the common perpendicular between Π_1 and Π_2 be l_k. It is a lift of a return path λ_k for some $k \geq 1$. Hence we have a right angled hexagon in $\tilde{N}$ with alternating sides of l_1, l_2 and l_k as shown in figure 4. By applying the right angled hexagon rule we obtain

$$
\begin{aligned}
cosh(d_{12}) &= \frac{cosh(l_1)cosh(l_2) + cosh(l_k)}{sinh(l_1)sinh(l_2)} \\
&\geq \frac{cosh(l_1)cosh(l_2) + cosh(l_1)}{sinh(l_1)sinh(l_2)} \\
&= \frac{cosh(l_1)(cosh(l_2) + 1)}{sinh(l_1)sinh(l_2)} \\
&= \tanh(l_1)\sqrt{1 + \frac{2}{cosh(l_2) - 1}}
\end{aligned}
$$
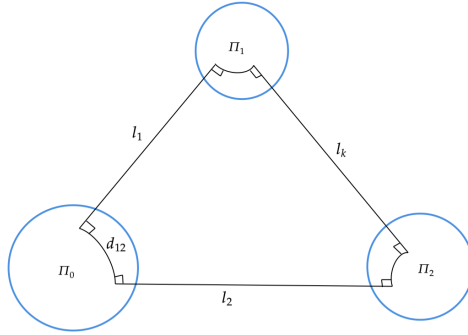
Figure 4: Relating d_{12} to l_2

Hence we have

$$cosh(l_2) \geq 1 + \frac{2}{cosh^2(d_{12})tanh^2(l_1) - 1} \tag{1}$$

Similarly we can find another inequality relating l_2 to d_{22}. In this case we have a right

17

angled hexagon with alternating sides l_2, l_2 and l_k for some $k \geq 1$. By applying the right angled hexagon rule to this case we obtain

$$
\begin{aligned}
cosh(d_{22}) &= \frac{cosh(l_2)cosh(l_2) + cosh(l_k)}{sinh(l_2)sinh(l_2)} \\
&\geq \frac{cosh^2(l_2) + cosh(l_1)}{sinh^2(l_2)}
\end{aligned}
$$

Hence we have

$$
cosh(l_2) \geq \sqrt{1 + \frac{cosh(l_1) + 1}{cosh(d_{22}) - 1}} \tag{2}
$$

Recall that the $M_{l_1} \cap \partial N$ is two disks with radius R_1. Let's denote these two disks by U_1 and U_2. First define a new quantity R'_1 as

$$
cosh(R'_1) = 3 - cosh(R)
$$

We claim that R'_1 is the maximum radius of two disks that can be embedded in $\partial N \backslash (U_1 \cup U_2)$. Suppose there are two disks with radius $r > R'_1$ embedded in $\partial N \setminus (U_1 \cup U_2)$. Sum of the areas of these two disks and U_1 and U_2 are then equal to

$$
2 * 2\pi(cosh(R_1) - 1) + 2 * 2\pi(cosh(r) - 1)
$$
$$
> 4\pi(cosh(R_1) - 1) + 4\pi(cosh(R'_1) - 1)
$$
$$
= 4\pi
$$

But the area of ∂N is 4π as $\chi(\partial N) = -2$. Hence the last inequality is a contradiction as the sum of the areas of the four embedded disks can not exceed the area of the boundary.

Now consider two disks embedded in $\partial N \setminus (U_1 \cup U_2)$ that are centered at the feet of λ_2. Let's denote them by V_1 and V_2. Let r' be the maximum radius these two disks can take while remain embedded in $\partial N \setminus (U_1 \cup U_2)$. Hence r' is less than R'_1.

Since r' is the maximum radius V_1 and V_2 can take while remain embedded in $\partial N - (U_1 \cup U_2)$, one of the following must be true.

18

- One of V_1 or V_2 touch its own boundary
- Boundary of V_1 touches the boundary of V_2
- Boundary of a V_i touches the boundary of a U_i

In the first or second scenario we have $d_{22} \leq 2r' \leq 2R_1'$.

In the third scenario we have $d_{12} \leq R_1 + r' \leq R_1 + R_1'$. We know one of these two things should be true. If $R_1 + R_1' \geq d_{12}$ is true then we can use 1 to obtain

$$cosh(l_2) \geq \sqrt{1 + \frac{cosh(l_1) + 1}{cosh(R_1 + R_1') - 1}}$$

If $2R_1' \geq d_{22}$ is true then we can use 2 to obtain

$$cosh(l_2) \geq \sqrt{1 + \frac{cosh(l_1) + 1}{cosh(2R_1') - 1}}$$

Now we define the following.

$$cosh(E_1) = \sqrt{1 + \frac{cosh(l_1) + 1}{cosh(R_1 + R_1') - 1}}$$

$$cosh(F_1) = \sqrt{1 + \frac{cosh(l_1) + 1}{cosh(2R_1') - 1}}$$

These are exactly the right hand sides of last two inequalities and also depend entirely on x_1. Hence there are two functions E_1 and F_1 of x_1 such that one of the following must always be true.

- $l_2 \geq E_1$
- $l_2 \geq F_1$

Recall that when selecting a height H_1 for the collar of $\partial N \setminus (U_1 \cup U_2)$, we need to have $H \leq \min\left\{A_1, l_2/2\right\}$. With what was proved in this section, we can take $H_1 = \min\left\{A_1, E_1/2, F_1/2\right\}$. This height for H_1 makes sure the collar we consider will not run into itself. But the bounds E_1 and F_1 are far from being sharp. In fact for large x_1 values, they turn out to be smaller than even l_1. Hence the choice for H_1 is slightly modified as below.

$$H_1 = max\left\{min\left\{\frac{E_1}{2}, \frac{F_1}{2}, A_1\right\}, \frac{l_1}{2}\right\}$$

3.3   Half ideal muffin

To handle the region of intersection between the collar and the cusp neighbourhood , we use another hyperbolic solid of rotation, about λ_0. We call this object as the "Half ideal muffin".(see figure 5)
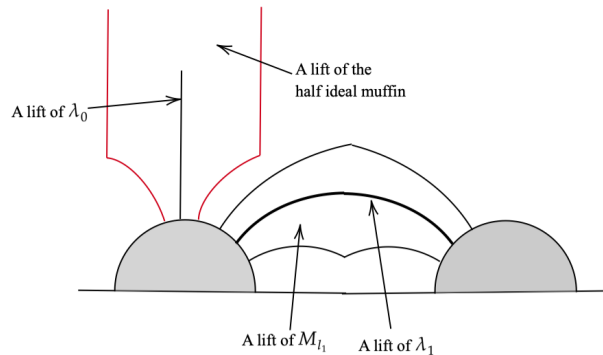
Figure 5: Lifts of M_{l_1} and the half ideal muffin

To figure out correct dimensions for the half ideal muffin so that it's embedded and does not

intersect M_{l_1} first we need to understand the shortest distance between the foot of λ_0 and feet of λ_0 on ∂N ; d_{01}. Using the trigonometry proved in [6] we have the following lower bound of d_{01}.

$$cosh(d_{01}) \geq \frac{cosh(l_1) + 1}{sinh(l_1)} = \sqrt{\frac{x_1 + 1}{x_1 - 1}} \tag{3}$$

$acosh\left(\sqrt{x_1 + 1/x_1 - 1}\right)$ is hence a lower bound for d_{01}. Let's denote it by $(d_{01})_{min}$.

Now we are ready to define dimensions of the half ideal muffin properly. There are two parameters that completely determine a half ideal muffin ; base radius and side altitude. We chose them as follows.

- Base radius $= (d_{01})_{min} - R_1$
- Side altitude $= A_1$
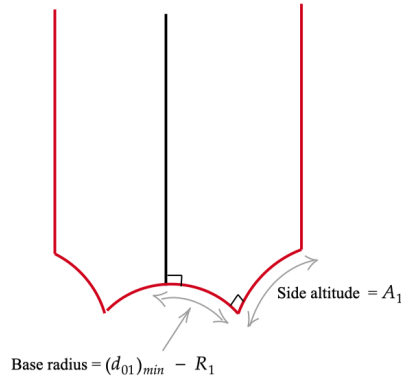
Figure 6: Dimensions of the half ideal muffin

Now the part of the cusp neighbourhood outside the half ideal muffin can be dropped further to encompass more volume. The complete arrangement as scene in $\partial \tilde{N}$ is shown in figure 7

21
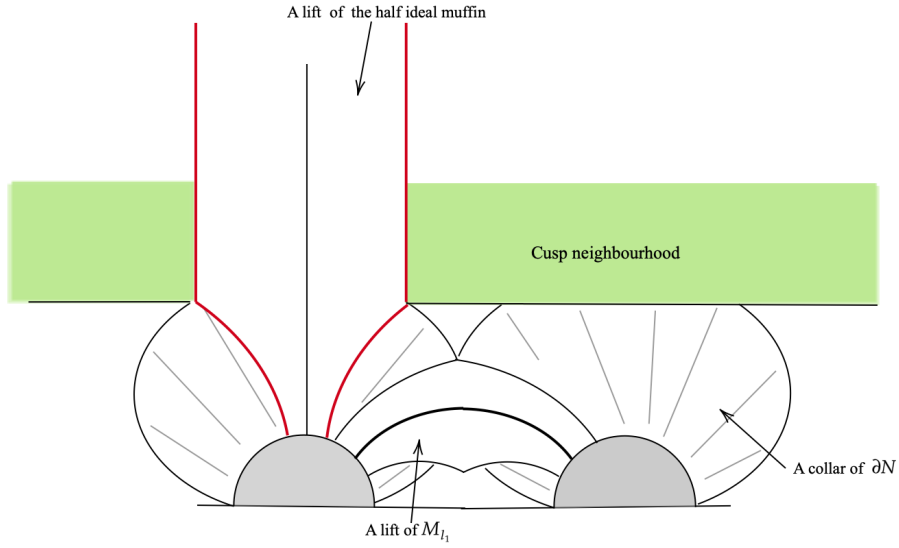
Figure 7: Complete arrangement seen in $\partial \tilde{N}$

3.4 Volumes

In this section we compute volumes of solids mentioned earlier.

3.4.1 Volume of the muffin around shortest return path

M_{l_1} is a solid of a rotation and it's volume is given by [2]

$$V_{M_{l_1}}(x_1) = 2\pi \left(A_1 cosh(R_1) - \frac{l_1}{2} \right)$$

3.4.2 Volume of the half ideal muffin

We divide the half ideal muffin into two parts.(see figure 8)

- A compact part which is the solid of rotation of a Lambert quadrilateral. Sides of this Lambert quadrilateral are $(d_{01})_{min}, A_1, \rho$ and K' in terms of the notation in figure 8.
- A non compact part.
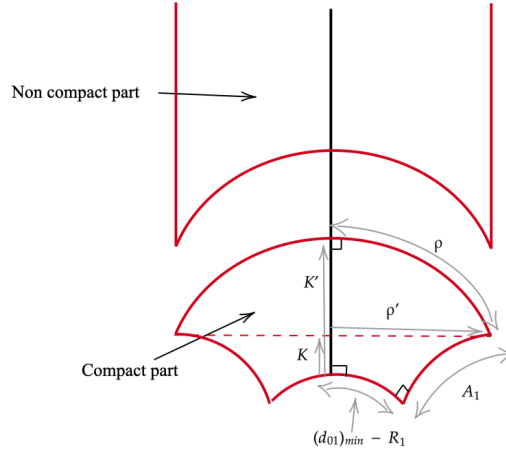
Figure 8: Two parts of the half ideal muffin

Lemma 3.4.1. *All the measurements in figure 8 entirely depend on x_1. They are given by*

$$tanh(K') = \frac{tanh(A)}{cosh((d_{01})_{min})}$$

$$sech^2(\rho) = \frac{tanh^2(d_{01})_{min}}{1 - \frac{sech^2(A_1)}{sinh^2((d_{01})_{min}) + sech^2(A_1)}}$$

$$K = K' - log(cosh(\rho)$$

$$\rho' = sinh(\rho)$$

23

Proof. Consider the Lambert quadrilateral shown in figure 9. Such a quadrilateral satisfies the rule $tanh(c) = cosh(b)tanh(a)$[2].

Now we apply this rule to the Lambert quadrilateral in figure 8, rotation of which forms the compact part of the half ideal muffin. By taking $a = K', b = (d_{01})_{min}, c = A_1$ we obtain

$$tanh(A_1) = cosh((d_{01})_{min})tanh(K')$$

We now reflect this quadrilateral along the diagonal through the acute angle and apply the same quadrilateral rule again. This time we have $a = (d_{01})_{min}, b = K', c = \rho$ and hence

$$tanh(\rho) = cosh(K')tanh((d_{01})_{min})$$

By solving these two equations, we can obtain K' and ρ as given in the statement.

Now consider a lift of λ_0 that is a vertical line segment that goes to ∞ in the universal cover and the lift of the half ideal muffin around that vertical line. To compute K and ρ', without loss of generality we assume radius of the Euclidean hemisphere that bounds the non compact part of the lift of half ideal muffin below is 1 and centered at $(0,0)$ on $\partial\mathbb{H}^3$ (see figure 11).Let h be as shown in the same figure.

The curve from $(0,0,1)$ to $(\sqrt{1-h^2}, 0, h)$ can be parameterized by $r(t) =< sin(t), 0, cos(t) >$ for $0 \leq t \leq cos^{-1}(h)$. Since the hyperbolic length of this arc is ρ we have

$$\rho = \int_0^{cos^{-1}(h)} \frac{|r'(t)|}{cos(t)}dt$$
$$=log(sec(t) + tant(t))\Big|_0^{cos^{-1}(h)}$$
$$=log\left(\frac{1+\sqrt{1-h^2}}{h}\right)$$

By solving this equation for h, we obtain $h = sech(\rho)$. The vertical line segment from $(0,0,h)$

24

to $(0, 0, 1)$ can be parameterized by $< 0, 0, t >$ for $h \leq t \leq 1$. Hence its hyperbolic length is equal to

$$\int_h^1 \frac{1}{t} dt = -log(h) = log(cosh(\rho))$$

Therefore $K = K' - log(cosh(\rho))$

Finally, ρ' is an arc that lie in a horosphere of ∞ (a horizontal Euclidean plane). It can be parameterized by $< t, 0, h >$ for $0 \leq t \leq \sqrt{1 - h^2}$. So its length ρ' is equal to

$$\int_h^{\sqrt{1-h^2}} \frac{1}{h} dt = \frac{\sqrt{1 - h^2}}{h} = sinh(\rho)$$

$\square$
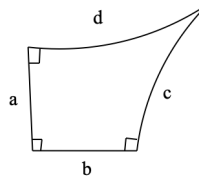
Figure 9: A Lambert quadrilateral

Some of the quantities in the previous lemma will be needed to compute the volume of the half ideal muffin while others will be needed later to estimate the volume of the cusp neighbourhood.
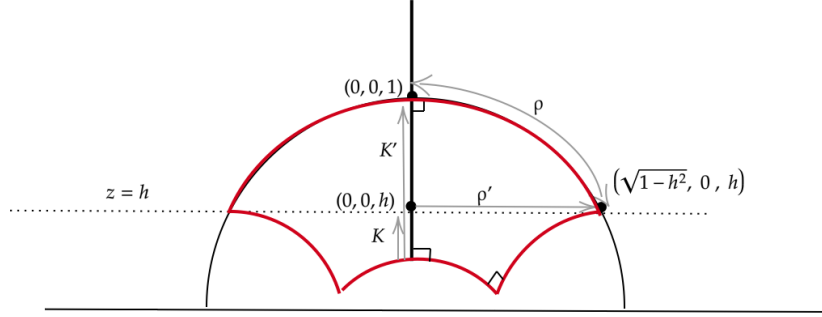
Figure 10: Computations in $\mathbb{H}^3$

Lemma 3.4.2. *The volume of the compact part of the half ideal muffin is*
$\pi(A_1 cosh((d_{01})_{min} - R_1) - K')$ *where K' and ρ are functions of x_1 given in the previous lemma*

Proof. We just have to use the volume formula for the solid obtained by rotating a Lambert quadrilateral proved in [12] (Same formula used in [2] to find the volume of M_{l_1}). $\square$

Lemma 3.4.3. *Volume of the non compact part of the half ideal muffin is given by $\pi log(cosh(\rho))$*

Proof. Here we use the same set up used to compute K and ρ' in lemma 3.1. We consider a lift of λ_0 that is a vertical line segment that goes to ∞ in the universal cover and the lift of the half ideal muffin around that vertical line and assume radius of the Euclidean hemisphere that bounds the non compact part of the lift of half ideal muffin below is 1 and centered at $(0,0)$ on $\partial \mathbb{H}^3$; i.e its the Euclidean hemisphere $z = \sqrt{1 - x^2 - y^2}$.

Hence the projection of the non compact part onto $\partial \mathbb{H}^3$ is a Euclidean disk with radius $\sqrt{1 - h^2}$ and centered at the origin. Denote this disk by D. Hence the volume of the non

26

compact part is given by

$$\text{Volume of the non compact part} = \iint_D \int_{\sqrt{1-x^2-y^2}}^{\infty} \frac{1}{z^3} dz dx dy$$

$$= -\frac{1}{2}.2\pi \int_0^{\sqrt{1-h^2}} \frac{rdr}{1-r^2}$$

$$= -\frac{1}{2}.\pi.log(h^2)$$

$$= \pi log(1/h)$$

Since $h = sech(\rho)$, the volume of the non compact part of the half ideal muffin is $\pi log(cosh(\rho))$.

□
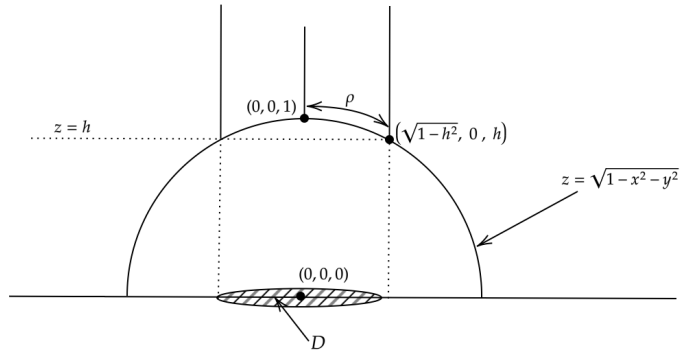
Figure 11: Computing the volume of the non compact part of the half ideal muffin

Hence we have the volume of the half ideal muffin is given by

$$V_{\text{HIM}}(x_1) = \pi(A_1 cosh((d_{01})_{min} - R_1) - K') + \pi log(cosh(\rho))$$

3.4.3 Volume of the collar of the remaining part of ∂N

Intersection of M_{l_1} with ∂N is the union of two disks with radius R_1. Each of these disks has an area of $2\pi(cosh(R_1) - 1)$. Intersection of the half ideal muffin with ∂N is a disk with radius $(d_{01})_{min} - R_1$ and it has an area of $2\pi(cosh((d_{01})_{min} - R_1) - 1)$.

Hence the area of the part of ∂N that does not intersect the two muffins is $4\pi - 4\pi(cosh(R_1) - 1) - 2\pi(cosh((d_{01})_{min} - R_1) - 1)$.

We take a collar of this part with height H_1. In the product metric space , it's volume is given by

$$V_{\text{col}}(x_1) = \left(4\pi - 4\pi(cosh(R_1) - 1) - 2\pi\left(cosh((d_{01})_{min} - R_1) - 1\right) \right)\left(\frac{2H_1 + sinh(2H_1)}{4} \right)$$

.

3.4.4 Volume of the remaining part of the cusp neighbourhood

The cusp neighbourhood we consider is distance K away from ∂N. Boroczky's theorem theorem provides a way to estimate the volume of this cusp neighbourhood if we know the maximal radius of a disk that can be embedded in its boundary.

Let q be the point of intersection between λ_0 and the boundary of this cusp neighbourhood. So we would like to understand how large of a disk can be embedded in the cusp cross section centered at q. Suppose the radius of the largest such a disk is $\theta/2$.

If ∞ is a lift of the cusp point in $\tilde{N}$ then a lift of the boundary of the cusp neighbourhood

would be a horosphere of ∞ which is a horizontal Euclidean plane. Denote this Euclidean plane by Λ. It contains some of the lifts of q. Then the length of the horocyclic arc on Λ between any two lifts of q should be at least θ.

Suppose q_1 and q_2 be two lifts of q that attains this distance. Let $\tilde{\lambda}'_0$ and $\tilde{\lambda}"_0$ be lifts of λ_0 that contains those two points and Π_1 and Π_2 be the components of $\partial\tilde{N}$ that contain the initial points of these two lifts. (See figure 12)
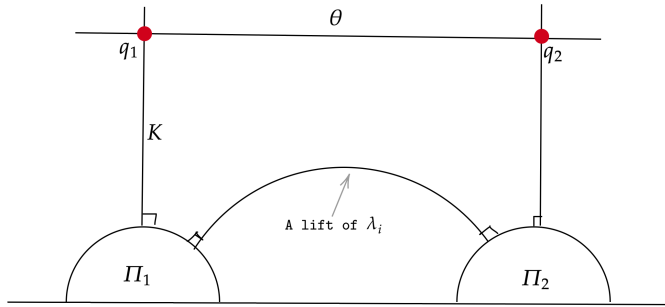
Figure 12: Common perpendicular to two components in $\partial\tilde{N}$ contain two lifts of λ_0 is a lift of λ_i

If the common perpendicular to Π_1 and Π_2 is a lift of λ_i then θ depends on l_i. Using hyperbolic trigonometry results in [6] we can write θ explicitly in terms of l_i as below.

$$\theta = \frac{\sqrt{2(cosh(l_i) + 1)}}{e^K} \tag{4}$$

Using the Boroczky's theorem , we can bound the area of this cusp cross section as follows.

$$\text{Area of the cusp cross section at height K} \geq \frac{2\sqrt{3}}{\pi}\left(\pi\left(\frac{\theta}{2}\right)^2\right) = \frac{\sqrt{3}\theta^2}{2}$$

29

But within this cross section a disk of radius ρ' will be covered by the half ideal muffin. Hence the area of the remaining part of the cusp cross section is bounded below by $\frac{\sqrt{3}\theta^2}{2} - \pi(\rho')^2$

Note that the volume of a cusp neighbourhood is one half of the area of its boundary (Proposition 4.1.7 [13]). Hence the volume of the remaining part of the cusp cross section is bounded below by

$$\frac{1}{2}\left(\frac{\sqrt{3}\theta^2}{2} - \pi(\rho')^2\right) \tag{5}$$

3.5   Final Estimations

In the arrangement shown in figure 7, we have 4 sources contributing to the volume of N.

- M_{l_1}
- Half ideal muffin
- Collar of the remaining part of ∂N
- Remaining part of the cusp neighbourhood

In the previous section we computed volumes of the first three explicitly as functions of x_1. We also obtained a lower bound for the volume of the fourth which was recorded in (5). This lower bound depend on both x_1 and θ.

Recall that if two components of $\partial\tilde{N}$ that contain lifts of λ_0 going to ∞ has a lift of λ_i as their common perpendicular (see figure 12) then θ depends on l_i. The explicit relation between θ and l_i is recorded in (4). We have to consider two cases.

Case 1 : $i = 1$

First using the trigonometric results proved in [6] , we showed $d_{01} = (d_{01})_{min}$ in this case. This forces $\theta/2$ to be same as ρ'. Hence the bound in equation (5) can be rewritten as

$$\frac{1}{2}\left(\frac{2\sqrt{3}}{\pi}(\pi(\rho')^2) - \pi(\rho')^2\right) = \frac{1}{2}\left(\frac{2\sqrt{3}}{\pi} - 1\right)(\pi(\rho')^2)$$

Denote this function as $V_{\text{cusp}}(x_1)$.

Now define

$$V(x_1) = V_{M_{l_1}}(x_1) + V_{\text{HIM}}(x_1) + V_{\text{col}}(x_1) + V_{cusp}(x_1)$$

Then V bound the volume of N by below ; $Vol(N) \geq V(x_1)$. Graph of $V(x_1)$ is shown in figure 13 and value of V at $x_1 = 1.2158$ exceeds 7.8. In particular for a manifold N that falls into the category of case 1, we have $Vol(N) > Vol(N_0)$ if $x_1 > 1.2158$.

Case 2 : $i \geq 2$

In this case θ is not a function of x_1. Since $l_i \geq l_2$ we have the following.

$$\theta \geq \frac{\sqrt{2(cosh(l_2) + 1)}}{e^K}$$

Since $l_2 \geq min\{E_1, F_1\}$, we take $V_{\text{cusp}}(x_1)$ to be

$$V_{\text{cusp}}(x_1) = \frac{1}{2}\left[\left[\frac{2\sqrt{3}}{\pi}\left(\pi(\theta'/2)^2\right)\right] - \pi(\rho')^2\right]$$

where $\theta' = \frac{\sqrt{2(cosh(min\{E_1,F_1\})+1)}}{e^K}$

This $V_{\text{cusp}}(x_1)$ bounds the volume of the remaining part of the cusp neighbourhood by below in case 2.

Similar to case 1, we define

$$V(x_1) = V_{M_{l_1}}(x_1) + V_{\text{HIM}}(x_1) + V_{\text{col}}(x_1) + V_{\text{cusp}}(x_1)$$

Graph of $V(x_1)$ for this case is also shown in figure 13. Value of V at $x_1 = 1.208$ exceeds 7.8. In particular for a manifold N that falls into the category of case 2 $Vol(N) > Vol(N_0)$ if $x_1 > 1.208$.(Note that this holds true even for some x_1 values less than that in this case. But this bound is suffice for now as x_1 values less than 1.208 will be separately addressed in the next chapter.)

This completes the main result of this chapter which is
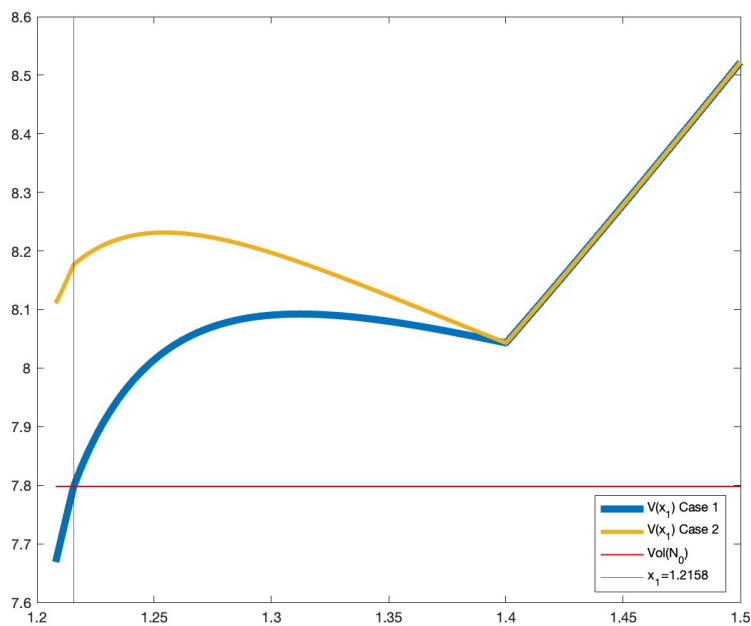
Figure 13: Plots of $V(x_1)$

Theorem 1. *If the smallest manifold in $\mathcal{N}_{c,c}$ belongs to the type described in case 1 then it's x_1 value is less than 1.2158. If it belongs to case 2 then it's x_1 value is less than 1.208.*

In the next chapter we will show that no manifold in $N_{c,c}$ can have an x_1 value less than 1.208 eliminating the possibility of the latter case in 1. In chapters 5,6 and 7 we explain our approach to tackle the former case.

4.0   Centered Dual Decomposition

The main goal of this chapter is to find a lower bound for the x_1 value of the smallest manifold in $\mathcal{N}_{c,c}$. In proposition 2.4.5 we recorded the lower bound computed by Kojima and Miyamoto for the x_1 of any hyperbolic manifold. This value is 1.183. In this chapter, we will prove this lower bound can be pushed higher when the manifold is cusped. Recall that in chapter 3 we proved an upper bound for the x_1 value of the smallest manifold in $\mathcal{N}_{c,c}$ which turns out to be 1.2158.

Throughout this chapter N will be a manifold in $\mathcal{N}_{c,c}$ with $\chi(\partial N) = -2$ and an **x_1 value between 1.183 and 1.2158**. Most of our work in this chapter will be on the boundary of N. We study its geometry using the machinery of "Centered Dual Decomposition" introduced in [7] by DeBlois to understand the geometry of ∂N. Then we relate the geometry of ∂N to the geometry of N using the trigonometry of right angled hyperbolic hexagons.

4.1 (i, j, k) hexagons

Let's first record the hexagon rule for the right angled hexagons. Let a be the hyperbolic length of a side of such a hexagon. Suppose b and c are the side lengths of adjacent sides of a and d is the length of the side opposite to a. Right angled hexagon rule (Theorem 3.5.14, [14])says sides a, b and c determines the entire hexagon and

$$cosh(a) = \frac{cosh(b)cosh(c) + cosh(d)}{sinh(b)sinh(c)}$$

Let Π_1, Π_2 and Π_3 be distinct components of $\partial \tilde{N}$. Suppose the common perpendiculars to these are lifts of λ_i, λ_j and λ_k. Then these lifts are contained in a geodesic plane of $\mathbb{H}^3$.

The right angled hexagon which has the above lifts as alternating sides in contained in $\tilde{N}$ [4]. Other three sides of the hexagon are geodesic arcs in $\partial\tilde{N}$. Such a hexagon is called as an $(\mathbf{i},\mathbf{j},\mathbf{k})$ **hexagon.** Sides of the hexagon which are lifts of return paths are called as internal edges and the sides which are geodesic arcs in $\partial\tilde{N}$ are called as external edges of the hexagon.
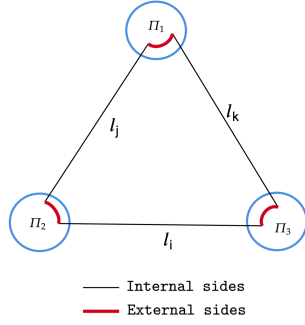
Figure 14: An (i,j,k) hexagon in $\tilde{N}$ seen from above

Recall that d_{11} is the distance between the feet of λ (shortest return path) on the boundary. Suppose λ'_1 and $\lambda"_1$ are two lifts of λ_1 such that both of them has an end point in the same boundary component Π of $\partial\tilde{N}$ and d_{11} is the distance of the geodesic arc between these two points on Π. This geodesic arc on Π together with λ'_1 and $\lambda"_1$ determines a right angled hexagon in $\tilde{N}$. If the third internal side of the hexagon is a lift of $k-$th shortest return path then this is a $(1,1,k)$ hexagon. By applying the right angled hexagonal rule we have the following.

$$\begin{aligned} cosh(d_{11}) &= \frac{cosh^2(l_1) + cosh(l_k)}{sinh^2(l_1)} \\ &\geq \frac{cosh^2(l_1) + cosh(l_1)}{sinh^2(l_1)} \\ &= \frac{cosh(l_1)(cosh(l_1) + 1)}{cosh^2(l_1) - 1} \\ &= 1 + \frac{1}{cosh(l_1) - 1} \end{aligned}$$

35

The inequality in the second line follows from $l_k \geq l_1$. Hence this inequality becomes and equation if and only if the third internal side is also a lift of λ_1 (or in other words if and only if $\tilde{N}$ has a $(1,1,1)$ hexagon.)

DeBlois and Shalen [4] showed manifolds with $x_1 < 1.215$ contain a $(1,1,1)$ hexagon in it's universal cover. This is further improved to $x_1 < 1.23$ in [5]. Since the x_1 values of the manifolds we consider in this chapter are also in this range, we have following relation which describe d_{11} explicitly in terms of x_1.

$$cosh(d_{11}) = 1 + \frac{1}{cosh(l_1) - 1} = 1 + \frac{1}{x_1 - 1} \tag{6}$$

Using this relation between x_1 and d_{11} we can rewrite $(d_{01})_{min}$ from chapter 3 (3) in terms of d_{11}.

$$cosh((d_{01})_{min}) = \sqrt{2cosh(d_{11}) - 1}$$

We also have the following which will be more useful later in this chapter.

$$sinh((d_{01})_{min}) = \sqrt{2(cosh(d_{11}) - 1)} \tag{7}$$

4.2   Centered Dual Decomposition

Below we provide a brief summary on the centered dual decomposition (sections 1 and 2, [15]). Let $\mathcal{S} \subset \mathbb{H}^2$ be a locally finite set. We start with the Voronoi tessellation of $\mathbb{H}^2$ with respect to $\mathcal{S}$. For each $s \in \mathcal{S}$, there is a unique corresponding Voronoi 2 -cell in the

tessellation given by

$$V_s = \big\{\, x \mid d(x,s) \le d(x,s') \quad \forall s' \in \mathcal{S} \,\big\}$$

Each 1-cell of the tessellation is given by the intersection of two Voronoi 2-cells and each vertex is the intersection of three or more Voronoi 2-cells.

Consider a k-cell $V = \bigcap_{s \in \mathcal{S}_0} V_s$ of the Voronoi tessellation where $\mathcal{S}_0 \subset \mathcal{S}$. Then it's geometric dual is the closed convex hull of $\mathcal{S}_0$ in $\mathbb{H}^2$ which has the dimension $2-k$. We denote this by C_V. Collection of geometric duals of Voronoi cells form the **Geometric Dual Complex** of $\mathcal{S}$.

An edge e in the Voronoi tessellation is said to be **non centered** if it's geometric dual edge does not intersect $int(e)$. Collection of non centered Voronoi edges is called as the **non centered Voronoi subgraph** .

Then the **Centered Dual Decomposition** can be thought as a coarsened version of the geometric dual complex where some of the 2-cells in the latter is grouped in a way to give a larger 2-cells , one corresponding to each component of the non centered Voronoi subgraph.

To be precise, if T is a component of the non centered Voronoi subgraph then we define a $2-$ cell of the centered dual decomposition by $C_T = \bigcup_{v \in T^0} C_v$ where T^0 is the set of vertices of T.

Now consider an orientable complete hyperbolic surface $\mathcal{H}$ and a finite set $\mathcal{S} \subset \mathcal{H}$. Let $\pi : \mathbb{H}^2 \to \mathcal{H}$ be the universal cover. We can consider the centered dual decomposition of $\mathbb{H}^2$ with respect to $\pi^{-1}(\mathcal{S})$. Corollary 5.6 of [15] says, this centered dual decomposition is invariant under deck transformations and π embeds the interior of each cell in $\mathcal{H}$. The projection of these cells under the covering map forms **the centered dual decomposition of** $\mathcal{H}$ **with respect to** $\mathcal{S}$.

For a manifold N in $\mathcal{N}_{c,c}$ we consider the Centred Dual Decomposition of ∂N with re-

spect to feet of λ_1 on ∂N ; i.e vertices of the Centered Dual Decomposition decomposition are feet of λ_1. Then d_{11} is the minimum length of edges in the decomposition.

Each 2-cell in this decomposition is a union of geometric duals. Note that vertices of any geometric dual are equidistant from the corresponding Voronoi vertex; hence lie on a metric circle centered at that Voronoi vertex. We call such polygons as cyclic polygons. These were studied heavily in [16] and we devote the next section to record some of the pertinent results proved there.

4.3   Cyclic polygons

Definition 4.3.1. Consider a hyperbolic polygon P with n vertices. If all the vertices of P lie on a metric circle , we call it as a **cyclic polygon**. This metric circle is called as the **circumcircle** of P.

For an example any $2-$cell in a geometric dual described earlier is a cyclic polygon. Calculus of cyclic polygons are of utmost importance for us in the remainder of this chapter. Below we record some of the results proved in [7] and [16] which we use regularly.

Let P be a cyclic polygon and $v_0, v_1, \ldots, v_{n-1}$ be it's vertices ordered cyclically. Denote the edge lengths of P by $q_0 = dist(v_0, v_{n-1})$ and $q_i = dist(v_{i-1}, v_i)$. Edge lengths of a cyclic polygon satisfy

$$sinh(q_i/2) < \sum_{j \neq i} sinh(q_j/2) \quad \forall i \in \{0, \ldots, n-1\}$$

This tuple $(q_0, \ldots q_{n-1})$ of positive numbers upto a cyclic permutation uniquely determine P upto an orientation preserving isometry. Hence we define the set of cyclic hyperbolic

polygons with n sides by

$$\mathcal{AC}_n = \left\{ (q_0, \ldots q_{n-1}) \subset \mathbb{R}^n \mid sinh(q_i/2) < \sum_{j \neq i} sinh(q_j/2) \quad \forall i \in \{0, \ldots, n-1\} \right\}$$

Proposition 4.3.2. *(Proposition 3.3 ,[7]) There exist smooth functions*
$D_0 : \mathcal{AC}_n \to \mathbb{R}_+$ *and* $J : \mathcal{AC}_n \to \mathbb{R}_+$ *that assigns a cyclic polygon it's area and the radius of it's circumcircle respectively.*

Definition 4.3.3. A cyclic polygon P is **centered** if the center of it's circumcircle is contained in the interior of P. We denote the set of centered polygons with n sides by $\mathcal{C}_n \subset \mathcal{AC}_n$. P is **semicyclic** if the center of the circumcircle lie on an edge of P. Set of semicyclic polygons with n sides is denoted by $\mathcal{BC}_n \subset \mathcal{AC}_n$

Proposition 4.3.4. *(Proposition 3.7 ,[7]) There exist a smooth function*
$b_0 : \mathbb{R}_+^{n-1} \to \mathbb{R}_+$ *such that* $(b_0(\bar{q}), \bar{q}) \in \mathcal{BC}_n$ *for any* $\bar{q} \in \mathbb{R}_+^{n-1}$.

If P is the semicyclic polygon determined by $(b_0(\bar{q}), \bar{q})$ then $b_0(\bar{q})$ is it's largest edge and $J(P) = b_0(\bar{q})/2$. Furthermore if $p_i \leq q_i$ for all i then $b_0(p_1, \ldots p_{n-1}) \leq b_0(q_1, \ldots q_{n-1})$

Below we record circumcircle radii and area formulas for hyperbolic triangles and quadrilaterals. Formulas for circumcircle radii follows from general results in hyperbolic trigonometry. Area formulas were proved in [17] and [17] for triangles and quadrilaterals respectively.

Proposition 4.3.5. *Consider a hyperbolic triangle with sides a, b and c. Let $A = sinh(a/2), B = sinh(b/2)$ and $C = sinh(c/2)$. Then the circumcircle radius $J(a, b, c)$ of this triangle is given by*

$$sinh(J(a, b, c)) = \frac{2ABC}{\sqrt{(A+B+C)(A+B-C)(A-B+C)(-A+B+C)}}$$

and the area $D_0(a, b, c)$ of this triangle is given by

$$\cos\left(\frac{D_0(a, b, c)}{2}\right) = \frac{A^2 + B^2 + C^2 + 2}{2\cosh(a/2)\cosh(b/2)\cosh(c/2)}$$

Proposition 4.3.6. *Consider a hyperbolic quadrilateral with sides a, b, c and d. Let $A = \sinh(a/2)$ and so on. Then the circumcircle radius $J(a, b, c, d)$ of this quadrilateral is given by*

$$\sinh(J(a, b, c, d)) = 2\sqrt{\frac{(AB + CD)(AC + BD)(AD + BC)}{(A + B + C - D)(A + B - C + D)(A - B + C + D)(-A + B + C + D)}}$$

and the area $D_0(a, b, c, d)$ of this quadrilateral is given by

$$\cos\left(\frac{D_0(a, b, c, d)}{2}\right) = \frac{A^2 + B^2 + C^2 + D^2 - 2ABCD + 2}{2\cosh(a/2)\cosh(b/2)\cosh(c/2)\cosh(d/2)}$$

Behaviours of the functions J and D_0 defined above vary on $\mathcal{C}_n$ and it's complement in $\mathcal{AC}_n$. Next two propositions were proved in [16] and will play a very important role later in this chapter.

Proposition 4.3.7. *(Proposition 1.20, [16]) For $\bar{q} = (q_o, \ldots, q_{n-1}) \in \mathcal{AC}_n$*

$$\begin{cases} 0 < \frac{\partial J}{\partial q_i}(\bar{q}) < \frac{1}{2} & \text{if } \bar{q} \in \mathcal{C}_n \text{ and } i \in \{0, 1, \ldots, n-1\} \\ \frac{\partial J}{\partial q_i}(\bar{q}) > \frac{1}{2} & \text{if } \bar{q} \in \mathcal{AC}_n - (\mathcal{C}_n \cup \mathcal{BC}_n) \text{ and } q_i = max\{q_0, \ldots, q_{n-1}\} \\ \frac{\partial J}{\partial q_i}(\bar{q}) < 0 & \text{if } \bar{q} \in \mathcal{AC}_n - (\mathcal{C}_n \cup \mathcal{BC}_n) \text{ and } q_i \neq max\{q_0, \ldots, q_{n-1}\} \end{cases}$$

Furthermore if $q_i < q_j$ then $\left|\frac{\partial J}{\partial q_i}(\bar{q})\right| < \left|\frac{\partial J}{\partial q_j}(\bar{q})\right|$

Proposition 4.3.8. *(Proposition 2.3 ,[16]) For $\bar{q} = (q_o, \ldots, q_{n-1}) \in \mathcal{AC}_n$*

$$\frac{\partial D_0}{\partial q_i}(\bar{q}) = \begin{cases} -\sqrt{\frac{1}{cosh^2(q_i/2)} - \frac{1}{cosh^2(J(\bar{q})}} & \text{if } \bar{q} \in \mathcal{AC}_n - (\mathcal{C}_n \cup \mathcal{BC}_n) \text{ and } q_i = max\{q_0, \ldots, q_{n-1}\} \\ \\ \sqrt{\frac{1}{cosh^2(q_i/2)} - \frac{1}{cosh^2(J(\bar{q})}} & \text{otherwise} \end{cases}$$

Corollary 4.3.9. *If $\bar{p} = (p_o, \ldots, p_{n-1}), \bar{q} = (q_o, \ldots, q_{n-1}) \in \mathcal{C}_n$ and $p_i < q_i$ after a cyclic permutation then $D_0(\bar{p}) < D_0(\bar{q})$ and $J(\bar{p}) < J(\bar{q})$*

4.4 Centered Dual Decomposition of ∂N with respect to the feet of shortest return path

For manifolds in $\mathcal{N}_{c,c}$ we already have a lower bound for d_{01} in terms of x_1 given in (3). Now our goal is to obtain an upper bound for d_{01} in terms of x_1. Recall that manifolds N we consider in this chapter has x_1 values in the interval $[1.183, 1.2158]$ and for such N, d_{11} can be given explicitly in terms of x_1 by (6). Hence we will first obtain the upper bound of d_{01} we seek in terms of d_{11} and then use (6) to rewrite them in terms of x_1.

First fix a d_{11} value. For a manifold N with this d_{11} value, we define $\mathcal{Q}_{d_{11}}$ to be the space of all the possible centered dual decompositions of ∂N with respect to the feet of its shortest return path. For any such decomposition $\mathcal{F}$ in $\mathcal{Q}_{d_{11}}$, edge lengths are bounded below by d_{11}. Areas of $2-$cells of $\mathcal{F}$ should also add up to 4π ; the area of a genus 2 surface.

The types of polygons that can appear as $2-$cells of a decomposition $\mathcal{F}$ in $\mathcal{Q}_{d_{11}}$ depend on the value of d_{11}. In section 4.5 we classify the ranges of d_{11} values according to the polygons that can appear as $2-$cells of the decompositions in $\mathcal{Q}_{d_{11}}$.

Definition 4.4.1. For a fixed d_{11} value and a decomposition $\mathcal{F} \in \mathcal{Q}_{d_{11}}$ define

$$J_{\mathcal{F}} = max\{\, J(\Delta_i) \mid \Delta_i \text{ is a 2-cell of } \mathcal{F}\,\}$$

and then $J_{d_{11}}$ is defined to be

$$J_{d_{11}} = max\{\, J_{\mathcal{F}} \mid \mathcal{F} \in \mathcal{Q}_{d_{11}}\,\}$$

.

In sections 4.6, 4.7 and 4.8 we investigate $J_{d_{11}}$ for the ranges of d_{11} values classified in section 4.3. We either compute $J_{d_{11}}$ explicitly as a function of d_{11} or derived functions of d_{11} that bound $J_{d_{11}}$ by above when explicit computations are tedious to carry out.

Note that for a manifold N with a given d_{11} value, $J_{d_{11}}$ defined above is the maximum distance between any point in ∂N and the feet of shortest return path on ∂N. In particular, it bounds d_{01} by above. Hence the explicit functions or upper bounds we compute in sections 4.6, 4.7 and 4.8 bound d_{01} by above.

4.5 d_{11} value of a manifold and 2-cells of the centered dual decomposition of its boundary

Area bounds for $2-$cells in a centered dual decomposition were proved in [7] and [15]. In this section, we use these bounds to classify ranges of d_{11} values based on the polygons appearing as $2-$cells in the decompositions in $\mathcal{Q}_{d_{11}}$.

Lemma 4.5.1. *If all 2-cells in the centered dual decomposition are triangles then $d_{11} \leq d_\alpha \approx arccosh(6.464)$ where d_α satisfy*

$$8D_0(d_\alpha, d_\alpha, d_\alpha) = 4\pi$$

Proof. If all $2-$cells are triangles then an Euler characteristic computation show there are 8 faces , say Δ_i for $i = 0, \ldots 7$. All these 2-cells are centered and lengths of all the edges in the decomposition are bounded below by d_{11}. If $d_{11} > d_\alpha$ then by corollary 4.3.9 we have

$$4\pi = \sum_{i=0}^{7} \Delta_i \geq 8D_0(d_{11}, d_{11}, d_{11}) > 8D_0(d_\alpha, d_\alpha, d_\alpha) = 4\pi$$

which is a contradiction. Hence $d_{11} \leq d_\alpha$.

$\square$

Lemma 4.5.2. *If one of the 2−cells in the centered dual decomposition is a rectangle then $d_{11} \leq d_\beta \approx arccosh(6.299)$ where d_β satisfy*

$$6D_0(d_\beta, d_\beta, d_\beta) + 2A_m(d_\beta) = 4\pi$$

Here $A_m(d_\beta)$ is the area of a semi cyclic triangle with two sides of d_β.

Proof. Let Δ_0 be the rectangular 2−cell. As proved in [7] , area of such a 2−cell is bounded below by $2A_m(d_{11})$. There are 6 other 2−cells in the decomposition, all of which are centered triangles.(say Δ_i for $i = 1, \ldots 6$). If $d_{11} > d_\beta$ then using corollary 4.3.9 we have

$$4\pi = \sum_{i=0}^{6} \Delta_i \geq 2A_m(d_{11}) + 6D_0(d_{11}, d_{11}, d_{11}) > 2A_m(d_\beta) + 6D_0(d_\beta, d_\beta, d_\beta) = 4\pi$$

which is a contradiction. Hence $d_{11} \leq d_\beta$ in this case. $\qquad \square$

In general , area of a centered dual 2− cell with n sides is bounded below by $(n-2)A_m(d_{11})$[7]. But improved area bounds for $n > 4$ were proved in [15]. Using these improved bounds and arguments similar to the ones used in previous two lemmas, we can find upper bounds for d_{11} when pentagons and hexagons appear in the centered dual decomposition. We record these bounds below.

Lemma 4.5.3. *If one of the 2−cells in the centered dual decomposition is a pentagon then $d_{11} \leq d_\theta \approx arccosh(6.059)$. If one of the 2−cells in the centered dual decomposition is a hexagon then $d_{11} \leq d_\delta \approx arccosh(5.801)$.*

These three lemmas determine the possibilities for 2−cells in centered dual decomposition for a fixed d_{11} value in a certain intervals. We summarise them below.

Corollary 4.5.4. *Suppose $cosh(d_{11}) \in [5.801, 6, 464]$*

- *If $d_{11} \in [d_\beta, d_\alpha]$ ($\Leftrightarrow cosh(d_{11}) \in [6.299, 6.464] \Leftrightarrow x_1 \in [1.183, 1.189]$) then CDD can have only triangles*
- *If $d_{11} \in [d_\theta, d_\beta]$ ($\Leftrightarrow cosh(d_{11}) \in [6.059, 6.299] \Leftrightarrow x_1 \in [1.189, 1.197]$) then CDD can only have triangles or rectangles.*

- If $d_{11} \in [d_\delta, d_\theta]$ ($\Leftrightarrow cosh(d_{11}) \in [5.801, 6.059] \Leftrightarrow x_1 \in [1.197, 1.208]$) *then CDD can have only triangles ,rectangles or pentagons.*

4.6 When $d_{11} \in [d_\beta, d_\alpha]$

Consider a fixed d_{11} in this interval. By corollary 4.5.4 , a centered dual decomposition of ∂N with respect to feet of shortest return parth of a manifold N with this d_{11} can only have triangles. This means all these triangles are centered and these are also the $2-$ cells in the geometric dual ; i.e CDD coincides with the geometric dual.

First we want to parameterize $\mathcal{Q}_{d_{11}}$, the space of all the possible centered dual decompositions for this fixed d_{11}.

As mentioned in lemma 4.5.1, such a decomposition have 8 centered triangles. Following the notation used there, we denote them by Δ_j for $j = 0, \ldots, 7$.

Denote edges of Δ_j by $\gamma_{3j}, \gamma_{3j+1}, \gamma_{3j+2}$ and their lengths by $q_{3j}, q_{3j+1}, q_{3j+2}$.
Each γ_i is glued exactly to another edge which we denote by $\gamma_{\iota(i)}$. Hence $q_i = q_{\iota(i)}$.

Hence we parameterize $\mathcal{Q}_{d_{11}}$ as all the tuples $(q_0, q_1, \ldots q_{23})$ in $\mathbb{R}_+^{24}$ that satisfy following conditions.

- $d_{11} \leq min\{\, q_i \mid 0 \leq i \leq 23 \,\}$
- $4\pi = \sum_{j=0}^{7} D_0(q_{3j}, q_{3j+1}, q_{3j+2})$
- $\Delta_j = (q_{3j}, q_{3j+1}, q_{3j+2}) \in \mathcal{C}_n$ for each $j \in \{0, \ldots, 7\}$
- $\exists$ an involution $\iota \in S_{24}$ such that $q_i = q_{\iota(i)}$ for $0 \leq i \leq 23$

Recall that for a decomposition $\mathcal{F} \in \mathcal{Q}_{d_{11}}$ we have $J_{\mathcal{F}} = max\{\, J(\Delta_i) \mid 0 \le i \le 7\,\}$ and $J_{d_{11}} = max\{\, \mathcal{F} \mid \mathcal{F} \in \mathcal{Q}_{d_{11}},\,\}$. Now we want to identify the decomposition $\mathcal{F} \in Q_{d_{11}}$ such that $J_{\mathcal{F}} = J_{d_{11}}$.

Lemma 4.6.1. *For any $d_{11} \in [d_\beta, d_\alpha]$ there is a unique $s(d_{11}) \in [d_{11}, b_0(d_{11})]$ such that*

$$6D_0(d_{11}, d_{11}, d_{11}) + 2D_0(s(d_{11}), d_{11}, d_{11}) = 4\pi$$

Proof. By definition , we can take $s(d_\alpha) = d_\alpha$ and $s(d_\beta) = b_0(d_\beta)$. Now suppose $d_{11} \in (d_\beta, d_\alpha)$. Define $f(x) = 6D_0(d_{11}, d_{11}, d_{11}) + 2D_0(x), d_{11}, d_{11})$. We need to prove f attains 4π in the interval $(d_{11}, b_0(d_{11}))$.

By corollary 4.3.9 we have the following.

$f(d_{11}) = 8D_0(d_{11}, d_{11}, d_{11}) < 8D_0(d_\alpha, d_\alpha, d_\alpha) = 4\pi$ and
$f(b_0(d_{11})) = 6D_0(d_{11}, d_{11}, d_{11}) + 2A_m(d_{11}) > 6D_0(d_\beta, d_\beta, d_\beta) + 2A_m(d_\beta) = 4\pi$.

It follows from the same corollary, $f(x)$ is an increasing function when $x \in [d_{11}, b_0(d_{11})]$. Hence the result follows. $\square$

Note that the lemma above provides an element $\mathcal{F}_0 \in \mathcal{Q}_{d_{11}}$ which can be represented by a tuple in $\mathbb{R}^{24}$ with exactly two entries of $s(d_{11})$ and all the remaining entries of d_{11}. i.e $\mathcal{F}_0 = \big(s(d_{11}), d_{11}, d_{11}, s(d_{11}), d_{11}, d_{11}, \ldots, d_{11}\big)$ (see figure 15)

Lemma 4.6.2. *Suppose $\mathcal{F} \in \mathcal{Q}_{d_{11}}$ Length of any edge in $\mathcal{F}$ can not exceed $s(d_{11})$.*
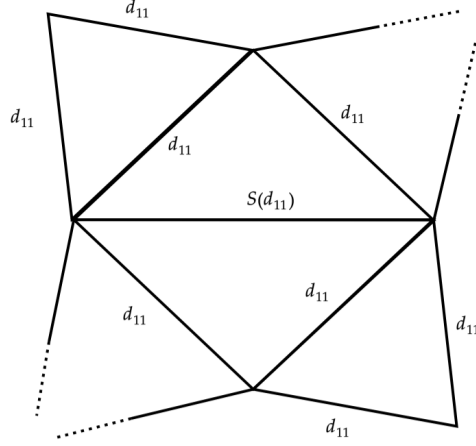
Figure 15: Two-cells of $\mathcal{F}_0$

Proof. W.l.o.g suppose an edge in Δ_0 has length greater than $s(d_{11})$ and it is glued to an edge in Δ_1. Lengths of all edges in the decomposition are bounded below by d_{11}.

Hence $D_0(\Delta_0), D_0(\Delta_1) > D_0(s(d_{11}), d_{11}, d_{11})$ and $D_0(\Delta_i) \geq D_0(d_{11}, d_{11}, d_{11})$ for $i = 2, \dots, 7$.

Then we have $4\pi = \sum_{i=0}^{7} D_0(\Delta_i) > 2D_0(s(d_{11}), d_{11}, d_{11}) + D_0(d_{11}, d_{11}, d_{11}) = 4\pi$ which is contradiction.

$\square$

Theorem 4.6.3. *(Lemma 8.14 ,[18])* $J_{d_{11}} = J_{\mathcal{F}_0} = J(s(d_{11}), d_{11}, d_{11})$ *where* $\mathcal{F}_0$ *is the decomposition given in lemma 4.6.1.*

Proof. We start with any $\mathcal{F} \in \mathcal{Q}_{d_{11}}$. Let $\{ \Delta_j \mid 0 \leq j \leq 7 \}$ be it's 2 -cells and edge lengths of Δ_j be $q_{3j}, q_{3j+1}, q_{3j+2}$. Then we have the following.

$$d_{11} \leq min\{ q_i \mid 0 \leq i \leq 23 \}$$

$$\sum_{j=0}^{7} D_0(\Delta_j) = 4\pi$$

Without loss of generality assume following.

- $J(\mathcal{F}) = J(\Delta_0) = max\{\, J(\Delta_i) \mid 0 \le i \le 7 \,\}$
- q_0 is the longest edge of Δ_0 and it's glued to an edge in Δ_1

By lemma 4.6.1 $q_0 \le s(d_{11})$. Suppose $q_0 < s(d_{11})$. Then there should be an edge q_i different from q_0 and $\iota(q_0)$ with length greater than d_{11}. If not all the edges except for a pair with length q_0 will have the length d_{11} leading to the contradiction

$$4\pi = \sum_{j=0}^{7} D_0(\Delta_j) < 6D_0(d_{11}, d_{11}, d_{11}) + 2D_0(s(d_{11}), d_{11}, d_{11}) = 4\pi$$

Let Δ_{j_0} and Δ_{j_1} be the triangles that has q_i and $\iota(q_i)$ as edges.

Now we deform $(q_0, \ldots, q_{23})$ as follows.

- Increase q_0 ; take $q_0(t) = q_0 + t$
- Do not change lengths of any other glued edge pair except for q_i
- Change q_i such that area sum of all 2-cells remains a constant $(= 4\pi)$

We claim this deformation increase $J(\Delta_0)$ while preserving the inclusion of $\mathcal{F}$ in $\mathcal{Q}_{d_{11}}$. For the simplicity , we denote this deformation by $\mathcal{T}$. We have to consider 3 cases.

Case 1:$\{\Delta_0, \Delta_1\} = \{\Delta_{j_0}, \Delta_{j_1}\}$

In this case both Δ_0 and Δ_1 has one edge each with with lengths q_0 and q_i. Let $\tilde{q}$ and $\tilde{\tilde{q}}$ be lengths of the remaining edge in Δ_0 and Δ_1 respectively.
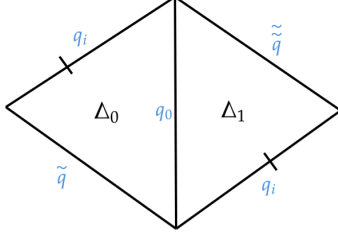
Figure 16: Edge gluings for case 1

The deformation $\mathcal{T}$ increase q_0 while keeping

$$D_0(\Delta_0) + D_0(\Delta_1) = D_0(q_0(t), q_i(t), \tilde{q}) + D_0(q_0(t), q_i(t), \tilde{\tilde{q}})$$

a constant.

By differentiating this with respect to t we obtain

$$\frac{\partial(D_0(\Delta_0))}{\partial q_0} + \frac{\partial(D_0(\Delta_0))}{\partial q_i}\frac{dq_i(t)}{dt} + \frac{\partial(D_0(\Delta_1))}{\partial q_0} + \frac{\partial(D_0(\Delta_1))}{\partial q_i}\frac{dq_i(t)}{dt} = 0$$

All the partial derivatives above can be computed using proposition 4.3. Hence we have

$$\frac{dq_i(t)}{dt} = -\frac{\left(\sqrt{\frac{1}{cosh^2(q_0(t)/2)} - \frac{1}{cosh^2(J(\Delta_0))}} + \sqrt{\frac{1}{cosh^2(q_0(t)/2)} - \frac{1}{cosh^2(J(\Delta_1))}}\right)}{\sqrt{\frac{1}{cosh^2(q_i(t)/2)} - \frac{1}{cosh^2(J(\Delta_0))}} + \sqrt{\frac{1}{cosh^2(q_i(t)/2)} - \frac{1}{cosh^2(J(\Delta_1))}}}$$

As $q_0 > q_i$ by assumption at least for $t > 0$, we observe the absolute value of the left hand side of above equation is less than 1. Hence $-1 < \frac{dq_i}{dt} < 0$.

On the other hand we have $\frac{dJ(\Delta_0)}{dt} = \frac{\partial J(\Delta_0)}{\partial q_0} + \frac{\partial J(\Delta_0)}{\partial q_i}\frac{dq_i}{dt}$.

By proposition 4.3.7 $\frac{\partial J(\Delta_0)}{\partial q_0} > \frac{\partial J(\Delta_0)}{\partial q_i}$. This together with the fact $-1 < dq_i/dt < 0$ implies $\frac{dJ(\Delta_0)}{dt} >$ is positive , hence the deformation $\mathcal{T}$ increase $J(\Delta_0)$.

Case 2: $\Delta_{j_0}, \Delta_{j_1} \neq \Delta_0$

In this case , only edge in Δ_0 that changes under $\mathcal{T}$ is q_0. Hence this case is trivial as $\frac{dJ(\Delta_0)}{dt} = \frac{dJ(\Delta_0)}{dq_0}$ is positive from proposition 4.3.7 .

Case 3: $\Delta_0 = \Delta_{j_0}$ and $\Delta_1 \neq \Delta_{j_1}$

In this case Δ_0 and Δ_1 share an edge each with lengths q_0 and Δ_0 and Δ_{j_1} share an edge each with length q_i. We can assume all other edges of Δ_1 and Δ_{j_1} has lengths equal to d_{11}.(If not we can apply case 1 or 2 and decrease them to d_{11}). So $2-$cells we are interested in are as follows.

- $\Delta_0 = (q_0(t), q_i(t), \tilde{q})$
- $\Delta_1 = (q_0(t), d_{11}, d_{11})$
- $\Delta_{j_1} = (q_i(t), d_{11}, d_{11})$
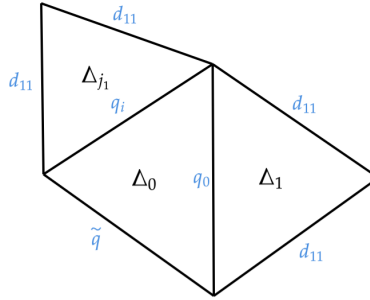
Figure 17: Edge gluings for case 3

Deformation $\mathcal{T}$ keep $D_0(\Delta_0) + D_0(\Delta_{j_1}) + D_0(\Delta_1)$ a constant. By differentiating this with respect to t we obtain

$$\frac{dq_i(t)}{dt} = -\frac{\left(\sqrt{\frac{1}{\cosh^2(q_0(t)/2)} - \frac{1}{\cosh^2(J(\Delta_0))}} - \sqrt{\frac{1}{\cosh^2(q_0(t)/2)} - \frac{1}{\cosh^2(J(\Delta_{j_1}))}}\right)}{\sqrt{\frac{1}{\cosh^2(q_i(t)/2)} - \frac{1}{\cosh^2(J(\Delta_0))}} + \sqrt{\frac{1}{\cosh^2(q_i(t)/2)} - \frac{1}{\cosh^2(J(\Delta_1))}}}$$

50

First term in the numerator is less than the first term in the denominator.

To show it's the same for second terms in the numerator and the denominator, we define a function $f(x) = \frac{1}{cosh^2(x)} - \frac{1}{J(x,d_{11}.d_{11})}$. From 8.14.1 in [18] $f(x)$ is a decreasing function of x. Hence the second term in the numerator $= \sqrt{f(q_0(t))}$ is less than the second term in the denominator $= \sqrt{f(q_i(t))}$. Hence similar to case 1, we have $-1 < \frac{dq_i}{dt} < 0$ and it follows $dJ(\Delta_0)/dt$ is positive.

In all 3 cases , we proved the deformation of $(q_0, \dots q_{23})$ described above increase $J(\Delta_0)$. These 3 cases exhaust all the possible edge gluings of q_0 and q_i. Hence we can continue the deformation $\mathcal{T}$ and increase $J_\mathcal{F}$ till the length of every edge pair except for q_o is equal to d_{11} at which instance $J_\mathcal{F}$ is a maximum. But by lemma 4.6.1 q_0 will be equal to $s(d_{11})$ when all remaining pairs of edges have the length d_{11}. Hence we can identify the decomposition that has the maximum $J_\mathcal{F}$ among all the decompositions in $\mathcal{Q}_{d_{11}}$ be $\mathcal{F}_0$.

$\square$

Theorem 4.6.4. *No manifold in $\mathcal{N}_{c,c}$ has a $d_{11} \in [d_\beta, d_\alpha]$*

Proof. In Theorem above we showed $J_{d_{11}} = J_{\mathcal{F}_0} = J(s(d_{11}), d_{11}, d_{11})$. Using 4.3.5 *sinh* value of this circumcircle radius can be computed to

$$sinh(J_{\mathcal{F}_0}) = \frac{2sinh^2(\frac{d_{11}}{2})}{\sqrt{4sinh^2(d_{11}/2 - sinh^2(s(d_{11})/2}}$$

We know $s(d_{11}) \leq b_0(d_{11}, d_{11})$ because all the triangles are centered.

Also $sinh(\frac{b_0(d_{11}, d_{11})}{2}) = \sqrt{2}sinh(d_{11}/2)$ [16]

51

Hence we have the following upper bound for $sinh(J_{\mathcal{F}_0})$.

$$sinh(J_{\mathcal{F}_0}) \leq \frac{2sinh^2(\frac{d_{11}}{2})}{\sqrt{2sinh^2(\frac{d_{11}}{2})}} = \sqrt{2}sinh\left(\frac{d_{11}}{2}\right)$$

Denote this upper bound of $sinh(J_{\mathcal{F}_0})$ by $sinh(J_{\mathcal{F}_0})^{ub}$. We compare its plot with that of $sinh(d_{01})_{min}$ given in 7.(see figure 18). We observe $(J_{\mathcal{F}_0})^{ub} < (d_{01})_{min}$ when $d_{11} \in [d_\beta, d_\alpha]$ which is a contradiction. Hence the theorem is proved.
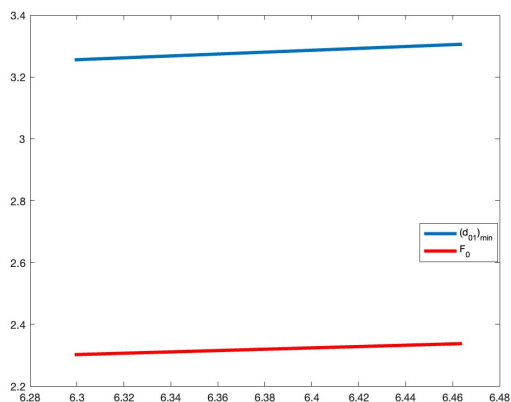
Figure 18: Comparing upper and lower bounds of $(d_{01})_{min}$ when $d_{11} \in [d_\beta, d_\alpha]$

$\square$

4.7 When $d_{11} \in [d_\theta, d_\beta]$

Consider a fixed d_{11} in this interval. By corollary 4.5.4, centered dual decomposition of ∂N of a manifold with this d_{11} can have triangles or quadrilaterals as $2-$cells.

We will first introduce two possible decompositions $\mathcal{F}_1$ and $\mathcal{F}_2$ in $\mathcal{Q}_{d_{11}}$. We will then either explicitly compute or estimate $J_{\mathcal{F}_1}$ and $J_{\mathcal{F}_1}$ and compare it with $(d_{01})_{min}$. We will see both $J_{\mathcal{F}_1}$ and $J_{\mathcal{F}_2}$ are less than $(d_{01})_{min}$ in this range of d_{11} values. Finally we will show any centered dual decomposition for $\mathcal{F} \in \mathcal{Q}_{d_{11}}$, $J_{\mathcal{F}}$ is less than one of $J_{\mathcal{F}_1}$ of $J_{\mathcal{F}_2}$, leading to a contradiction. This means we will be able to conclude that no manifold in $\mathcal{N}_{c,c}$ has a d_{11} value in this range.

Below we describe $\mathcal{F}_1$ and $\mathcal{F}_2$ them below and compute or estimate $J_{\mathcal{F}_i}$ for each case.

Decmposition 1 ; $\mathcal{F}_1$

There are 7 two-cells in $\mathcal{F}_1$; 1 rectangle and 6 triangles.

- $\Delta_0 = (u(d_{11}), d_{11}, u(d_{11}), d_{11}) \in \mathcal{C}_4$. Two sides of length $u(d_{11})$ are glued to each other.

- $\Delta_i = (d_{11}, d_{11}, d_{11}) \in \mathcal{C}_3$ for $i = 1, 2, , \ldots, 6$

Then we have

$$J_{\mathcal{F}_1} = J(\Delta_0) = J(u(d_{11}), d_{11}, u(d_{11}), d_{11})$$

and it satisfies $sinh(J(\Delta_0)) = \sqrt{sinh^2(\frac{u(d_{11})}{2}) + sinh^2(\frac{d_{11}}{2})}$ by prop 4.3.5

Now consider the area sum equation

$$4\pi = D_0(u(d_{11}), d_{11}, u(d_{11}), d_{11}) + 6D_0(d_{11}, d_{11}, d_{11})$$

Each term in the right hand side can be computed using proposition 4.3.6. By solving this equation for $u(d_{11})$ in terms of d_{11} we obtain the following

$$sinh^2\left(\frac{u(d_{11})}{2}\right) = \frac{cosh^2\left(d_{11}/2\right)(g(d_{11}) - 1)}{2 - cosh^2\left(d_{11}/2\right)(g(d_{11}) + 1)}$$

where $(g(d_{11}) - 1) = cos\left(6cos^{-1}\left(\frac{3sinh^2(d_{11}/2)+2}{2cosh^3(d_{11}/2)}\right)\right)$

Then plug in this solution to the previous equation of $sinh(J(\Delta_0))$ and obtain $sinh(J(\Delta_0))$ as a function of d_{11} explicitly.

Decomposition 2 ; $\mathcal{F}_2$

Again there are 7 two-cells in $\mathcal{F}_2$; 1 rectangle and 6 triangles.

- $\Delta_0 = (v(d_{11}), d_{11}, d_{11}, d_{11}) \in \mathcal{C}_4$

- $\Delta_1 = (v(d_{11}), d_{11}, d_{11}) \in \mathcal{C}_3$

- $\Delta_i = (d_{11}, d_{11}, d_{11}) \in \mathcal{C}_3$ for $i = 2, , \ldots, 6$

Then we have

$$J_{\mathcal{F}_2} = J(\Delta_0) = J(v(d_{11}), d_{11}, d_{11}, d_{11})$$

and it satisfies $sinh(J(\Delta_0)) = 2\sqrt{\frac{sinh^3(d_{11}/2)}{3sinh(d_{11}/2)-sinh(v(d_{11}))}}$ by proposition 4.3.5

Obtaining $v(d_{11})$ as a function of d_{11} explicitly require the tedious task of solving the area sum equation

$$4\pi = D_0(v(d_{11}), d_{11}, d_{11}, d_{11}) + D_0(v(d_{11}), d_{11}, d_{11}) + 5D_0((d_{11}, d_{11}, d_{11})$$

for $v(d_{11})$. Instead we differentiate the area sum with respect to d_{11}.

$$\frac{\partial D_0(\Delta_0)}{\partial v(d_{11})}v'(d_{11}) + 3\frac{\partial D_0(\Delta_0)}{\partial d_{11}} + \frac{\partial D_0(\Delta_1)}{\partial v(d_{11})}v'(d_{11}) + 2\frac{\partial D_0(\Delta_1)}{\partial d_{11}} + 15\frac{\partial D_0(d_{11}, d_{11}, d_{11})}{\partial d_{11}} = 0$$

All the partial derivatives in the above equation are positive by prop 4.3. Hence $v'(d_{11})$ is negative. Hence $v(d_{11}) \leq v(d_\theta)$ for any $d_{11} \in [d_\theta, d_\beta]$.

Therefore we have $sinh(J_{\mathcal{F}_2}) = sinh(J(\Delta_0)) \leq 2\sqrt{\frac{sinh^3(d_{11}/2)}{3sinh(d_{11}/2)-sinh(v(d_\theta))}}$

Denote this upper bound of $sinh(J_{\mathcal{F}_2})$ by $sinh(J_{\mathcal{F}_2})^{ub}$. A comparison of plots of $sinh(J_{\mathcal{F}_1})$ and $sinh(J_{\mathcal{F}_2})^{ub}$ with $sinh((d_{01})_{min})$ as given in 7 is shown below (figure 19).
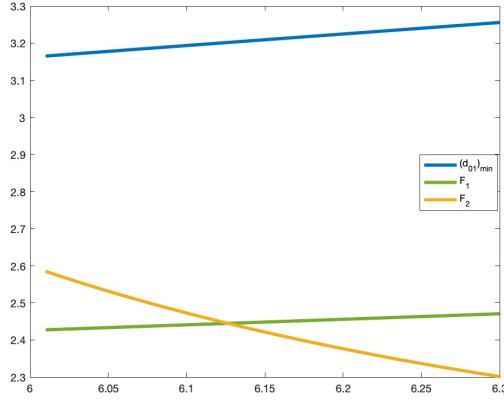
Figure 19: Comparing upper and lower bounds of $(d_{01})_{min}$ when $d_{11} \in [d_\theta, d_\beta]$

If we can show that for a d_{11} in this interval and for any decomposition $\mathcal{F} \in \mathcal{Q}_{d_{11}}$ that $J_{\mathcal{F}}$ is bounded above by one of $J_{\mathcal{F}_1}$ or $J_{\mathcal{F}}$ (or in other words $J_{d_{11}}$ is one of those two) then the above plot would raise a contradiction. The next subsection is devoted to this purpose.

4.7.1 $J_{d_{11}}$ is either $J_{\mathcal{F}_1}$ or $J_{\mathcal{F}}$

In this range of d_{11} values, its possible for the centered dual to have triangles or quadrilaterals as $2-$ cells. Main goal of this subsection is to show any $\mathcal{F}$ in $\mathcal{Q}_{d_{11}}$ can be deformed through a series of operations, all of which continue to increase $J_{\mathcal{F}}$, till $\mathcal{F}$ is deformed into one of $\mathcal{F}_1$ or $\mathcal{F}_2$.

While this is exactly the process we followed in the previous sections when centered dual only has triangles, in this section(and also in the next) there are significantly higher number of cases we have to go through. Hence below we describe the process and some of the notations we will be using to keep things concise.

Basic steps : We start with a $\mathcal{F}$ in $\mathcal{Q}_{d_{11}}$. We look at its 2-cell that has the largest circumcircle radius. We denote this 2-cell by Δ_0. Hence $J_{\mathcal{F}} = J(\Delta_0)$. Then we send $\mathcal{F}$ through an operation with the goal of increasing $J(\Delta_0)$.

A typical operation that can do this looks as below. We increase a length of an edge of Δ_0 (say l) and change the length of only one other selected edge (say q) in the centered dual such that sum of the areas of all the 2-cells remain constant at 4π. We simply denote this operation as follows.

Deformation : Increase l and change q

Note that we do not explicitly mention area sum remain constant but it is always the case and the notation above implicitly assumes it.

If we denote increment of l by $l(t) = l + t$ then we can compute $q'(t)$ by differentiating the area sum using proposition 4.3. When differentiating the area sum, we need to differentiate the function D_0 with respect to some edge lengths. Hence we will frequently see the

terms such as

$$\sqrt{\frac{1}{cosh^2(u/2)} - \frac{1}{cosh^2(J(\Delta))}}$$

where u is a length of an edge of a 2-cell Δ. **For the convenience, we will denote this kind of a term simply by** $f(u, \Delta)$.

By differentiating the area sum, we can write $q'(t)$ as a quotient which is a combination of several terms of the form $f(u, \Delta)$. We can not find the exact value of $q'(t)$ but we can determine an interval of values it can take by using properties of $f(u, \Delta)$. We list these properties in the lemma below.

Lemma 4.7.1. *Let* $f(u, \Delta)$ *be as above.*

- $f(u, \Delta) > f(u', \Delta)$ *for a 2-cell* Δ *with* u *and* u' *its edges if* $u < u'$
- $f(x, \Delta_1) > f(y, \Delta_2)$ *if* $\Delta_1 = (x, d, d) \in \mathcal{C}_3$, $\Delta_2 = (y, d, d) \in \mathcal{C}_3$ *and* $x < y$
- $f(y, \Delta_1) > f(x, \Delta_2)$ *if* $\Delta_1 = (x, d, d) \in \mathcal{AC}_3 - \mathcal{C}_3$, $\Delta_2 = (y, d, d) \in \mathcal{AC}_3 - \mathcal{C}_3$ *and* $x < y$

Proof. The first one is obvious. Second and third one are followed from claim 8.14.1 in [18] □

Then we show $J'(\Delta_0) > 0$ by using proposition 4.3.7 and $q'(t)$ if necessary.

It shows this operation increases $J(\Delta_0)$. Finally we mention till when we can continue this operation. Typically there are multiple cases that can force us to terminate this kind of an operation. q decreased to d_{11} is one of them.

Then for terminating case, we send the decomposition through another operation that further increase $J(\Delta)$. Whenever an operation is forced to terminate, we continue to analyse those terminating cases through a sequence of operations till we reach one of $\mathcal{F}_1$ or $\mathcal{F}_2$. Now we are ready to begin our analysis.

When $\mathcal{F}$ has a quadrilateral as a 2-cell

We'll start with a $2-$cell that is a quadrilateral which is formed by gluing a centered triangle Δ_0 to a non centered triangle Δ_1 and all other 2-cells in the centered dual are centered triangles. In this case non centered tree has a single edge and $J(\Delta_0) > J(\Delta_1)$.

Let l be the length of the side shared by Δ_0 and Δ_1. We have to consider two main cases.

- Case A : No other edge of Δ_0 is glued to and edge of Δ_1
- Case B : One more edge of Δ_0 is glued to an edge of Δ_1

Case A : We now address case A. First we check to see if there are edges that are not glued to either of Δ_0 and Δ_1 and has length greater than d_{11}. Suppose there is such an edge with length $q > d_{11}$. Then exists perform the following deformation. If no such edge exists, proceed to case A.2.

Deformation : Increase l and change only q

By differentiating the area sum with respect to t , by proposition 4.3 we obtain

$$q'(t) = -\left(\frac{f(l, \Delta_0) - f(l, \Delta_1)}{f(s, \Delta_i) + f(s, \Delta_j)}\right)$$

where Δ_i and Δ_j be the triangles that share edge q. We observe s' is negative as long as $f(l, \Delta_0) > f(l, \Delta_1)$ or equivalently $J(\Delta_0) > J(\Delta_1)$ and hence s is decreasing. On the other hand $J(\Delta_0)$ is increasing as Δ_0 is centered and the deformation increase length of one of its edges without changing other edges. To be precise we have

$$J'(\Delta_0) = \frac{\partial J(\Delta_0)}{\partial l} \in (0, 1/2) \quad \text{(by 4.3.7)}$$

We also have the following

$$J'(\Delta_1) = \frac{\partial J(\Delta_1)}{\partial l} > 1/2 \quad \text{(by 4.3.7)}$$

So both $J(\Delta_0)$ and $J(\Delta_1)$ are increasing but $J(\Delta_1)$ increases at a higher rate. We can continue this deformation till one of the following two things happen.

- Case A.1 : $J(\Delta_0) = J(\Delta_1)$
- Case A.2 : q is decreased to d_{11}

Case A.1 When $J(\Delta_0) = J(\Delta_1)$, two triangles Δ_0 and Δ_1 will together form a single centered rectangle. Let's denote this rectangle by Δ. None of the edges of Δ is glued to another edge of the rectangle.(follows from the assumption of case A.) Now let s be the length of the longest edge in Δ and Δ' be the other $2 - cell$ (which is a centered triangle) it's glued to.

Again take a side with length q that is not glued to any other edge of the Δ.

Deformation : Increase s and change q

We have

$$q'(t) = -\left(\frac{f(s, \Delta) + f(s, \Delta')}{f(s, \Delta_i) + f(s, \Delta_j)} \right)$$

We observe q is decreasing and similar to the previous case $J(\Delta)$ is increasing. Note that Δ' can not become non centered as that would form a pentagon in the centered dual which is not permissible in this interval of d_{11} values. Hence we can continue to increase $J(\Delta)$ till q is decreased to d_{11}.

Now we can assume all the edges that are not glued to Δ has lengths d_{11}. Now let u be the length of another edge of Δ and $\Delta'' = (u, d_{11}, d_{11})$ be the triangle its glued to.

Increase s and change u

By differentiating the area sum and using lemma 4.7.1 we obtain

$$u'(t) = -\left(\frac{f(s,\Delta) + f(s,\Delta')}{f(s,\Delta) + f(s,\Delta'')}\right) \in (-1,0)$$

Hence we have

$$J'(\Delta) = \frac{\partial J(\Delta)}{\partial s} + \frac{\partial J(\Delta)}{\partial u} u' > 0$$

This follows from the fact $\frac{\partial J(\Delta)}{\partial s} > \frac{\partial J(\Delta)}{\partial u}$ as $s > u$ by proposition 4.3.7. So we can continue this operation and increase $J(\Delta)$ till u is decreased to d_{11}. Hence $J(\Delta)$ is the maximum when every single edge of the centered dual decomposition except the longest edge of the rectangle (with length s) is equal to d_{11}. This is decomposition $\mathcal{F}_2$.

Case A.2 In this case we can assume all the edges that are not glued to Δ_0 or Δ_1 has length d_{11}. Now take q to be the length of an edge of Δ_1 other than l and $\Delta' = (q, d_{11}.d_{11})$ be the triangle its glued to.

Deformation : Increase l and change q

By differentiating the area sum we have

$$q'(t) = -\left(\frac{f(l,\Delta_0) - f(l,\Delta_1)}{f(q,\Delta_1) + f(s,\Delta')}\right)$$

and $J(\Delta_0)$ is increasing because its centered and the only transformation on it was the increment of one of its sides. We can continue this till one of the following two things happen

- Case A.2.1 :   q is decreased to d_{11}
- Case A.2.1 : $J(\Delta_0) = J(\Delta_1)$

60

Case A.2.1 Now we can assume all the edges in the centered dual except for the ones belong to Δ_0 has length d_{11}. Suppose the other two lengths of Δ_0 are s and u (wlog $s > u$). Let $\Delta' = (s, d_{11}, d_{11})$ and $\Delta'' = (u, d_{11}, d_{11})$ be the other triangles s and u glued to respectively.

Deformation : Increase s and change u

$$u'(t) = -\left(\frac{f(s, \Delta_0) + f(s, \Delta')}{f(s, \Delta_0) + f(s, \Delta'')}\right) \in (-1, 0)$$

Hence from proposition 4.3.7 we have

$$J'(\Delta_0) = \frac{\partial J(\Delta_0)}{\partial s} + \frac{\partial J(\Delta)}{\partial u}u' > 0$$

We continue this deformation till u is decreased to d_{11}. Once that happens , only two edges in the entire centered dual has a length greater than d_{11}. These are the edges in Δ_0 with lengths l (shared with Δ_1) and s. Finally we increase l and change s. Under this deformation we have

$$s'(t) = -\frac{f(s, \Delta_0) - f(s, \Delta_1)}{f(s, \Delta_0) + f(s, \Delta')} \in (-1, 0)$$

We can continue this deformation till either $J(\Delta_0) = J(\Delta_1)$ or till s is decreased to d_{11}.

If $J(\Delta_0) = J(\Delta_1)$ then the union of Δ_0 and Δ_1 forms a single centered quadrilateral. This is same as Case 1.1.

If s is decreased to d_{11} then $\Delta_0 = (l, d_{11}, d_{11})$ has same edge lengths as Δ_1. Since Δ_1 is non centered , Δ_1 should also be. But this is not possible as two non centered triangles glued together then form a $2-$ cell with five edges in the centered dual which is not possible in the range of d_{11} we consider. Hence we conclude s can not be decreased to d_{11}.

Case A.2.2 In this case we have a centered quadrilateral formed by the union of Δ_0 and Δ_1. This is again same as case A.1

Case B : Now we address Case B where another edge of Δ_0 is glued to Δ_1. Denote

the length of this edge by s. Just like in Case A first we want to reduce the lengths of edges that are not glued to either of Δ_0 or $\Delta)1$ to d_{11}. If q is the length of any such edge, we increase l and change only q. When we do that, similar to Case A, one of the two things will happen.

- Case B.1 : $J(\Delta_0) = J(\Delta_1)$
- Case B.2 : q is decreased to d_{11}

Case B.1 When $J(\Delta_0) = J(\Delta_1)$, union of Δ_0 and Δ_1 will form a single centered quadrilateral. Let's denote it by Δ. Two sides with length s in Δ are glued to each other.

We know there are still edges that are not glued to Δ with lengths greater than d_{11}. We want to continue decreasing them to d_{11}. Again we take q to be a length of such edge.

Deformation : Increase s and change q

Similar to Case A.1, this deformation increase $J(\Delta)$ and decrease q and we can continue it till q is d_{11}.

Now we can assume all the edges that are not glued to Δ has lengths d_{11}. Now let u be the length of another edge of Δ and $\Delta'' = (u, d_{11}, d_{11})$ be the centered triangle its glued to.

Deformation : Increase s and change u

By differentiating the area sum and using lemma 4.7.1 we get
$$u'(t) = -\frac{2f(s, \Delta)}{f(u, \Delta) + f(u, \Delta'')} \in (-2, 0)$$
Hence by proposition 4.3.7 we have
$$J'(\Delta) = 2\frac{\partial J(\Delta)}{\partial s} + \frac{\partial J(\Delta)}{\partial u}u' > 0$$

62

So we can continue this operation and increase $J(\Delta)$ till u is decreased to d_{11}. $J(\Delta)$ is a maximum when every single edge of the centered dual decomposition except the two edges in Δ (with length s) that are glued to each other has lengths d_{11}. This is the decomposition $\mathcal{F}_1$

Case B.2 Similar to $A.2$ we can assume all the edges that are not glued to Δ_0 or Δ_1 has lengths d_{11}. Now take q to be the length of the edge in Δ_1 that is not glued to Δ_0. Let $\Delta' = (q, d_{11}, d_{11})$ be the centered triangle its glued to.

Deformation : Increase l and change q

By differentiating the area sum and using lemma 4.7.1 we have

$$q'(t) = -\left(\frac{f(l, \Delta_0) - f(l, \Delta_1)}{f(q, \Delta_1) + f(q, \Delta')} \right)$$

So q is decreasing. This deformation will increase $J(\Delta_0)$ because it increases length of one edge without changing other edges of the centered triangle Δ_0. We can continue this transformation till one of the following two things happen.

- Case B.2.1 : q is decreased to d_{11}
- Case B.2.2 : $J(\Delta_0) = J(\Delta_1)$

Case B.2.1 : Now we can assume all the edges in the centered dual except for the ones in Δ_0 has edge lengths d_{11}. Suppose u be the length of the edge of Δ_0 that is not glued to Δ_1. Let $\Delta'' = (u, d_{11}, d_{11})$ be the other centered triangle its glued to.

Deformation : Increase l and change u

By differentiating the area sum and using lemma 4.7.1 we have

$$u'(t) = -\left(\frac{f(l, \Delta_0) - f(l, \Delta_1)}{f(u, \Delta_0) + f(q, \Delta'')} \right) \in (-1, 0)$$

63

Hence by proposition 4.3.7 we have

$$J'(\Delta) = \frac{\partial J(\Delta)}{\partial l} + \frac{\partial J(\Delta)}{\partial u} u' > 0$$

So we can continue the deformation till either $J(\Delta_0) = J(\Delta_1)$ or u is decreased to d_{11}. If $J(\Delta_0) = J(\Delta_1)$, then the union of Δ_0 and Δ_1 forms a centered quadrilateral. This belongs to Case B.1 and we will end up with decomposition $\mathcal{F}_1$ in this case.

If u is decreased to d_{11} then $\Delta_0 = (l, s, d_{11})$ has same edge lengths as the non centered triangle Δ_1. So it should also be non centered, making a pentagonal $2-$ cell in the centered dual which is not possible in this range of d_{11}. Hence we conclude u can not be decreased to d_{11}.

Case B.2.2 In this case the union of Δ_0 and Δ_1 forms a centered quadrilateral. Again this belongs to Case B.1 and we will end up with decomposition $\mathcal{F}_1$.

Above subcases of Case A and B exhaust all the possibilities when the centered dual has a quadrilateral formed by a centered triangle and a non centered triangle.

If the centered dual has a 2-cell that is a centered quadrilateral then it is same as Case A.1 If the centered dual has only centered triangles, then we can start in a way similar to the previous section but before the length of the largest edge reach $s(d_{11})$, one of the triangles will be non centered meaning we will be at the beginning of Case A OR Case B and continue from there.

Following two figures summarise the sequences of operations we followed in Case A and Case B.

Case A

Decrease all the edges except for the ones glued to Δ_0 and Δ_1 to d_{11}

Case A.1

$J(\Delta_0)$ becomes same as $J(\Delta_1)$ making their union a single centered quad Δ

Decrease all the edges except for the ones glued to Δ to d_{11}

Increase s (the largest edge length of Δ) and decrease all of its other edges

$\mathcal{F}_2$

Case A.2

All the edges except for the ones glued to Δ_0 and Δ_1 has length d_{11}

Increase l and decrease all other the edges of Δ_1 to d_{11}

Case A.2.1

All other edges Δ_1 has length d_{11}

Increase s and decrease u

Increase l and decrease s

$J(\Delta_0)$ becomes same as $J(\Delta_1)$ making their union a single centered quad Δ

Same as A.1

Case A.2.2

$J(\Delta_0)$ becomes same as $J(\Delta_1)$ making their union a single centered quad Δ

Same as A.1

Figure 20: Quadrilaterals : Case A

65
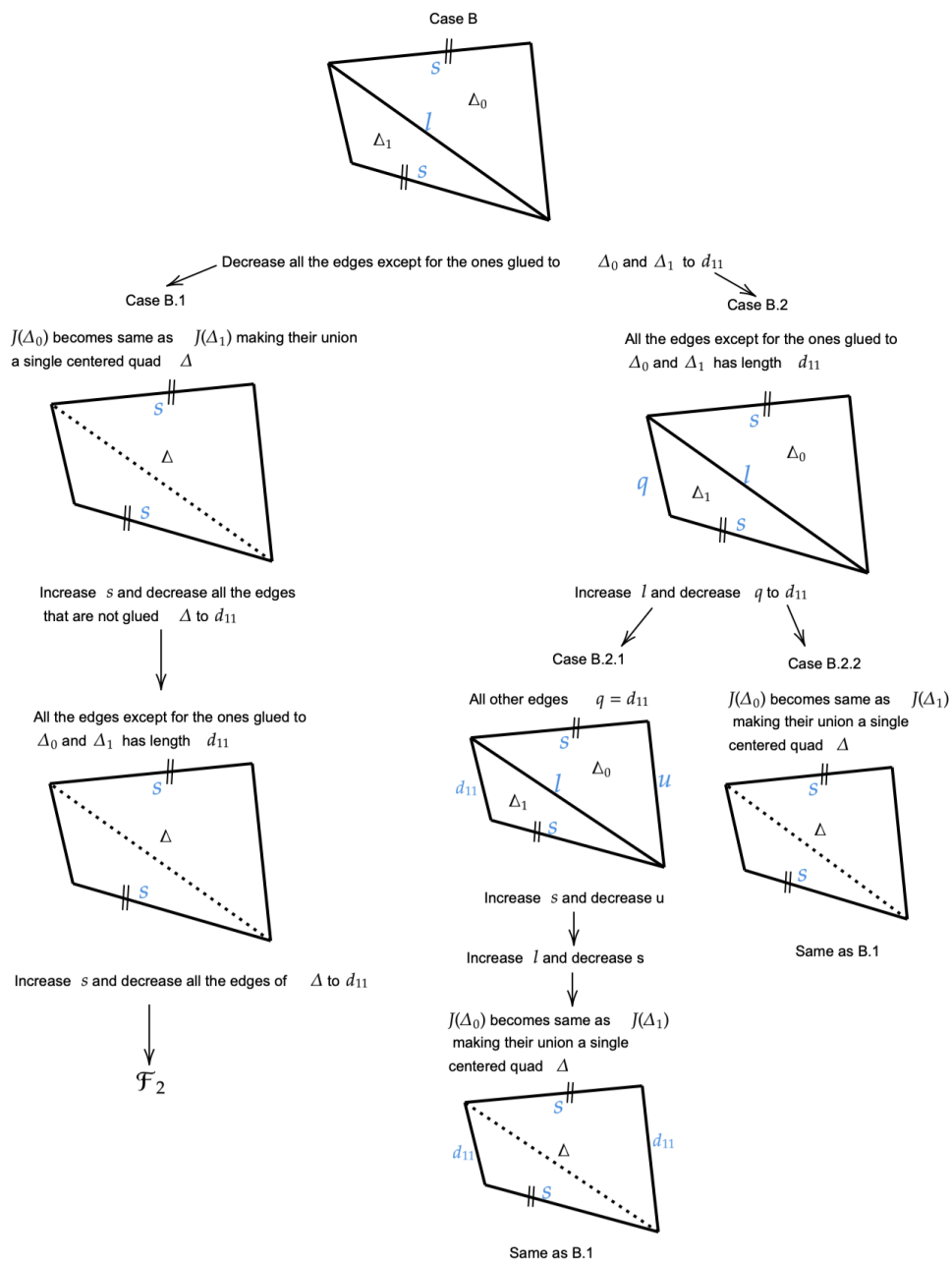
Figure 21: Quadrilaterals : Case B

66

4.8   When $d_{11} \in [d_\delta, d_\theta]$

Consider a fixed d_{11} in this interval. By corollary 4.5.4, centered dual decomposition of ∂N of a manifold with this d_{11} can have triangles, quadrilaterals or pentagons as $2-$cells.

Similar to the case with quadrilaterals, we will first introduce few possible decompositions in $\mathcal{Q}_{d_{11}}$. We will then describe find upper bounds for $J_\mathcal{F}$ for each of these decompositions in terms of d_{11} and compare it with $(d_{01})_{min}$. We will again see $J_\mathcal{F}$ of these decompositions are less than $(d_{01})_{min}$ in this range of d_{11} values too. Finally we will show any centered dual decomposition for $\mathcal{F}' \in \mathcal{Q}_{d_{11}}$, $J_{\mathcal{F}'}$ is less than one of $J_\mathcal{F}$s we discussed , leading to a contradiction. This means we will again be able to conclude that no manifold in $\mathcal{N}_{c,c}$ has a d_{11} value in this range.

Below we describe several decompositions that belong to $\mathcal{Q}_{d_{11}}$ when $d_{11} \in [d_\delta, d_\theta]$ and then bound their circumcircle radii by a function of d_{11}

Decomposition 1 ; $\mathcal{F}_1$

There are 6 two-cells in $\mathcal{F}_1$; 1 pentagon and 5 triangles.

- $\Delta_0 = (p(d_{11}), d_{11}, d_{11}, d_{11}, d_{11}) \in \mathcal{C}_5$.

- $\Delta_1 = (p(d_{11}), d_{11}, d_{11}) \in \mathcal{C}_3$ with edge length $p(d_{11})$ glued to the edge in the pentagon with same length.

- $\Delta_i = (d_{11}, d_{11}, d_{11}) \in \mathcal{C}_3$ for $i = 2, \ldots, 5$

Consider the area sum equation

$$4\pi = D_0(p(d_{11}), d_{11}, d_{11}, d_{11}, d_{11}) + D_0(p(d_{11}), d_{11}, d_{11}) + 4D_0((d_{11}, d_{11}, d_{11})$$

By differentiating this with respect to d_{11} we obtain.

$$\frac{\partial D_0(\Delta_0)}{\partial p(d_{11})}p'(d_{11}) + 4\frac{\partial D_0(\Delta_0)}{\partial d_{11}} + \frac{\partial D_0(\Delta_1)}{\partial p(d_{11})}p'(d_{11}) + 2\frac{\partial D_0(\Delta_1)}{\partial d_{11}} + 12\frac{\partial D_0(d_{11}, d_{11}, d_{11})}{\partial d_{11}} = 0$$

We can compute each of the partial derivatives above using proposition 4.3. We then solve the equation for $p'(d_{11})$.

$$p'(d_{11}) = -\left(\frac{4f(d_{11}, \Delta_0) + 2f(d_{11}, \Delta_1) + 12f(d_{11}, \Delta_2)}{4f(p(d_{11}), \Delta_0) + f(p(d_{11}), \Delta_1)}\right)$$
$$-4\left(\frac{f(d_{11}, \Delta_0) + \frac{1}{2}f(d_{11}, \Delta_1) + 3f(d_{11}, \Delta_2)}{4f(p(d_{11}), \Delta_0) + f(p(d_{11}), \Delta_1)}\right)$$

Using the properties of the quantity f from lemma 4.7.1, we have the following.

- $f(d_{11}, \Delta_0) > f(p(d_{11}), \Delta_0)$
- $f(d_{11}, \Delta_1) > f(p(d_{11}), \Delta_1)$
- $f(d_{11}, \Delta_2) > f(p(d_{11}), \Delta_2) > \frac{1}{6}f(p(d_{11}), \Delta_1)$

Then we have

$$f(d_{11}, \Delta_0) + \frac{1}{2}f(d_{11}, \Delta_1) + 3f(p(d_{11}), \Delta_2) > f(p(d_{11}), \Delta_0) + \frac{1}{2}f(p(d_{11}), \Delta_1) + \frac{1}{2}f(p(d_{11}), \Delta_1)$$
$$= f(p(d_{11}), \Delta_0) + f(p(d_{11}), \Delta_1)$$

This proves $p'(d_{11}) < -4$.

We also have $J'(\Delta_0) = \frac{\partial J(\Delta_0)}{\partial p}p' + 4\frac{\partial J(\Delta_0)}{\partial d_{11}}$.

From proposition 4.3.7 we know $\frac{\partial J(\Delta_0)}{\partial p} > \frac{\partial J(\Delta_0)}{\partial d_{11}}$. Since $p'(d_{11}) < -4$ we conclude $J'(\Delta_0) < 0$. Hence $J_{\mathcal{F}_1}$ is decreasing in d_{11}.

This means for any d_{11} value in the interval $[d_\delta, d_\theta]$, $\mathcal{F}_1 \in \mathcal{Q}_{d_{11}}$ has its $J_{\mathcal{F}_1}$ bounded above by the J value of $\mathcal{F}_1 \in \mathcal{Q}_{d_\delta}$. In other words we have

$$J_{\mathcal{F}_1} < J(p(d_\delta), d_\delta, d_\delta, d_\delta, d_\delta) \tag{8}$$

Computing $p(d_\delta)$

We first divide the centered pentagon into a square and a triangle as shown in figure 22. Both of those should have the same circumcircle radius. We compute them using 4.3.5 and set them equal.
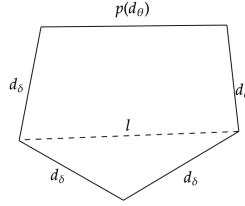
Figure 22: Computing the value of $p(d_\delta)$

$$\frac{D^2}{\sqrt{4D^2 - L^2}} = \frac{D^2(D^2 + PL)}{4D^2 - (L - P)^2}$$

where $D = sinh(d_\delta/2), L = sinh(l/2)$ and $P = sinh(p(d_\delta)/2)$. The above equation can be reduced to the cubic equation

$$L^3 - 2D^2 L - D^2 S = 0$$

We also have the area sum equation

$$D_0(p(d_\delta), d_\delta, d_\delta, d_\delta, d_\delta) + D_0(p(d_\delta), d_\delta, d_\delta) + 4D_0(d_\delta, d_\delta, d_\delta)$$

We can compute each term in the above equation in terms of $d_\delta, p(d_\delta)$ and l using proposition 4.3.5.

We first solve the cubic equation for L which allows us to write l in terms of $p(d_\delta)$. Then we plug that expression into the area sum equation. This makes $p(d_\delta)$ the only variable in the area sum equation. By solving it we obtain $p(d_\delta) \approx 2.8598$

Decomposition 2 ; $\mathcal{F}_2$

There are 6 two-cells in $\mathcal{F}_1$; 1 pentagon and 5 triangles.

- $\Delta_0 = (q(d_{11}), r(d_{11}), d_{11}, d_{11}, r(d_{11})) \in \mathcal{C}_5$. $q(d_{11})$ is the longest edge. Two edges with length $r(d_{11})$ are glued to each other

- $\Delta_1 = (q(d_{11}), d_{11}, d_{11}) \in \mathcal{C}_3$ with edge length $q(d_{11})$ glued to the edge in the pentagon with same length.

- $\Delta_i = (d_{11}, d_{11}, d_{11}) \in \mathcal{C}_3$ for $i = 2, \ldots, 5$

First we would like to understand how r varies with q. Again we consider the area sum equation

$$4\pi = D_0(q(d_{11}), r(d_{11}), d_{11}, d_{11}, r(d_{11})) + D_0(q(d_{11}), d_{11}, d_{11}) + 4D_0((d_{11}, d_{11}, d_{11})$$

We keep d_{11} fixed and differentiate the area sum equation with respect to q while considering r as a function of q.

$$2\frac{\partial D_0(\Delta_0)}{\partial r(q)}r'(q) + \frac{\partial D_0(\Delta_0)}{\partial q} + \frac{\partial D_0(\Delta_1)}{\partial q} = 0$$

All the partial derivatives above are positive because 2-cells are centered. (Prop 4.3). So r

decreases if we increase q. Hence q can attain a maximum when r is at its minimum which is d_{11}. But when $r = d_{11}$, we have exactly the decomposition $\mathcal{F}_1$ described above. Hence the maximum value q can take is equal to $p(d_{11})$. So both q and r are less than $p(d_{11})$.

Now compare Δ_0 with a centered pentagon Δ given by

$$\Delta = \left(p(d_{11}), p(d_{11}), d_{11}, d_{11}, p(d_{11}) \right)$$

.

Since $q, r < p(d_{11})$ we have the following from corollary 4.3.9.

$$J(\Delta_0) < J(\Delta)$$

So $J_{\mathcal{F}_2} = J(\Delta_0)$ is bounded above by $J(\Delta)$. But its not easy to compute $J(\Delta)$ explicitly. Hence we will find an upper bound for it as shown below. We differentiate the circumcircle radius of $\Delta = (p(d_{11}), p(d_{11}), d_{11}, d_{11}, p(d_{11}))$ with respect to d_{11} now. We have

$$J'(\Delta) = 3\frac{\partial J(\Delta)}{\partial p(d_{11})}p'(d_{11}) + 2\frac{\partial J(\Delta)}{\partial d_{11}}$$

From proposition 4.3.7 we know $\frac{\partial J(\Delta)}{\partial p(d_{11})} > \frac{\partial J(\Delta)}{\partial d_{11}}$. Earlier we showed the derivative of $p(d_{11})$ with respect to d_{11} is less than -4. Hence $J'(\Delta) < 0$. So the circumcircle radius of Δ decreases with d_{11}. Hence we have

$$J(\Delta) < J(p(d_\delta), p(d_\delta), d_\delta, d_\delta, p(d_\delta))$$

We have already shown $J_{\mathcal{F}_2} < J(\Delta)$. So we have

$$J_{\mathcal{F}_2} < J(p(d_\delta), p(d_\delta), d_\delta, d_\delta, p(d_\delta)) \tag{9}$$

Recall that earlier we bounded $J_{\mathcal{F}_1}$ by the circumcircle radius of a centered pentagon with a

71

side of $p(d_\delta)$ and four sides of d_δ. (8). By corollary 4.3.9 that circumcircle radius is less than the circumcircle radius in the right hand side of equation 9. Hence $J_{\mathcal{F}_1}$ and $J_{\mathcal{F}_2}$ can both be bounded above by the circumcircle radius in the right hand side of equation 9.

$$J_{\mathcal{F}_1}, J_{\mathcal{F}_2} < J(p(d_\delta), p(d_\delta), d_\delta, d_\delta, p(d_\delta)) \tag{10}$$

Decomposition 3 ; $\mathcal{F}_3$

There are 6 two-cells in $\mathcal{F}_1$; 1 pentagon and 5 triangles.

- $\Delta_0 = (m(d_{11}), d_{11}, m(d_{11}), d_{11}, d_{11}) \in \mathcal{C}_5$. $q(d_{11})$. Two edges with length $m(d_{11})$ are glued to each other

- $\Delta_i = (d_{11}, d_{11}, d_{11}) \in \mathcal{C}_3$ for $i = 1, 2, \ldots, 5$

By differentiating the area sum equation with respect to d_{11} we obtain the following.

$$
\begin{aligned}
m'(d_{11}) = - &\left(\frac{3f(d_{11}, \Delta_0) + 15f(d_{11}, \Delta_1)}{2f(m(d_{11}), \Delta_0)} \right) \\
&- 3 \left(\frac{f(d_{11}, \Delta_0) + 5f(d_{11}, \Delta_1)}{2f(m(d_{11}), \Delta_0)} \right)
\end{aligned}
$$

Since $f(d_{11}, \Delta_0) > f(m(d_{11}), \Delta_0)$ we have $m'(d_{11}) < -3/2$.

We also have $J'(\Delta_0) = 2\frac{\partial J(\Delta_0)}{\partial m} m' + 3\frac{\partial J(\Delta_0)}{\partial d_{11}}$.

From proposition 4.3.7 we know $\frac{\partial J(\Delta_0)}{\partial m} > \frac{\partial J(\Delta_0)}{\partial d_{11}}$. Since $m'(d_{11}) < -3/2$ we conclude $J'(\Delta_0) < 0$. Hence $J_{\mathcal{F}_3} = J(\Delta_0)$ is decreasing in d_{11}.

This means for any d_{11} value in the interval $[d_\delta, d_\theta]$, $\mathcal{F}_3 \in \mathcal{Q}_{d_{11}}$ has $J_{\mathcal{F}_3}$ bounded above by the J value of $\mathcal{F}_3 \in \mathcal{Q}_{d_\delta}$. In other words we have

$$J_{\mathcal{F}_3} < J(m(d_\delta), d_\delta, m(d_\delta), d_\delta, d_\delta) \tag{11}$$

While, we have an upper bound for $J_{\mathcal{F}_3}$ as above, its not easy to directly compute the circumcircle radius in the right hand side of 11 using the formulas given in 4.3.5. Instead we will show below $m(d_\delta) < p(d_\delta)$ and use it to find an upper bound for $J_{\mathcal{F}_3}$

Lemma 4.8.1. $m(d_\delta) < p(d_\delta)$

Proof. First we split the pentagon $(m(d_\delta), d_\delta, m(d_\delta), d_\delta, d_\delta)$ into a quadrilateral and a tri-
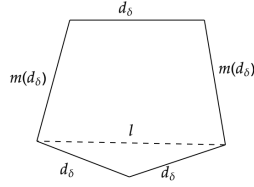
Figure 23: Comparing $m(d_\delta)$ with $p(d_\delta)$

angle as shown in figure 23. They both have the same circumcircle radius. Hence we have

$$\frac{D^2}{\sqrt{4D^2 - L^2}} = \sqrt{\frac{(M^2 + DL)(S^2}{4S^2 - (L - D)^2}}$$

where $D = sinh(d_\delta/2), M = sinh(m(d_\delta)/2)$ and $L = sin(l/2)$. This can be again reduced to a cubic equation

$$DM^2L^3 + (M^4 - D^4)L^2 + (2D^5 - 4D^3M^2)L - 4D^2M^2(M^2 - D^2) = 0$$

We define a function $C_1(x, y)$ by

$$C_1(x, y) = DX^2Y^3 + (X^4 - D^4)Y^2 + (2D^5 - 4D^3X^2)Y - 4D^2X^2(x^2 - D^2)$$

where $X = sinh(x/2)$ and $Y = sinh(y/2)$.

We also have the area sum equation

$$D_0(m(d_\delta), d_\delta, m(d_\delta), l) + D_0(l, d_\delta, d_\delta) + 5D_0(d_\delta, d_\delta, d_\delta) = 4\pi$$

We define another function

$$C_2(x, y) = D_0(x, d_\delta, x, y) + D_0(y, d_\delta, d_\delta) + 5D_0(d_\delta, d_\delta, d_\delta) - 4\pi$$

So we have $C_1(m(d_\delta), l) = 0$ and $C_2(m(d_\delta), l) = 0$

By plotting the graph of C_1 in the interval $x \in [2.85, \infty)$ we observe the following.

- For $x > 2.85$, y values that makes $C_1(x, y) = 0$ are always greater than 3.307
- For $x > 2.85$, y values that makes $C_1(x, y) = 0$ are either less than 2.901 or greater than 3.853

Also note that since d_δ, d_δ and l are sides of a hyperbolic triangle we have $sinh^2(l/2) < 2sinh^2(d_\delta/2)$ which implies $l < 3.698$. This fact together with above observations means $m(d_\delta)$ has to be less than 2.85. In particular it is less than $p(d_\delta)$. $\qquad\square$

We just proved $m(d_\delta) < p(d_\delta)$. Hence the circumcircle radius of the centered pentagon with two sides of $m(d_\delta)$ and three sides of d_δ (pentagon in the right hand side of equation 11) should be less than that of the centered pentagon with three sides of $p(d_\delta)$ and two sides of d_δ (pentagon in the right hand side of equation 9) . Hence we conclude $J_{\mathcal{F}_3}$ is also bounded above by $J(p(d_\delta), p(d_\delta), d_\delta, d_\delta p(d_\delta))$. We update equation 12 by also adding $J_{\mathcal{F}_3}$.

$$J_{\mathcal{F}_1}, J_{\mathcal{F}_2}, J_{\mathcal{F}_3} < J(p(d_\delta), p(d_\delta), d_\delta, d_\delta p(d_\delta)) \tag{12}$$

Computing $J(p(d_\delta), p(d_\delta), d_\delta, d_\delta p(d_\delta))$

Let's denote the pentagon by P. Again we divide it into a quadrilateral and a triangle
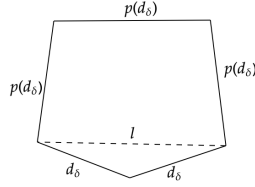
Figure 24: Computing $J(P)$

and then set their circumcircle radii equal as in figure 24 We have

$$\frac{D^2}{\sqrt{4D^2 - L^2}} = \sqrt{\frac{P^3}{3P - L}}$$

which can be reduced to $P^3 L^2 - D^4 L + 3PD^4 - 4P^3 D^2 = 0$. Here D, P, L has usual meanings ; $D = sinh(d_\delta/2)$ and so on. Using the values of $d_\delta = acosh(5.8)$ and $p(d_\delta) = 2.8598$, we compute L to be 2.6764. Then we have $J(p(d_\theta), p(d_\theta), d_\theta, d_\theta, p(d_\theta)) = J(l, d_\theta, d_\theta, d_\theta) = asinh(1.5374)$. Finally we compare this value with $(d_{01})_{min}$. (See figure 25)
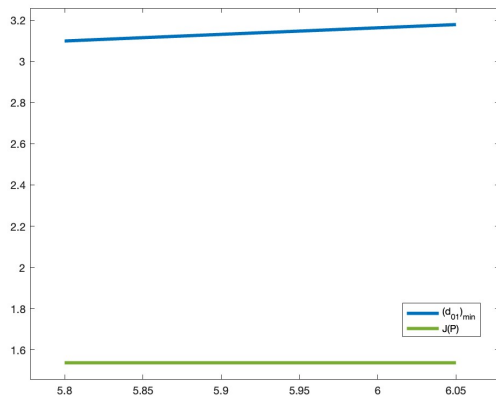
Figure 25: Plots of $sinh(J(P))$ and $sinh((d_{01})_{min})$

Decomposition 4 ; $\mathcal{F}_4$

There are 7 two-cells in $\mathcal{F}_4$; 1 quadrilateral and 6 triangles.

- $\Delta_0 = (w(d_{11}), d_{11}, d_{11}, d_{11}) \in \mathcal{C}_4$.

- $\Delta_1 = (w(d_{11}), d_{11}, d_{11}) \in \mathcal{AC}_3 \setminus \mathcal{C}_3$

- $\Delta_i = (d_{11}, d_{11}, d_{11}) \in \mathcal{C}_3$ for $i = 2, \ldots, 6$

Consider a centered quadrilateral with sides x, d_{11}, d_{11} and d_{11}. If we increase d_{11} while keeping x constant, then the area of this quadrilateral will be increased. Same is true for a non centered triangle with sides x, d_{11} and d_{11}. Area of a centered triangle with all three sides of d_{11} also increase its area with d_{11}. We define the following function

$$C(x, d_{11}) = D_0(x, d_{11}, d_{11}, d_{11}) + D_0(x, d_{11}, d_{11}) + 5D_0(d_{11}, d_{11}, d_{11}) - 4\pi$$

for $d_{11} \in [d_\delta, d_\theta]$ and $x > d_{11}$. As described above C is increasing in d_{11}.

By plotting the graphs of $C(x, d_{11})$ for fixed d_{11} values, we observe that there is $x > d_{11}$ such that $C(x, d_{11}) = 0$ for $d_{11} = cosh^{-1}(6.023)$. Furthermore when $d_{11} < cosh^{-1}(6.023)$ $C(x, d_{11}) < 0$ for all $x > d_{11}$. Hence for $d_{11} \in [d_\delta, cosh^{-1}(6.023))$ there is no $w(d_{11})$ such that $D_0(w(d_{11}), d_{11}, d_{11}, d_{11}) + D_0(w(d_{11}), d_{11}, d_{11}) + 4D_0(d_{11}, d_{11}, d_{11}) = 4\pi$. This is the area sum equation for $\mathcal{F}_4$. We conclude the decomposition $\mathcal{F}_4$ described above is possible only if when $d_{11} \in [cosh^{-1}(6.023), d_\theta]$

Now for $d_{11} \in [cosh^{-1}(6.023), d_\theta]$ we differentiate the above area sum equation with respect to d_{11}

$$\frac{\partial D_0(\Delta_0)}{\partial w}w' + 3\frac{\partial D_0(\Delta_0)}{\partial d_{11}} + \frac{\partial D_0(\Delta_1)}{\partial w}w' + 2\frac{\partial D_0(\Delta_0)}{\partial d_{11}} + 15\frac{\partial D_0(\Delta_2)}{\partial d_{11}} = 0$$

Hence we have

$$w'(d_{11}) = \left(\frac{3f(d_{11}, \Delta_0) + 2f(d_{11}, \Delta_1) + 15f(d_{11}, \Delta_2)}{f(w(d_{11}), \Delta_0) - f(w(d_{11}), \Delta_1)}\right) > -3$$

Then it follows

$$J'(\Delta_0) = \frac{\partial J(\Delta_0)}{\partial w}w' + 3\frac{\partial J(\Delta_0)}{\partial d_{11}} < 0$$

Hence we have an upper bound for $J_{\mathcal{F}_4} = J(\Delta_0)$ as below

$$J_{\mathcal{F}_4} < J(w(d_{\delta'}), d_{\delta'}, d_{\delta'}, d_{\delta'}) \tag{13}$$

where $d_{\delta'} = acosh(6.023)$. Finally we compare the circumcircle radius $J(w(d_{\delta'}), d_{\delta'}, d_{\delta'})$ with $(d_{01})_{min}$ in the interval $d_{11} \in [d_{\delta'}, d_\theta]$. See figure 26.

In this section we described four decompositions $\mathcal{F}_1, \mathcal{F}_2, \mathcal{F}_3, \mathcal{F}_4$ in $\mathcal{Q}_{d_{11}}$ for $d_{11} \in [d_\delta, d_\theta]$ and showed each $J_{\mathcal{F}_i}$ is less than $(d_{01})_{min}$. If we can show that for any $\mathcal{F} \in \mathcal{Q}_{d_{11}}$ in this range of d_{11} values, $J_{\mathcal{F}} < J_{\mathcal{F}_i}$ for some $i \in \{1, 2, 3, 4\}$ then we will have $J_{\mathcal{F}} < (d_{01})_{min}$ which will be a contradiction . Our next section is devoted for this.
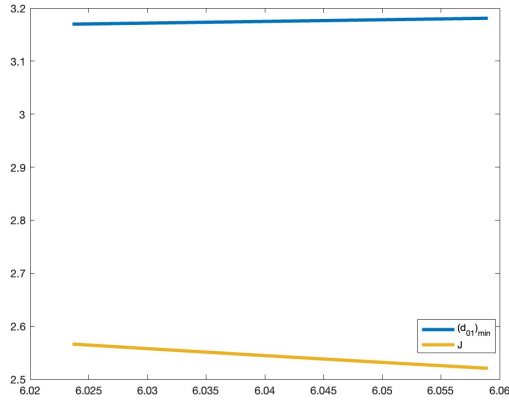
Figure 26: Comparing the upper bound of $J_{\mathcal{F}4}$ with $(d_{01})_{min}$

4.8.1 $J_{d_{11}} = J_{\mathcal{F}_i}$ for some i

Similar to the case in the quadrilaterals , we start with an $\mathcal{F} \in \mathcal{Q}_{d_{11}}$ and usually denote its $2-$ cell with largest circumcircle as Δ_0. We will then send $\mathcal{F}$ through a sequence of deformations , each of which increase $J(\Delta_0)$ till its not possible to do so further. When we reach such a terminating case we will show its always one of the four decompositions we described earlier. Similar to the quadrilaterals we can always first perform deformations to reduce lengths of edges that are not glued to Δ_0 while increasing $J(\Delta_0)$. Hence without loss of generality we will assume all such edges have lengths d_{11}.

Our first task is to show if Δ_0 is a centered pentagon, then it can be deformed into one of F_1, F_2 or F_3 while increasing its circumcircle radius. There are four separate cases need to be considered depending on the edge gluings of Δ_0. We show them in next four figures.
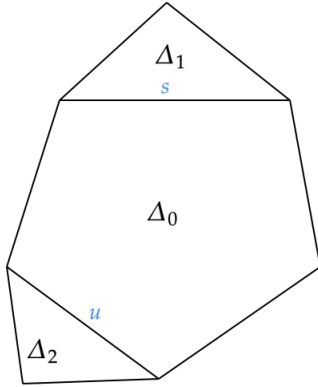
Centered pentagon case 1

Δ_0 is a centered pentagon with largest side length s

No edges of Δ_0 are glued to one of its other edges

Let u be another edge of Δ_0

Deformation : Increase s and change u

$$u' = \frac{-(f(s,\Delta_0) + f(s,\Delta_1))}{f(u,\Delta_0) + f(s,\Delta_2)} \in (-1,0)$$

$$\Rightarrow J'(\Delta_0) = \frac{\partial J(\Delta_0)}{\partial u}u' + \frac{\partial J(\Delta_0)}{\partial s} > 0$$

We can continue this deformation till $u = d_{11}$
Then do the same for other edges of Δ_0

This is $\mathcal{F}_1$

Figure 27: Centered pentagon case 1

Centered pentagon case 2

Δ_0 is a centered pentagon with largest side length s. This side is glued to another side of Δ_0

None of the remaining edges of Δ_0 are glued to one of its other edges

Let u be another edge of Δ_0

Deformation : Increase s and change u

$$u' = \frac{-2(f(s,\Delta_0))}{f(u,\Delta_0) + f(s,\Delta_2)} \in (-2,0)$$

$$\Rightarrow J'(\Delta_0) = \frac{\partial J(\Delta_0)}{\partial u}u' + 2\frac{\partial J(\Delta_0)}{\partial s} > 0$$
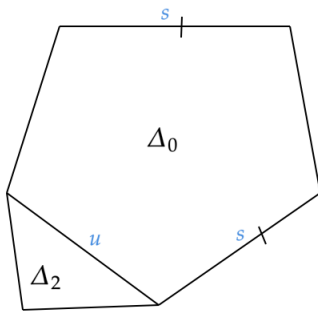
We can continue this deformation till $u = d_{11}$
Then do the same for other edges of Δ_0

This is $\mathcal{F}_3$

Figure 28: Centered pentagon case 2

Centered pentagon case 3
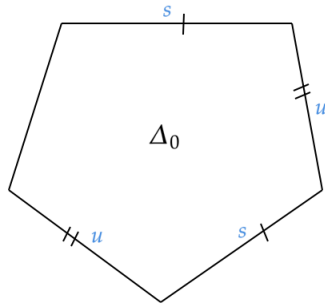
Δ_0 is a centered pentagon with largest side length s. This side is glued to another side of Δ_0

One other edge of Δ_0 is glued to another of its edges. Let u be the length of this edge

Deformation : Increase s and change u

$$u' = \frac{-2(f(s,\Delta_0))}{2f(u,\Delta_0)} \in (-1,0)$$

$$\Rightarrow J'(\Delta_0) = 2\frac{\partial J(\Delta_0)}{\partial u}u' + 2\frac{\partial J(\Delta_0)}{\partial s} > 0$$

We can continue this deformation till $u = d_{11}$
Then increase s while changing the other remaining edge of Δ_0

This is $\mathcal{F}_3$

Figure 29: Centered pentagon case 3
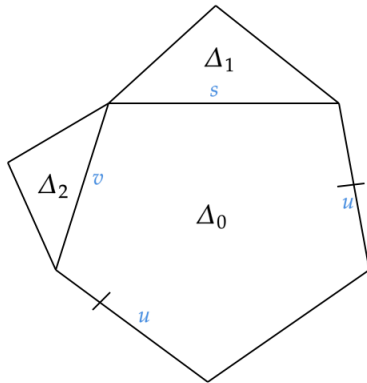
Centered pentagon case 4

Δ_0 is a centered pentagon with largest side length s

One edge of Δ_0 (different from s) is glued to one of its other edges
Let u be the length of that edge

Let v be the length of the remaining edge

Deformation : Increase s and change v

$$v' = \frac{-(f(s,\Delta_0) + f(s,\Delta_1))}{f(v,\Delta_0) + f(v,\Delta_2)} \in (-1,0)$$

$$\Rightarrow J'(\Delta_0) = \frac{\partial J(\Delta_0)}{\partial v}v' + \frac{\partial J(\Delta_0)}{\partial s} > 0$$

We can continue this deformation till $v = d_{11}$
This is $\mathcal{F}_2$

Figure 30: Centered pentagon case 4

80

Now we consider $\mathcal{F}$ which has a pentagonal 2−cell that is formed by the union of two non centered triangle and a centered triangle. Depending on their edge gluings, there are 8 cases to consider. We label them by case A, case B and so on. The next 8 figures show that in each of these case, we can increase $J(\Delta)$ through a series of deformations till we reach one of the four decompositions described earlier.

Case A
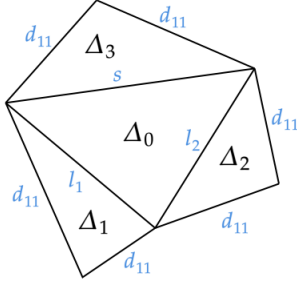
Δ_0 is centered

Δ_1 and Δ_2 are non centered

$\Delta_0 \cup \Delta_1 \cup \Delta_2$ is the a pentagonal 2-cell in the centered dual.

Wlog $s < l_1 < l_2$

Deformation : Increase l_2 and change s

$$s' = \frac{-(f(l_2,\Delta_0) - f(l_2,\Delta_2))}{f(s,\Delta_0) + f(s,\Delta_3)} \in (-1,0)$$

$$\Rightarrow J'(\Delta_0) = \frac{\partial J(\Delta_0)}{\partial s}s' + \frac{\partial J(\Delta_0)}{\partial l_2} > 0$$

Case A.1 : $s = d_{11}$

Deformation : Increase l_2 and change l_1

$$l_1' = \frac{-(f(l_2,\Delta_0) - f(l_2,\Delta_2))}{f(l_1,\Delta_0) - f(l_1,\Delta_1)} \in (-1,0) \quad \Rightarrow J'(\Delta_0) = \frac{\partial J(\Delta_0)}{\partial l_1}l_1' + \frac{\partial J(\Delta_0)}{\partial l_2} > 0$$

Case A.1.1 : $l_1 = d_{11}$ Not possible as it makes Δ_0 non centered

Case A.1.2 : $J(\Delta_0) = J(\Delta_2)$ This is $\mathcal{F}_4$

Case A.2 : $J(\Delta_0) = J(\Delta_2)$

$\Delta_0 \cup \Delta_2 = \Delta$ forms a single centered quad

Deformation : Increase l_1 and change s

$$s' = \frac{-(f(l_1,\Delta) - f(l_1,\Delta_1))}{f(s,\Delta) + f(s,\Delta_3)} \in (-1,0) \quad \Rightarrow J'(\Delta) = \frac{\partial J(\Delta)}{\partial s}s' + \frac{\partial J(\Delta)}{\partial l_1} > 0$$

Case A.2.1 : $s = d_{11}$ This is $\mathcal{F}_4$

Case A.2.2 : $J(\Delta) = J(\Delta_1)$ Forms a single centered pentagon

Figure 31: Pentagons : Case A

Case B

Δ_0 is centered

Δ_1 and Δ_2 are non centered

$\Delta_0 \cup \Delta_1 \cup \Delta_2$ is the a pentagonal 2-cell in the centered dual.

Wlog $s < l_1 < l_2$

Deformation : Increase l_2 and change s

$$s' = \frac{-(f(l_2, \Delta_0) - f(l_2, \Delta_2))}{f(s, \Delta_0) + f(s, \Delta_1)} \in (-1, 0)$$

$$\Rightarrow J'(\Delta_0) = \frac{\partial J(\Delta_0)}{\partial s} s' + \frac{\partial J(\Delta_0)}{\partial l_2} > 0$$

Case B.1 : $s = d_{11}$ Same as A.1

Case B.1.2 : $J(\Delta_0) = J(\Delta_2)$

$\Delta_0 \cup \Delta_2 = \Delta$ forms a single centered quad

Deformation : Increase l_1 and change s
Then same as A.2

Figure 32: Pentagons : Case B

Case C

Δ_0 is centered

Δ_1 and Δ_2 are non centered

$\Delta_0 \cup \Delta_1 \cup \Delta_2$ is the a pentagonal 2-cell in the centered dual.

Wlog $s < l_1 < l_2$

Deformation : Increase l_2 and change s

$$s' = \frac{-(f(l_2,\Delta_0) - f(l_2,\Delta_2))}{f(s,\Delta_0) + f(s,\Delta_3)} \in (-1,0)$$

$$\Rightarrow J'(\Delta_0) = \frac{\partial J(\Delta_0)}{\partial s}s' + \frac{\partial J(\Delta_0)}{\partial l_2} > 0$$

Case C.1 : $s = d_{11}$

Deformation : Increase l_1 and change u

$$u' = \frac{-(f(l_1,\Delta_0) - f(l_1,\Delta_1))}{f(u,\Delta_1) + f(u,\Delta2)} < 0 \qquad \text{and } J'(\Delta_0) = \frac{\partial J(\Delta_0)}{\partial l_1} > 0$$

Case C.1.1 : $u = d_{11}$ Same as A.1

Case C.1.2 : $J(\Delta_0) = J(\Delta_1)$

$\Delta_0 \cup \Delta_1 = \Delta$ forms a single centered quad

Deformation : Increase l_2 and change u

$u' < 0$ and $\Rightarrow J'(\Delta_0) > 0$ as earlier

Case C.1.2.1 : $u = d_{11}$ This is $\mathcal{F}_4$

Case C.1.2.1 : $J(\Delta) = J(\Delta_2)$ Forms a centered pentagon

---

Case C.2 : $J(\Delta_0) = J(\Delta_2)$

$\Delta_0 \cup \Delta_2 = \Delta$ forms a single centered quad with sides l_1, s, u, d_{11}

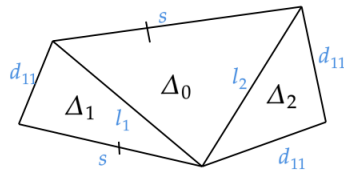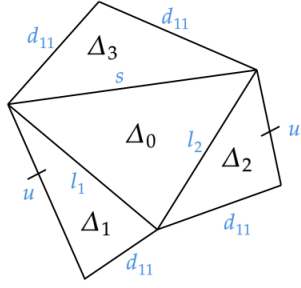*Deformation : Increase l_1 and change s*

$$s' = \frac{-(f(l_1,\Delta) - f(l_1,\Delta_1))}{f(s,\Delta) + f(s,\Delta_3)} \in (-1,0) \qquad \Rightarrow J'(\Delta) = \frac{\partial J(\Delta)}{\partial s}s' + \frac{\partial J(\Delta)}{\partial l_1} > 0$$

Case C.2.1 : $s = d_{11}$

Deformation : Increase l_1 and change u

$u' < 0$ and $\Rightarrow J'(\Delta) > 0$ as earlier

Case C.2.1.1 : $u = d_{11}$ This is $\mathcal{F}_4$

Case C.2.1.2 : $J(\Delta) = J(\Delta_1)$ Forms a centered pentagon

Case C.2.2 : $J(\Delta) = J(\Delta_1)$ Forms a centered pentagon

---

Figure 33: Pentagons : Case C

Case D
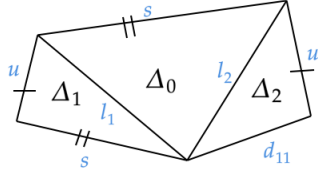
Δ_0 is centered

Δ_1 and Δ_2 are non centered

$\Delta_0 \cup \Delta_1 \cup \Delta_2$ is the a pentagonal 2-cell in the centered dual.

Wlog $s < l_1 < l_2$

Deformation : Increase l_2 and change s

$$s' = \frac{-(f(l_2, \Delta_0) - f(l_2, \Delta_2))}{f(s, \Delta_0) + f(s, \Delta_1)} \in (-1, 0)$$

$$\Rightarrow J'(\Delta_0) = \frac{\partial J(\Delta_0)}{\partial s} s' + \frac{\partial J(\Delta_0)}{\partial l_2} > 0$$

Case D.1 : $s = d_{11}$ Same as D.1

Case D.2 : $J(\Delta_0) = J(\Delta_2)$

$\Delta_0 \cup \Delta_2 = \Delta$ forms a single centered quad with sides s, u, d_{11}, l_1

Deformation : Increase l_1 and change s

$$s' = \frac{-(f(l_1, \Delta) - f(l_1, \Delta_1))}{f(s, \Delta) + f(s, \Delta_1)} \in (-1, 0) \qquad \Rightarrow J'(\Delta_0) = \frac{\partial J(\Delta_0)}{\partial s} s' + \frac{\partial J(\Delta_0)}{\partial l_2} > 0$$

Case D.2.1 : $s = d_{11}$
Deformation : Increase l_1 and change u
$u' \in (-1, 0)$ and $\Rightarrow J'(\Delta_0) > 0$ as earlier
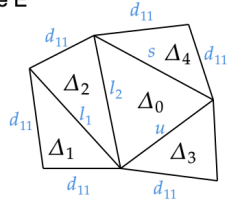
Case D.2.1.1 : $u = d_{11}$ This is $\mathcal{F}_4$
Case D.2.1.2 : $J(\Delta) = J(\Delta_1)$ Forms a centered pentagon

Case D.2.2 : $J(\Delta) = J(\Delta_1)$ Forms a centered pentagon

Figure 34: Pentagons : Case D

Case E

Δ_0 is centered

Δ_1 and Δ_2 are non centered

$\Delta_0 \cup \Delta_1 \cup \Delta_2$ is the a pentagonal 2-cell in the centered dual.

Deformation : Increase l_2 and change s

$$s' = \frac{-(f(l_2, \Delta_0) - f(l_2, \Delta_2))}{f(s, \Delta_0) + f(s, \Delta_4)} \in (-1, 0)$$

$$\Rightarrow J'(\Delta_0) = \frac{\partial J(\Delta_0)}{\partial s}s' + \frac{\partial J(\Delta_0)}{\partial l_2} > 0$$

Case E.1 : $s = d_{11}$

Deformation : Increase l_2 and change u

$u' \in (-1, 0)$ and $\Rightarrow J'(\Delta_0) > 0$ as earlier

Case E.1.1 : $u = d_{11}$ Not possible as it makes Δ_0 non centered

Case E.1.2 : $J(\Delta_0) = J(\Delta_2)$ Similar to as D.2.1

Case E.2 : $J(\Delta_0) = J(\Delta_2)$ Same as D.2

Figure 35: Pentagons : Case E

Case F
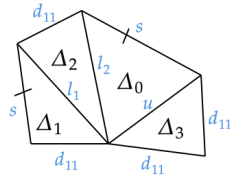
Δ_0 is centered

Δ_1 and Δ_2 are non centered

$\Delta_0 \cup \Delta_1 \cup \Delta_2$ is the a pentagonal 2-cell in the centered dual.

Deformation : Increase l_2 and change s

$$s' = \frac{-(f(l_2, \Delta_0) - f(l_2, \Delta_2))}{f(s, \Delta_0) + f(s, \Delta_1)} \in (-1, 0)$$

$$\Rightarrow J'(\Delta_0) = \frac{\partial J(\Delta_0)}{\partial s}s' + \frac{\partial J(\Delta_0)}{\partial l_2} > 0$$

Case F.1 : $s = d_{11}$ Same as E.1

Case F.2 : $J(\Delta_0) = J(\Delta_2)$

$\Delta_0 \cup \Delta_2 = \Delta$ forms a single centered quad with sides s, u, l_1, d_{11}

Deformation : Increase l_1 and change u

$$u' = \frac{-(f(l_1, \Delta) - f(l_1, \Delta_1))}{f(u, \Delta) + f(u, \Delta_3)} \in (-1, 0) \Rightarrow J'(\Delta) = \frac{\partial J(\Delta)}{\partial u}u' + \frac{\partial J(\Delta_0)}{\partial l_2} > 0$$

Case F.2.1 : $u = d_{11}$ Same as D.2.1

Case F.2.2 : $J(\Delta) = J(\Delta_1)$ Forms a centered pentagon

Figure 36: Pentagons : Case F

85

Case G

Δ_0 is centered

Δ_1 and Δ_2 are non centered

$\Delta_0 \cup \Delta_1 \cup \Delta_2$ is the a pentagonal 2-cell in the centered dual.

Deformation : Increase l_2 and change u

$$u' = \frac{-(f(l_2, \Delta_0) - f(l_2, \Delta_2))}{f(u, \Delta_0) + f(u, \Delta_2)} \in (-1, 0)$$

$$\Rightarrow J'(\Delta_0) = \frac{\partial J(\Delta_0)}{\partial u} u' + \frac{\partial J(\Delta_0)}{\partial l_2} > 0$$

Case G.1 : $u = d_{11}$ Same as E.1

Deformation : Increase l_2 and change s

$s' \in (-1, 0)$ and $\Rightarrow J'(\Delta_0) > 0$ as earlier

Case G.1.1 : $s = d_{11}$ Not possible as it makes Δ_0 non centered

Case G.1.2 : $J(\Delta_0) = J(\Delta_2)$ Same as A.2

Case G.2 : $J(\Delta_0) = J(\Delta_2)$

$\Delta_0 \cup \Delta_2 = \Delta$ forms a single centered quad with sides u, s, u, l_1

Deformation : Increase l_1 and change s

$s' \in (-1, 0)$ and $\Rightarrow J'(\Delta_0) > 0$ as earlier

Case G.2.1 : $s = d_{11}$

Deformation : Increase l_1 and change u

$$u' = \frac{-(f(l_1, \Delta) - f(l_1, \Delta_1))}{2 f(u, \Delta)} \in (-1/2, 0)$$

$$\Rightarrow J'(\Delta) = 2 \frac{\partial J(\Delta)}{\partial u} u' + \frac{\partial J(\Delta_0)}{\partial l_2} > 0 \quad \text{This is } \mathcal{F}_4$$

Case G.2.2 : $J(\Delta) = J(\Delta_1)$ Forms a centered pentagon

---

Figure 37: Pentagons : Case G

86

Case H

d_{11}

u s

Δ_2 l_2 Δ_0

l_1

s Δ_1 u

d_{11}

Δ_0 is centered

Δ_1 and Δ_2 are non centered

$\Delta_0 \cup \Delta_1 \cup \Delta_2$ is the a pentagonal 2-cell in the centered dual.

Deformation : Increase l_2 and change s

$$s' = \frac{-(f(l_2, \Delta_0) - f(l_2, \Delta_2))}{f(s, \Delta_0) + f(s, \Delta_1)} \in (-1, 0)$$

$$\Rightarrow J'(\Delta_0) = \frac{\partial J(\Delta_0)}{\partial s} s' + \frac{\partial J(\Delta_0)}{\partial l_2} > 0$$

Case H.1 : $s = d_{11}$ Same as G

Case H.2 : $J(\Delta_0) = J(\Delta_2)$

$\Delta_0 \cup \Delta_2 = \Delta$ forms a single centered quad with sides u, s, u, l_1
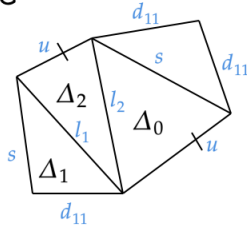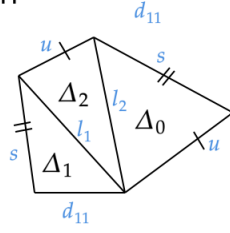
Deformation : Increase l_1 and change s

$s' \in (-1, 0)$ and $\Rightarrow J'(\Delta) > 0$ as earlier

Case H.2.1 : $s = d_{11}$ Same as G.2.1

Case H.2.2 : $J(\Delta) = J(\Delta_1)$ Forms a centered pentagon

Figure 38: Pentagons : Case H

Above cases exhaust all the possible decompositions in $\mathcal{Q}_{d_{11}}$ for $d_{11} \in [d_\delta, d_\theta]$. This leads us to the contradiction

Theorem 4.8.2. *No manifold in $\mathcal{N}_{c,c}$ has a d_{11} value in the interval $[d_\delta, d_\theta]$*

In the preceding subsections we analysed the three intervals of d_{11} values listed in the corollary 4.5.4. In each interval we compared the upper bound of d_{01} we obtained using the Centered Dual Decomposition with the lower bound of d_{01} which is $(d_{01})_{min}$. In each interval it turns out the supposed upper bound is smaller than $(d_{01})_{min}$. Hence we conclude no manifold in $\mathcal{N}_{c,c}$ has a d_{11} value in any of the three intervals listed in 4.5.4

Theorem 2. *No manifold in $\mathcal{N}_{c,c}$ has a d_{11} value in the interval $[d_\delta, d_\alpha]$ or equivalently an x_1 value in the interval $[1.183, 1.208]$*

5.0 Small Dehn Fillings

Main results in the previous two chapters (Theorem 1 and Theorem 2) imply the smallest element in $\mathcal{N}_{c,c}$ should satisfy the following.

- It should have an x_1 value in the interval $[1.208, 1.256]$
- It should be of the form of case 1 mentioned in chapter 3 or equivalently $d_{01} = (d_{01})_{min}$

We denote the subset of manifolds of $\mathcal{N}_{c,c}$ that satisfy these conditions by $\mathcal{N}'_{c,c}$.

Definition 5.0.1. $\mathcal{N}'_{c,c} = \left\{ N \in \mathcal{N}_{c,c} \mid x_1 \in [1.208, 1.256], d_{01} = (d_{01})_{min} \right\}$

5.1 Hexagons visible from the cusp

Let N be a manifold in $\mathcal{N}'_{c,c}$. Figure 39 shows key components in our volume estimation from chapter 3 for such a manifold. Consider the horosphere of ∞ in $\tilde{N}$ which is away from $\partial \tilde{N}$ by a distance of K. Let's denote this horosphere by Λ. It's a Euclidean horizontal plane. A lift of λ_0 which has an ideal end point at ∞ in $\tilde{N}$ goes through this horosphere Λ. Any such a lift would be a vertical line segment emanating from a boundary component of $\tilde{N}$ and has ∞ as the other end point. Intersection of such a lift with Λ is a point on Λ.

Now consider all such lifts of λ_0 that runs to ∞ and their intersections with Λ which is a set of discrete points. This set of discrete points create a lattice on Λ. Our focus in this chapter is on understanding this lattice. Let's start by defining these formally.

$$\Lambda = \left\{ (x, y, h) \mid x, y \in \mathbb{R} \right\} \quad \text{where } h \text{ is as in 11}$$

$$L = \left\{ \text{Lifts of } \lambda_0 \text{ in } \tilde{N} \text{ which has an ideal end point at } \infty \right\}$$

$$S = \left\{ \Lambda \cap \tilde{\lambda}_0 \mid \tilde{\lambda}_0 \in L \right\}$$

$$C = \left\{ \Pi \mid \Pi \text{ is a component of } \partial \tilde{N} \text{ and contains an intial point of some } \tilde{\lambda}_0 \text{ in } L \right\}$$

Lifts of λ_0

Horosphere Λ
of ∞

K

l_1

A lift of M_{l1}

Lifts of the cusp neightbourhood

Lifts of half ideal muffin

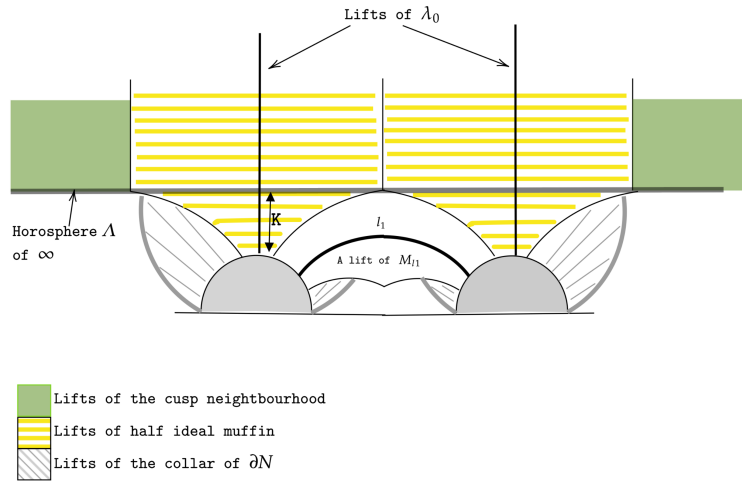Lifts of the collar of ∂N

Figure 39: Volume estimation for case 1 in chapter 3

Λ
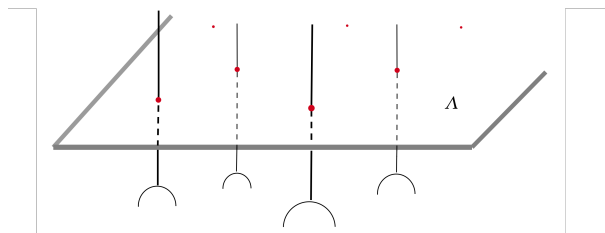
Figure 40: Lattice on Λ

Using the proposition 0.1 in [6] we can relate the horocyclic arc length between two points in the lattice on Λ to return paths.

Lemma 5.1.1. *Let $q_1 = \Lambda \cap \tilde{\lambda}_0'$ and $q_2 = \Lambda \cap \tilde{\lambda}_0''$ be two points in S and Π_1 and Π_2 be the components of $\partial \tilde{N}$ in C that contain the initial points of $\tilde{\lambda}_0'$ and $\tilde{\lambda}_0''$. If the common perpendicular to Π_1 and Π_2 is a lift of λ_i then the length of the horocyclic arc between q_1 and q_2 in Λ is given by*

$$\theta_i = \frac{\sqrt{2(\cosh(l_i) + 1)}}{e^K}$$
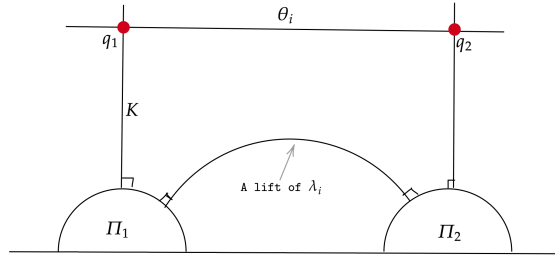
Figure 41: Horocyclic arc length between two lattice points on Λ

Now take any arbitrary triple Π_1, Π_2 and Π_3 of boundary components in C. Suppose the common perpendicular to these are lifts of λ_i, λ_j and λ_k. **The (i, j, k) hexagon which has these lifts as alternating sides is then called as an (i, j, k) hexagon visible from the cusp.** If q_1, q_2 and q_3 are the corresponding points in L then the lengths of horocyclic arcs on Λ between them are θ_i, θ_j and θ_k.

Recall that N belongs to $\mathcal{N}_{c,c}'$ means it satisfies the condition for case 1 mentioned in chapter 3. That is $\tilde{N}$ contains a pair of boundary components Π_1 and Π_2 that belongs C and has a lift of the shortest return path as their common perpendicular. This means $\tilde{N}$ has a $(1, j, k)$ hexagon visible from the cusp for some $1 \leq j \leq k$.
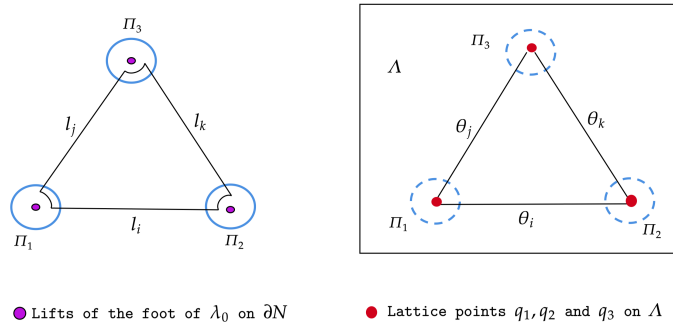
Figure 42: An (i,j,k) hexagon visible from the cusp(left) and the corresponding lattice points on Λ (right) viewed from infinity

The main goal of this chapter is to show that the only possible way for N to have a volume less than or equal to the volume of N_0 is by containing a $(1, 1, k)$ hexagon visible from the cusp in its universal cover $\tilde{N}$ for $k \geq 1$. We do so by producing a volume estimation that is very similar to the one we produced in chapter 3. Key components contributed to that estimation will remain the same here. The only modification will be made to the estimation of the cusp neighbourhood volume. Instead of the Boröczky's theorem, here we will use the information from the lattice on Λ by L to estimate the volume of the cusp neighbourhood. We begin with following two lemmas.

Lemma 5.1.2. *Let A, B, C and D be vertices of a parallelogram P in $\mathbb{R}^2$ such that vertices A, B and C lie on a Eucledian circle. If the interior angle of the parallelogram at the vertex opposite to D is greater than $90°$ then D lies inside the circle.*

Proof. We need to consider two cases ; depending on whether the center of the circle is inside P or not. We will start with the former case. (See figure 43 left.) Let O and r be the center and the radius of the circle respectively. Let l be the distance from O to D. Now assume the pair of interior angles $\alpha + \beta$ is greater than $90°$. Then the other pair should be

less than $90°$; $\theta + \alpha = \beta + \gamma < 90°$. In particular $\theta, \beta < 90°$.

Since the sum of the interior angles $2(\alpha + \beta) + (\alpha + \theta) + (\beta + \gamma) = 360°$ and $\theta + \alpha = \beta + \gamma$ we have $\theta = 180° - 2\alpha - \beta$. Therefore $\theta - \beta = 180° - 2\alpha - 2\beta < 0$ as $\alpha + \beta > 90°$ by assumption. So we have $\theta < \beta$ and hence $cos(\theta) > cos(\beta)$ as these are acute angles.

By applying the cosine rule to triangles OBC and ODA we have $l^2 = (AD)^2 + r^2 - 2arcos(\theta) = (BC)^2 + r^2 - 2arcos(\theta) < (BC)^2 + r^2 - 2arcos(\beta) = r^2$. Hence $l < r$.

In case 2 (figure 43 right) by arguing similarly we have $\theta + \alpha = \beta < 90°$ if $\alpha + \beta > 90°$. Hence we have $\theta, \beta < 90°$ and $\theta < \beta$. By applying the cosine rule to triangles OBC and ODA we can similarly obtain $l < r$.

$\square$

Now we consider the Delaunay tessellation of the lattice on Λ. Vertices of the tessellation
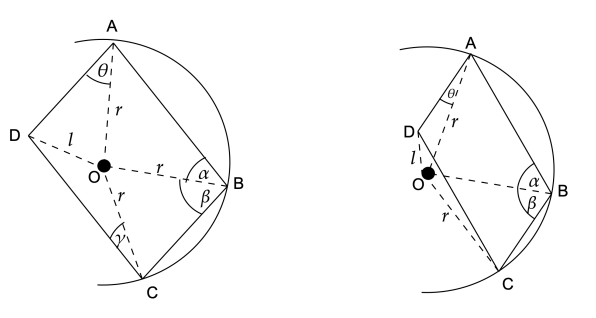

Figure 43:   Two cases in lemma 5.1.2

are lattice points and 2−cells are cyclic polygons. The special property that characterize the Delaunay tessellation is the fact that no vertices of the tessellation lie in the interior of a circumcircle corresponding to a 2−cell.

Lemma 5.1.3. *Delaunay tessellation of Λ determined by this lattice has triangles or rectangles as 2-cells.*

Proof. Let P be a 2-cell in the Delaunay tessellation and p be one of it's vertices. Let v_1 and v_2 be the vertices in this polygon that are adjacent to p. Then $\exists$ generators g_1, g_2 of Λ such that $g_1(p) = v_1$ and $g_2(p) = v_2$. Then $g_1 g_2(p)$ is also a vertex in the tessellation. Now consider the parallelogram with vertices v_1, p, v_2 and $g_1 g_2(p)$ .First three of its vertices lie on the circumcircle of P. The fourth vertex $g_1 g_2(p)$ cannot lie inside the circumcircle of P because by the definition of Dalauney tessellation, none of its vertices can lie inside a circumcircle. Hence By 5.1.2 the interior angle of P at p cannot exceed $90°$. But there is nothing special about this vertex p of P and the same argument can be applied to any of its other vertices. So no interior angle of P exceed $90°$. If number of sides of P is n then we have the following.

$$\text{Sum of interior angles} = (n-2)180 \leq 90n \Rightarrow n \leq 4$$

$\square$

5.2   Volume Estimation - slightly modified

Recall from chapter 3 we bounded the volume of a manifold N in $\mathcal{N}_{c,c}$ by a function of x_1. Key elements that contributed to this estimation were

- M_{l_1} ; Muffin around λ_1
- Half ideal muffin ; Muffin around λ_0
- Collar of the remaining part of the boundary of N
- An embedded cusp neighbourhood of N

Now we are going to modify the volume estimation slightly. While we keep our estimations for first three, we estimate the volume of the last component of the above list ; the embedded cusp neighbourhood of N by a different method using what we have proved so far in this chapter.

We just proved the Delaunay tessellation of Λ determined by the feet of lifts of λ_0 is ei-

ther a triangulation or contains rectangles. Below we estimate the volume of an embedded cusp neighbourhood of N which has Λ as its boundary for these two cases separately. It's important to note that the manifolds we consider in this chapter belongs to case 1 from chapter 3. That means two components of $\partial \tilde{N}$ that contain lifts of λ_0 going to ∞ has a lift of λ_1 as their common perpendicular. Hence such manifolds must contain a $(1, j, k)$ hexagon visible from the cusp and there is an edge in the Delaunay tessellation with length θ_1.

5.3 When the Delaunay tessellation of $\mathbb{R}^2$ determined by the feet of lifts of λ_0 is a triangulation

Lemma 5.3.1. *If the Delaunay tessellation of $\mathbb{R}^2$ determined by the feet of lifts of λ_0 is a triangulation then all triangles are centered.*

Proof. First we start with two adjacent triangles Δ_0 and Δ_1 of the Delaunay tessellation. Deck transformation of the cusp acts as Euclidean translation on horospheres. Hence there is no deck transformation that translates Δ_0 to Δ_1 or vice versa. Hence they belong to different orbits under the cusp group action. Since the universal cover is normal, cusp translations acts transitively on the lattice points of Λ. Hence there are translations in the cusp group that takes Δ_0 to triangles Δ_0' and Δ_0'' which are also adjacent to Δ_1. Hence lengths of both triangles Δ_0 and Δ_1 are equal and their union (which is a parallelogram) forms a fundamental domain of Λ under the cusp group action. As explained earlier there is a side on this tessellation with length θ_1. Hence we can take side lengths of these two triangles to θ_1, θ_j and θ_k. We can assume that the edge shared by the two triangles θ_k has the largest side length. (If not just replace Δ_0 by one of its translations Δ_0' or Δ_0'' such that the edge shared by both triangles has the largest side length.)

Now assume Δ_0 is non-centered. Then we can see that the interior angle at the vertex opposite to θ_k is greater than 90° by a simple application of the cosine rule. Since the union of Δ_0 and Δ_1 is a parallelogram , by applying the lemma 5.1.2 we conclude the vertex of Δ_1 opposite to θ_k should lie inside the circumcircle of Δ_0 which is a contradiction. Hence Δ_0 should be centered and hence Δ_1 is also centered. $\square$

Note that a Euclidean triangle with side lengths $a \leq b \leq c$ is centered iff $a^2 + b^2 > c^2$. Hence
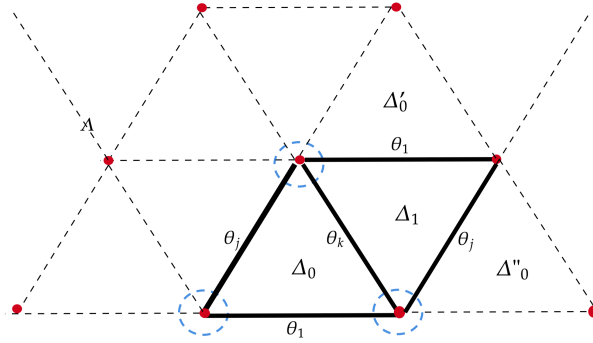
Figure 44: A fundamental domain for Λ

the condition for triangles Δ_0 and Δ_1 which has horocyclic arc lengths θ_1, θ_j and θ_K to be centered is

$$\theta_1^2 + \theta_j^2 > \theta_k^2 \tag{14}$$

In the proof of 5.3.1 we showed there are two triangles Δ_0 and Δ_1 on the horosphere Λ satisfying the following.

- Both triangles have same side lengths with horocyclic arcs of lenght θ_1, θ_j and θ_k for some integers j and k such that $1 \leq j \leq k$.
- They are glued along the edge with the longest side length θ_k
- Their union is a parallelogram and forms a fundamental domain for Λ under the cusp group action.

By Heron's formula, we can compute the Euclidean area of this parallelogram to be

$$\frac{1}{2}\sqrt{(\theta_1 + \theta_j + \theta_k)(\theta_1 - \theta_j + \theta_k)(\theta_1 + \theta_j - \theta_k)(-\theta_1 + \theta_j + \theta_k)}$$
$$=\frac{1}{2}\sqrt{((\theta_1 + \theta_j)^2 - \theta_k^2)(\theta_k^2 - (\theta_1 + \theta_j)^2)} \tag{15}$$

Going back to the volume estimation from chapter 1, we had a disk of radius $\theta_1/2$ in Λ embedded inside the half ideal muffin. Hence the volume of the part of the cusp neighbourhood which is outside the half ideal muffin is

$$\frac{1}{2}\sqrt{((\theta_1 + \theta_j)^2 - \theta_k^2)(\theta_k^2 - (\theta_1 + \theta_j)^2)} - \pi\left(\frac{\theta_1}{2}\right)^2$$

Note that Λ is a lift of the boundary of the cusp neighbourhood we consider. Hence the area of the boundary of the cusp neighbourhood is equal to the area of a fundamental domain which is given in 15. Volume of a cusp neighbourhood is equal to one half of the area of its boundary. Hence the volume of the part of the cusp neighbourhood outside the half ideal muffin is

$$\frac{1}{2}\left(\frac{1}{2}\sqrt{((\theta_1 + \theta_j)^2 - \theta_k^2)(\theta_k^2 - (\theta_1 + \theta_j)^2)} - \pi\left(\frac{\theta_1}{2}\right)^2\right) \tag{16}$$

Partial derivative of the expression $(\theta_1 + \theta_j)^2 - \theta_k^2)(\theta_k^2 - (\theta_1 + \theta_j)^2)$ with respect to θ_k is $2\theta_k^2(\theta_1^2 + \theta_j^2 - \theta_k^2)$ which is positive by 14. Similarly the partial derivative of the same expression with respect θ_j is $2\theta_j^2(\theta_1^2 + \theta_k^2 - \theta_j^2)$ and is also positive. Hence the volume of the cusp neighbourhood we consider increases as a function of θ_j and a function of θ_k. In other words when there is a $(1, j, k)$ hexagon visible from the cusp, volume of the cusp neighbourhood is bigger than when there is an $(1, j', k')$ hexagon visible from the cusp if $j' \leq j$ and $k' \leq k$.

As stated at earlier in this chapter, our goal is to show that a manifold N in $\mathcal{N}'_{c,c}$ has a volume exceeding that of N_0 unless it has a $(1, 1, 1)$ hexagon visible from the cusp. In the next two propositions, we will show that if a manifold in $\mathcal{N}'_{c,c}$ has a $(1, 2, 2)$ or a $(1, 1, 2)$ hexagon visible from the cusp then its volume is greater than that of N_0. The observation at

the end of the last paragraph means it is enough to consider only these two types of hexagons to rule out all other possible types of $(1, j, k)$ hexagons visible from the cusp except $(1, 1, 1)$ hexagons.

Proposition 5.3.2. *Let N be a manifold in $\mathcal{N}'_{c,c}$. Assume that the Delaunay tessellation of Λ determined by the lifts of λ_0 is a triangulation. If the side lengths of the triangles that forms the fundamental domain are $\theta_1, theta_2$ and θ_2 (or equivalently N has a $(1, 2, 2)$ hexagon visible from the cusp) then the volume of N is greater than the volume of N_0.*

Proof. Horocyclic arc lengths of the triangles are θ_1, θ_2 and θ_2. By taking $j = k = 2$ in 16 we can write the volume of the cusp neighbourhood outside the half ideal mas below.

$$\frac{1}{2}\left(\frac{\theta_1\sqrt{2(\theta_2)^2 - (\theta_1)^2}}{2} - \pi\left(\frac{\theta_1}{2}\right)^2\right)$$

By 5.1.1 we have θ_1 as a function of x_1.

$$\theta_1 = \frac{\sqrt{2(cosh(l_1) + 1)}}{e^K} = \frac{\sqrt{2(x_1 + 1)}}{e^K}$$

θ_2 can also be computed using 5.1.1. While it's not a function of x_1 , it can be bounded below by a function of x_1 as below and we denote it by $(\theta_2)_{min}$.

$$\theta_2 = \frac{\sqrt{2(cosh(l_2) + 1)}}{e^K}$$
$$\geq \frac{\sqrt{2(cosh(min\{E, F\}) + 1)}}{e^K} = (\theta_2)_{min}$$

The inequality above follows because $l_2 \geq min\{E, F\}$. Hence we have

$$\text{Volume of the cusp neighbourhood} \geq \frac{1}{2}\left(\frac{\theta_1\sqrt{2(\theta_2)^2_{min} - (\theta_1)^2}}{2} - \pi\left(\frac{\theta_1}{2}\right)^2\right)$$

Right hand side of the above inequality is a function of x_1. Let's denote it by $V_{\text{cusp}}^{(1,2,2)}(x_1)$. Now define

$$V_1(x_1) = V_{M_{l_1}}(x_1) + V_{\text{HIM}}(x_1) + V_{\text{col}}(x_1) + V_{\text{cusp}}^{(1,2,2)}(x_1)$$

where first three functions in the right hand side have the same meaning as in the volume estimation in chapter 1. They are volumes of the muffin around λ_1, half ideal muffin and the collar of the remaining part of the boundary of N respectively. V_1 defined as above bounds the volume of N by below. Graph of V_1 in the interval $[1.208, 1.216]$ is shown in figure 45. In that interval V_1 is always greater than 7.8. Hence we conclude volume of N is greater than that of N_0 in the presence of a $(1, 2, 2)$ hexagon visible from the cusp.
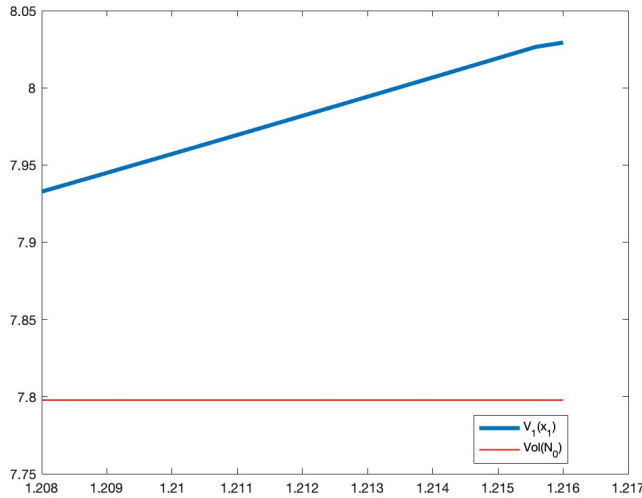
$\square$

Figure 45: Volume estimation when there is a $(1, 2, 2)$ hexagon visible from the cusp

Similarly we can analysis the presence of $(1, 1, 2)$ hexagons.

Proposition 5.3.3. *Let N be a manifold in $\mathcal{N}'_{c,c}$. Assume that the Delaunay tessellation of Λ determined by the lifts of λ_0 is a triangulation. If the side lengths of the triangles that*

forms the fundamental domain are θ_1, θ_1 and θ_2 (or equivalently N has a $(1, 1, 2)$ hexagon visible from the cusp) then the volume of N is greater than the volume of N_0.

Proof. In this case we need to take $j = 1$ and $k = 2$ in 16. Then the volume of the cusp neighbourhood outside the half ideal is.

$$\frac{1}{2} \left(\frac{\theta_2 \sqrt{4(\theta_1)^2 - (\theta_2)^2}}{2} - \pi \left(\frac{\theta_1}{2} \right)^2 \right)$$

The partial derivative of the square of the quantity $(\theta_2 \sqrt{4(\theta_1)^2 - (\theta_2)^2})$ with respect to θ_2 is $4\theta_2(2(\theta_1)^2 - (\theta_2)^2$ which is positive by 14. Hence the right hand side of the above equation increases with θ_2. By replacing θ_2 with its minimum value $(\theta_2)_{min}$ we can bound the volume of cusp by a function of x_1 as below.

$$\text{Volume of the remaining part of the cusp} \geq \frac{1}{2} \left(\frac{(\theta_2)_{min} \sqrt{4(\theta_1)^2 - (\theta_2)^2_{min}}}{2} - \pi \left(\frac{\theta_1}{2} \right)^2 \right)$$

Since $(\theta_2)_{min}$ is a function of x_1 the entire right hand side above also is a function of x_1. Let's denote it by $V_{\text{cusp}}^{(1,1,2)}(x_1)$. Now define

$$V_2(x_1) = V_{M_{l_1}}(x_1) + V_{\text{HIM}}(x_1) + V_{\text{col}}(x_1) + V_{\text{cusp}}^{(1,1,2)}(x_1)$$

Again first three functions in the right hand side above have same meanings as earlier and V_2 defined as above bounds the volume of N by below. Graph of V_2 in the interval $[1.208, 1.216]$ is shown in figure 46. In that interval V_2 is always greater than 7.8. Hence we conclude volume of N is greater than that of N_0 in the presence of a $(1, 1, 2)$ hexagon visible from the cusp.

$\square$

Now we are ready for the main result of this section that address the general case of $(1, j, k)$ hexagons visible from the cusp.
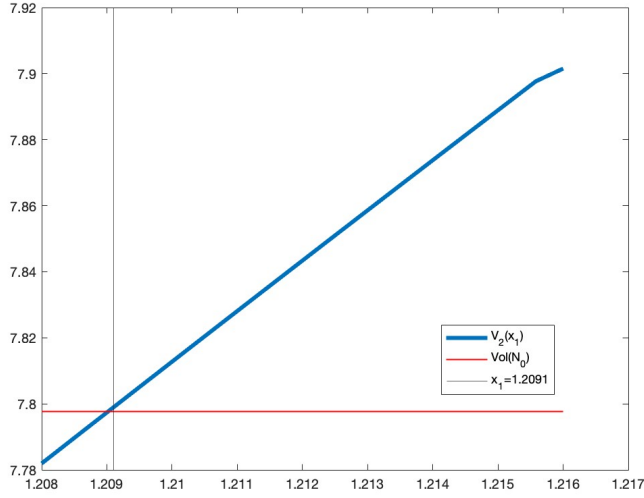
Figure 46: Volume estimation when there is a $(1, 1, 2)$ hexagon visible from the cusp

Proposition 5.3.4. *Let N be a manifold in $\mathcal{N}'_{c,c}$. Assume that the Delaunay tessellation of Λ determined by the lifts of λ_0 is a triangulation. If the volume of N does not exceed the volume of N_0 then one of the following is true.*

1. *$\tilde{N}$ has a $(1, 1, 1)$ hexagon visible from the cusp.*

2. *$\tilde{N}$ has a $(1, 1, k)$ hexagon visible from the cusp for some $k \geq 1$ and x_1 of N is between 1.208 and 1.2091.*

Proof. We know $\tilde{N}$ has a $(1, j, k)$ hexagon visible from the cusp $(1 \leq j \leq k)$. Horocyclic arc lengths of the triangles Δ_0 and Δ_1 that forms the fundamental domain of Λ are then θ_1, θ_j and θ_k. Using 16 we can write the volume of the part of the cusp outside the half ideal muffin as below.

$$\frac{1}{2}\left(\frac{\sqrt{(\theta_1 + \theta_j + \theta_k)(\theta_1 - \theta_j + \theta_k)(\theta_1 + \theta_j - \theta_k)(-\theta_1 + \theta_j + \theta_k)}}{2} - \pi\left(\frac{\theta_1}{2}\right)^2 \right)$$

This is a function of θ_1(hence of x_1), θ_j and θ_k. For simplicity let's denote it by $W(x_1, \theta_j, \theta_k)$. Note that W is not a function of x_1 entirely as θ_j and θ_k are not functions of x_1. As discussed earlier partial derivatives of W with respect to θ_j and θ_k are positive. Hence $W(x_1, \theta_j, \theta_k)$ increases with respect to both θ_j and θ_k

First assume $1 < j \leq k$. Then $\theta_2 \leq \theta_j \leq \theta_k$. Hence $W(x_1, \theta_j, \theta_k) > W(x_1, \theta_2, \theta_2)$. Note that

$$W(x_1, \theta_2, \theta_2) = \frac{1}{2}\left(\frac{\theta_1\sqrt{2(\theta_2)^2 - (\theta_1)^2}}{2} - \pi\left(\frac{\theta_1}{2}\right)^2\right) > V_{\text{cusp}}^{(1,2,2)}(x_1)$$

where $V_{\text{cusp}}^{(1,2,2)}(x_1)$ is the function in proposition 5.3.

Therefore we can bound the volume of N as below.

$$\text{Volume of N} \geq V_{M_{l_1}}(x_1) + V_{\text{HIM}}(x_1) + V_{\text{col}}(x_1) + W(x_1, \theta_j, \theta_k)$$
$$\geq V_{M_{l_1}}(x_1) + V_{\text{HIM}}(x_1) + V_{\text{col}}(x_1) + V_{\text{cusp}}^{(1,2,2)}(x_1) = V_1(x_1)$$

We already know $V_1(x_1)$ is always greater than 7.8 in the interval $[1.208, 1.216]$. Hence the volume of N exceeds the volume of N_0 if it has an $(1, j, k)$ hexagon visible from the cusp where $1 < j \leq k$.

If $1 = j < k$ then $\theta_1 = \theta_j < \theta_k$. Since W is increasing in θ_k we have $W(x_1, \theta_j, \theta_k) = W(x_1, \theta_1, \theta_k) > W(x_1, \theta_1, \theta_2)$. Note that

$$W(x_1, \theta_1, \theta_2) = \frac{1}{2}\left(\frac{\theta_2\sqrt{4(\theta_1)^2 - (\theta_2)^2}}{2} - \pi\left(\frac{\theta_1}{2}\right)^2\right) > V_{\text{cusp}}^{(1,1,2)}(x_1)$$

where $V_2\text{cusp}^{(1,2,2)}(x_1)$ is the function in proposition 5.3.3.

Therefore we can bound the volume of N as below.

$$\text{Volume of N} = V_{M_{l_1}}(x_1) + V_{\text{HIM}}(x_1) + V_{\text{col}}(x_1) + W(x_1, \theta_1, \theta_k)$$
$$\geq V_{M_{l_1}}(x_1) + V_{\text{HIM}}(x_1) + V_{\text{col}}(x_1) + V_{\text{cusp}}^{(1,1,2)}(x_1) = V_2(x_1)$$

We know $V_2(x_1)$ is greater than 7.8 in the interval $[1.2091, 1.216]$. Hence for a manifold with an x_1 value in this interval has a volume greater than that of N_0 if it has an $(1, 1, k)$ hexagon visible from the cusp for any $1 < k$.

Hence the only two possible scenarios where N has a volume less than that of N_0 are the ones listed in the statement. □

5.4 When the Delaunay tessellation of $\mathbb{R}^2$ determined by the feet of lifts of λ_0 contains a rectangle

The presence of rectangles in the tessellation of Λ can also be addressed using a similar volume bound. In fact, since the area of a rectangle involve only two pair of side lengths, computing a volume bound for the cusp neighbourhood as a function of x_1 is relatively easier.

Proposition 5.4.1. *Let N be a manifold in $\mathcal{N}'_{c,c}$. Assume that the Delaunay tessellation of Λ determined by the lifts of λ_0 has a rectangle as a $2-cell$. Then the volume of N is greater than the volume of N_0*

Proof. Let Δ be a $2 - cell$ in the Delaunay triangulation of Λ which is a rectangle. Deck transformations of the cusp act as Euclidean translations on Λ and transitively on the lattice points. Hence for each edge e of Δ there is a translation g in the cusp group such that $\Delta \cap g(\Delta)$ is e. Hence Δ forms a fundamental domain of Λ under the cusp group action. (Basically Δ plays the role $\Delta_0 \cup \Delta_1$ in the previous case where tessellation is a triangulation.) Again one pair of sides of Δ should have length θ_1. Let's take the side length of other pair to be θ_j

where $1 \leq j$. Then the area of the fundamental domain is $\theta_1 \cdot \theta_j$. Hence the volume of the part of the cusp neighbourhood outside the half ideal muffin is

$$\frac{1}{2}\left(\theta_1 \cdot \theta_j - \pi\left(\frac{\theta_1}{2}\right)^2\right)$$

Since $\theta_j \geq \theta_1$ we have the following.

$$\text{Volume of the remaining part of the cusp neighbourhood} \geq \frac{1}{2}\left(\theta_1^2 - \pi\left(\frac{\theta_1}{2}\right)^2\right)$$

Right hand side of the above inequality is a function of x_1 and let's denote it by $V_{\text{cusp}}^{\text{rec}}$. Finally define

$$V_3(x_1) = V_{M_{l_1}}(x_1) + V_{\text{HIM}}(x_1) + V_{\text{col}}(x_1) + V_{\text{cusp}}^{\text{rec}}(x_1)$$

where first three functions in the right hand side have the same meaning as earlier and V_3 defined as above bounds the volume of N by below. Graph of V_3 in the interval $[1.208, 1.216]$ is shown in figure 47. In this interval V_3 is always greater than 7.8. Hence we conclude volume of N is greater than that of N_0 in the presence of rectangles in the Delaunay tessellation of Λ. $\qquad\square$

We conclude this section by recording the following corollary which summarise our work so far in this chapter.

Corollary 5.4.2. *Let N be a manifold in $\mathcal{N}'_{c,c}$. If the volume of N does not exceed the volume of N_0 then one of the following is true.*

1. $\tilde{N}$ has a $(1,1,1)$ hexagon visible from the cusp.

2. $\tilde{N}$ has a $(1,1,k)$ hexagon visible from the cusp for some $k \geq 1$ and x_1 of N is between 1.208 and 1.2091.

Proof. By lemma 5.1.3, Delaunay tessellation of Λ in $\tilde{N}$ can only have triangles or rectangles. By 5.4 if it has rectangles then the volume of N is greater than the volume of N_0. If the tessellation is a triangulation then 5.3.4 says the volume of N exceeds the volume of N unless one of the two listed possibilities in the statement is true for N. $\qquad \square$
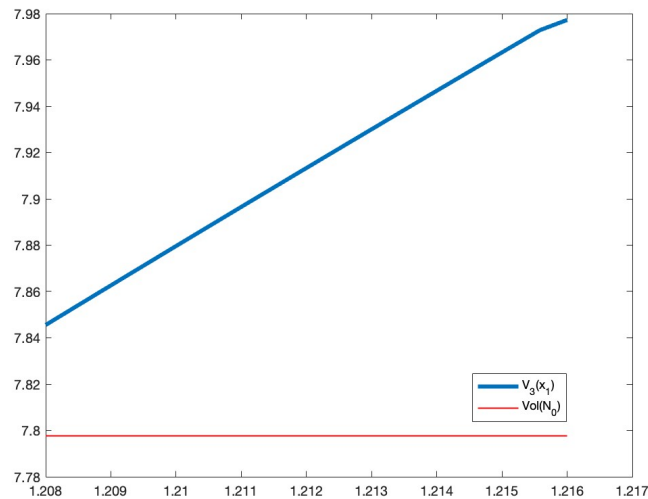

Figure 47: Volume estimation when there is a rectangular $2-$ cell in the lattice of Λ

In chapter 6 and 7 we will explain our work in dealing with a manifold N in $\mathcal{N}'_{c,c}$ which has a $(1, 1, 1)$ hexagon visible from the cusp. (case (1) in corollary 5.4.2)

6.0   With $(1, 1, 1)$ hexagons visible from the cusp

From now we assume N to be a manifold in $\mathcal{N}'_{c,c}$ such that $\tilde{N}$ has a $(1, 1, 1)$ hexagon visible from the cusp. Let H_0 be a one such $(1, 1, 1)$ hexagon in $\tilde{N}$. Then the corresponding Euclidean triangle on the lattice of Λ is equilateral and all three sides of it has horocyclic arc lengths θ_1. Let Δ_0 be this triangle. Then as explained in lemma 14 there is another equilateral triangle with same side lengths in the lattice that shares an edge with Δ_0. Let Δ_1 be this triangle. Since the horocyclic side lengths of Δ_1 is also θ_1 there is another $(1, 1, 1)$ hexagon visible from the cusp which lies underneath Δ_1. Let H_1 be this second $(1, 1, 1)$ hexagon. It shares an internal edge with H_0. (See figure 48)

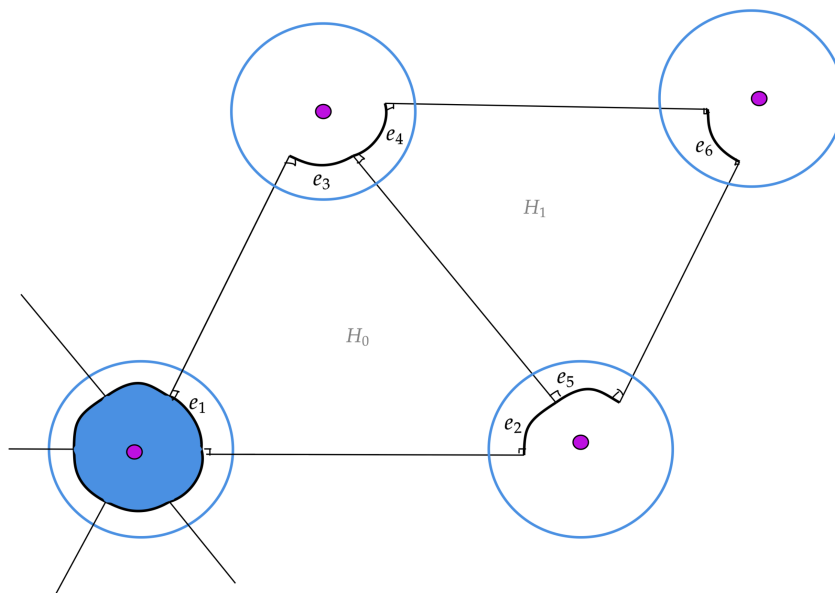Figure 48: Two $(1, 1, 1)$ hexagons visible from the cusp

Let's label the external edges of H_1 and H_2 by $e_1, e_2, \ldots e_6$ as shown in figure 48. It turns out the collection of exterior edges of H_0 and H_1 project under the covering map to form a graph on ∂N with two vertices and a complementary region which is a hexagon. To see this we will first need the following lemma.

Lemma 6.0.1. *The collection of interiors of external edges of H_1 and H_2 project homeomorphically onto ∂N.*

Proof. If two $(1,1,1)$ hexagons have external edges on the same boundary component in $\tilde{N}$ then their intersection is either empty or an interior edge.(Lemma 6.4, [4])

Suppose e_i and e_j be two distinct edges in the collection of exterior edges of H_0 and H_1 and the projection of their interiors under covering map has non empty intersection. Then there is a deck transformation g of $\tilde{N}$ such that $int(g(e_i)) \cap int(e_j) \neq \emptyset$. Without loss generality assume $e_1 \subset H_0$. Then $g(e_i)$ is an exterior edge of the $(1,1,1)$ hexagon $g(H_0)$.

If e_j is also another external edge of H_0 then $g(H_0) \cap H_0 \neq \emptyset$. Then it follows $g(H_0) = H_0$ by the property of $(1,1,1)$ hexagons mentioned at the beginning of the proof. Then g takes the corresponding Euclidean triangle Δ_0 to itself.

If e_j is an external edge of H_1 we have $g(H_0) = H_1$ as a consequence of the same property. Hence g takes Δ_0 to Δ_1.

Recall that $\Delta_0 \cup \Delta_1$ is a fundamental domain of Λ. Hence there is no non trivial deck transformation that takes Δ_0 takes itself or to Δ_1. Hence g has to be the identity. But this is a contradiction as e_i and e_j are distinct. □

We just proved that interiors of external edges of H_1 and H_2 project homeomorphically onto ∂N. These projections are geodesic arcs that connect the end points of λ_0 or loops at an end point of λ_0 and forms a graph on ∂N. This graph will play a prominent role in subsequent sections. We denote it by G.

Definition 6.0.2. $G =$ Graph on ∂N which has end points of λ_0 as vertices and projections of external edges of the two $(1,1,1)$ hexagons as edges.

Consider the region on a component of $\partial \tilde{N}$ bounded by these external edges and/or their deck transformations. (Blue hexagon in figure 48). Then the projection of this hexagon is a complementary region on ∂N. **Our next task is to understand the other complementary region(s)** that combined with the projection of the blue hexagon to form the boundary of N which is a genus 2 surface. We start by orienting H_1 and H_2 as described below.

First by slight abusing the notation, we give the same label to all the deck transformations of an external or an internal edge of H_0 or H_1. We also use the same label B_1 to denote a hexagon on a component of $\partial \tilde{N}$ bounded by external edges of H_1 and H_2 and its projection onto ∂N which is a complementary region. We orient both H_1 and H_2 counterclockwise as seen from above. If $\tilde{\lambda}_1, \tilde{\lambda}'_1$ and $\tilde{\lambda}''_1$ are the interior edges of H_0 as shown in figure 49 then we orient λ_0 in N such that projections of $\tilde{\lambda}_1$ and $\tilde{\lambda}'_1$ are orientation preserving homeomorphisms. Our approach varies depending on whether $\tilde{\lambda}''_1$; the remaining interior edge of H_0 is projected orientation preserving or reversing.
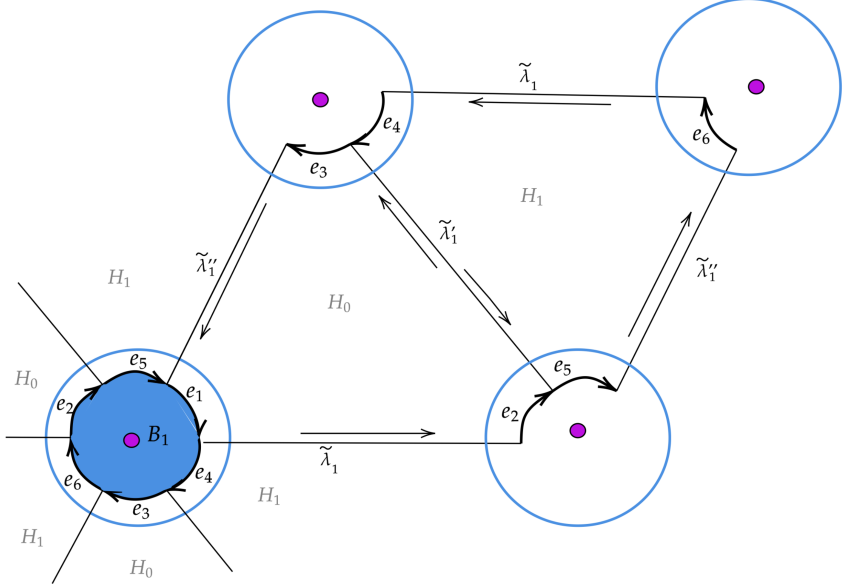

Figure 49: Orienting H_0 and H_1

107

6.1 Projection of $\tilde{\lambda}''_1$ an orientation preserving homeomorphism

Denote the feet of λ_0 on ∂N and their lifts on $\partial \tilde{N}$ by ⬤ and ▲. If interior edges $\tilde{\lambda}_1$ and $\tilde{\lambda}'_1$ of H_0 are from ⬤ to ▲, then we orient λ_0 in the same direction so that projections of $\tilde{\lambda}_1$ and $\tilde{\lambda}'_1$ are orientation preserving. If the projection of the remaining interior edge of H_0, $\tilde{\lambda}''_1$ is also OP then $\tilde{\lambda}''_1$ should also be directed from ⬤ to ▲ as shown in figure 50.
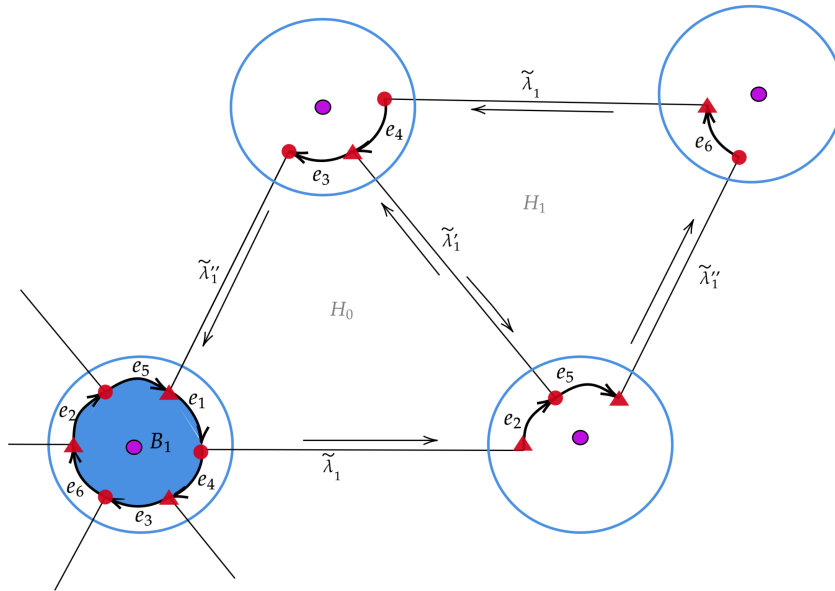
Figure 50: When $\tilde{\lambda}''_1$ is projected as an OP homeomorphism

With this orientation of H_0 and H_1, their exterior edges (and their projections) are directed from one feet of λ_0 to the other and creates a *theta* graph on ∂N with two vertices. Now let's look at B_1 which is of the complementary regions of the graph G in ∂N (See figure 51). B_1 is a hexagon and its boundary edges are same as the edges of the graph G on ∂N, hence directed from one feet of λ_0 to the other. In particular none of the edges of B_1 are loops. Now let's try to understand other complementary regions of ∂N. We know none of the edges of the hexagon B_1 are glued to another edge in B_1 (because the collection

of exterior edges were projected homeomorphically). So B_1 is simply connected and all of its edges must be glued together with edges of other complementary regions to form ∂N. These other complementary regions may not be simply connected. Our strategy is to add new edges to the graph we have till all complementary regions become simply connected. By doing so we obtain a cell decomposition of ∂N with two vertices such that these simply connected regions as its faces.
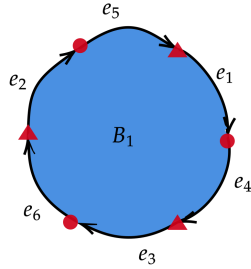
Figure 51: Complementary region of G in ∂N bounded by external edges of $(1,1,1)$ hexagons

There are certain edge gluings that needs to be avoided in a cell decomposition. These are depicted in figure 52. The one in the left yields an isolated vertex while the one in the right yields a non orientable quotient. Note that B_1 does not have any such gluing. The point is none of the complementary regions in the cell decomposition we are going to build can have these gluing patterns.

Figure 52: Edge gluings that are forbidden

All the remaining complementary regions are already simply connected without any additional edges :

In this case every boundary edge of B_1 is glued to an edge of a different complementary region and there are no other edges. Hence a cell decomposition of ∂N is given by 2 vertices and 6 edge classes. If f is the number of faces of the cell decomposition then we have $2 - 6 + f = -2$ as $\chi(\partial N)$ is -2. So $f = 2$ which means there is one complementary region other than B_1. Let's denote it by B_2. Since there are only 6 edge classes, B_2 must also be a hexagon and each of B_1 should be glued to an edge of B_2.

One additional edge is required to make all complementary regions simply connected :

In this case there are 7 edge classes. If f is the number of faces in the cell decomposition then we obtain $f = 3$ by doing the same Euler characteristic computation. Hence there are two complementary regions other than B_1. Let's denote them by B_2 and B_3. Total number of edges of B_2 and B_3 should add up to 8. 6 of those will be glued to edges of B_1 and the other 2 should be glued to each other to form the additional edge class we needed in this case to make all complementary regions simply connected. We have following possibilities.

- Both B_2 and B_3 are rectangles
- B_2 is a triangle and B_3 is a pentagon

Now let's investigate the possible edge gluings in each case. In the diagrams below we color an edge of a complementary component by black if it is glued to an edge of B_1. We color it by purple if it belongs to the additional edge class we needed.

If both B_1 and B_2 are rectangles, then there are only two possible ways of pairing edges. These are shown in the top row of figure 53. In the top left case once the purple edges are glued, union of B_1 and B_2 will be simply connected. But this contradicts with the assumption that purple edges are needed to make complementary regions simply connected. Top right case is also not possible because if the purple edges are glued that way, B_2 will not be simply connected.
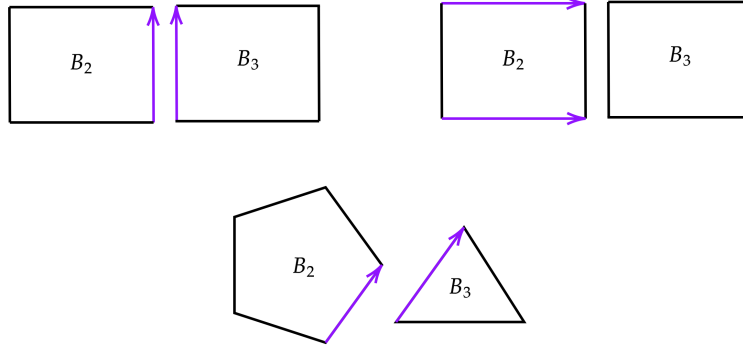
Figure 53: One added edge class

Now let's consider the second case when B_2 is a triangle and B_3 is a pentagon. If one of the complementary regions is a triangle then at least one of its edges is a loop. Since none of B_1's edges is a loop this means its not possible to pair all edges of the triangular region with edges of B_1. Hence one edge of the triangle should belongs to the additional edge class and must be glued to an edge of the pentagon. (Figure 53 bottom). This again yields a contradiction as B_2 and B_3 glued along the additional (purple) edge makes their union simply connected rendering the addition of a new edge class unnecessary.

Two additional edge are required to make all complementary regions simply connected :

In this case there are 8 edge classes. If f is the number of faces in the cell decomposition then we obtain $f = 4$ by doing the same Euler characteristic computation. Hence there are three complementary regions other than B_1 and let's denote them by B_2, B_3 and B_4. Total number of edges of these 3 regions must be 10 and 6 of those should again be glued to edges of B_1. Other other 4 must be paired to form the two additional edge class we needed to make all complementary regions simply connected. The only possibility is to have two triangles (say B_2 and B_3) and a rectangle. (B_4)

Let's try to understand the possible edge pairings for this arrangement. Let e_7 and e_8 be the two additional edge classes. As mentioned earlier, not all edges of a triangular region can be glued to edges of B_1. Hence in both B_2 and B_3 at least one edge must belong a new edge class. Suppose both triangles has an edge that belongs to the class e_7. If both edges of the class e_8 belong to B_4 then it would not be simply connected. (Figure 54 top left). If one edge of the class e_8 belongs to B_4 and the other belong to one of the triangles (top right)then the union of B_2, B_3 and B_4 glued along e_7 and e_8 will be simply connected. This contradicts with the assumption, e_7 and e_8 is needed to make complementary components simply connected. If both edges of e_8 also belong to triangles (bottom left) then the remaining edge of both these triangles that should be paired with edges of B_1 will be loops. But no edge of B_1 is a loop. Finally if no edge of B_2 is paired with an edge of B_3 (bottom right) then their edges that belongs to additional edge classes must be paired with edges of B_4. But this again makes the union of B_2, B_3 and B_4 glued along e_7 and e_8 simply connected.

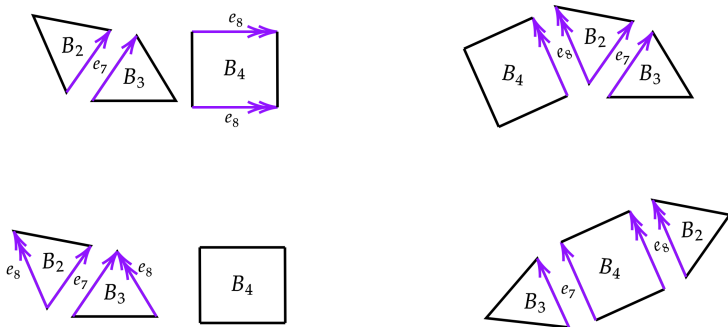Figure 54: Two added edge classes

Three additional edge are required to make all complementary regions simply connected :

In this case there are 9 edge classes. If f is the number of faces in the cell decomposition then we obtain $f = 5$ by the Euler characteristic computation. Hence there are four complementary regions other than B_1. Denote them by B_2, B_3, B_4 and B_5. Total number

of edges of these 4 regions must be 12. 6 of those should again be glued to edges of B_1. Other other 6 must be paired to form the three additional edge class we needed to make all complementary regions simply connected. The only way this could happen is when all four of B_2, B_3, B_4 and B_5 are triangles.

Let e_7, e_8 and e_9 be the three additional edge classes. Recall that not all edges of a triangular region can be glued to edges of B_1. Hence each of the four triangular regions have at least one edge that belongs to one of e_7, e_8 or e_9. Furthermore there should be at least one pair of triangles that are glued along one of these edges.

Without loss of generality assume B_2 and B_3 are glued along e_7. Now if one of these two triangles have an edge belong to e_8 or e_9 then the other can not have an edge that pairs with it. Otherwise it would create two loops that must be glued to B_1 (similar to the two triangles in bottom left of figure 54) or would force the remaining edges of B_2 and B_3 to be also paired by the remaining edge class between e_8 and e_9. Both these scenarios are not possible hence the claim that if one of B_2 or B_3 have an edge belong to e_8 or e_9 then the other can not have an edge that pairs with it is correct. Without loss of generality assume B_2 has an edge belong to e_8 and B_3 does not. Also assume B_4 is glued to B_2 along e_8. Hence one edge of B_5 must belong to class e_9 and glued to an edge in the union of B_2, B_3 and B_4 which are already glued along e_7 and e_8. Irrespective of with which edge its paired, the union of all four triangles will be simply connected once the pairing is done. This is the usual contradiction we obtained in previous cases. If both B_2 and B_3 have no edges belong to classes e_8 and e_9 then all four edges that belongs to these two classes will belongs to $B4$ and B_5. This will also yield a contradiction as it creates loops that should be glued to edges of B_1.

Note that it's not possible to add more than three new edges to create the cell decomposition of ∂N. To see this first note that he Euler characteristic computation shows that each added edge class increase the number of complementary regions by one. Also each added edge class contributes to only two new edges belong to complementary regions other than B_1. This means after some point there will not be enough edges to form all the com-

plementary regions. For an example with 4 added edges there will be five complementary regions other than B_1 but there are only 14 edges to make all of them which is not possible.

The discussion above was built around the main assumption interior edge $\tilde{\lambda}''_1$ of H_0 preserve orientation under the covering map. The discussion addressed the possible complementary regions of ∂N and it follows all the addressed cases except one yields contradictions. The only possibility that did not yield a contradiction is the first one ; no additional edges are required to make complementary regions simply connected. In this case there is only one other complementary region. We denoted it by B_2. Recall that B_2 is also a hexagon and each edge of B_2 is paired with an edge of B_1 to form ∂N.

6.2   Projection of $\tilde{\lambda}''_1$ an orientation reversing homeomorphism

If the projection of the remaining interior edge of H_0 , $\tilde{\lambda}''_1$ is OR then $\tilde{\lambda}''_1$ should be directed from ▲ to ● as shown in figure 55.

The complementary component B_1 in ∂N for this case is shown in figure 56 To figure out the possibilities for other complementary component(s) in this case, Euler characteristic arguments used in the previous section can also be used to some extent. The only difference is three edges in the graph G are loops now where as in the previous case when $\tilde{\lambda}'_1$ is projected OP, there were none. Recall that when when $\tilde{\lambda}'_1$ is projected OP, the only possibility for other complementary components in addition to B_1 was a single hexagon. But in this case, due to the presence of loops in G, we have one more possibility. These are listed below.

- No additional edges needed to make all complementary regions simply connected. There is only one complementary component in addition to B_1 and it's a hexagon.
- Two additional edge classes is needed to make all complementary regions simply connected. There are three more complementary components in addition to B_1 ; two trian-
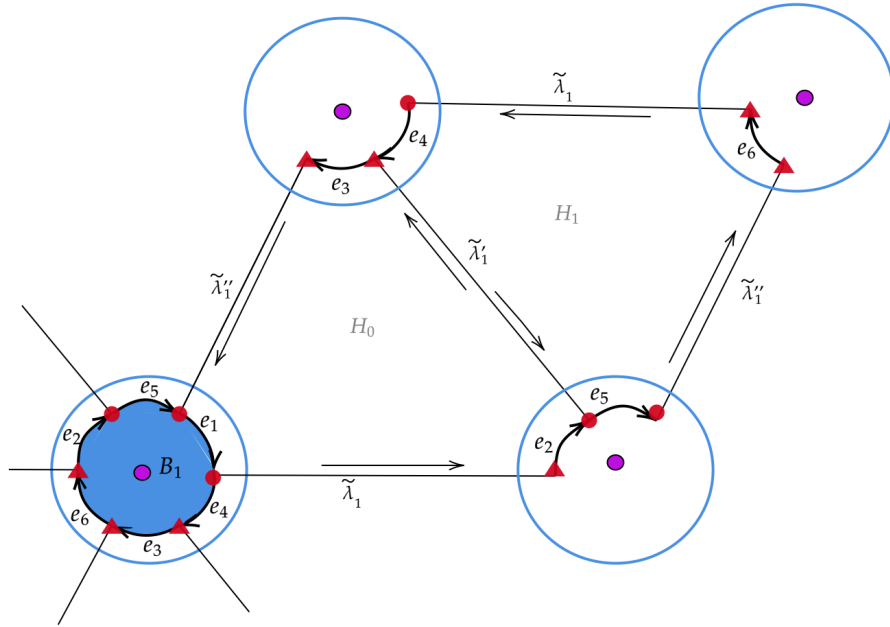
114

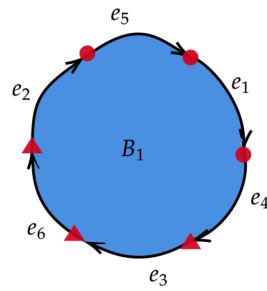Figure 55: When $\tilde{\lambda}_1''$ is projected as an OR homeomorphism

Figure 56: B_1 when $\tilde{\lambda}''_1$ is projected OR

gles and a rectangle. Two triangles are glued together to make an annulus.

6.3   When ∂N has two complementary regions

We know the interior edges of H_0 and H_1 bounds a hexagonal region in $\partial \tilde{N}$ which projects into a complementary region in ∂N. We denoted it by B_1. We oriented hexagons H_0 and H_1 which in turn induced an orientation on B_1. Figure 57 left shows B_1 with this induced orientation when $\tilde{\lambda}_1''$ is projected OP. Right hand side of the same figure is when $\tilde{\lambda}_1''$ is projected OR.
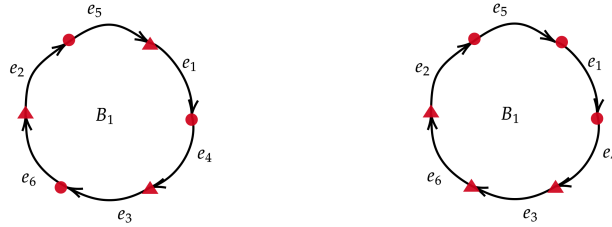
Figure 57: Edge labels of the complementary region B_1 when $\tilde{\lambda}_2''$ is projected OP(left) and OR(right)

In the last two sections we discussed other possible complementary regions for both of these cases. It follows from those discussions that there are only possibilities for other complementary regions.

- One more simply connected complementary region that is a hexagon. (Possible for both $\tilde{\lambda}_1''$ is projected OP and OR)
- Three more simply connected complementary regions ; Two triangles and a rectangle. (Possible only when $\tilde{\lambda}_1''$ is projected OR)

Throughout the remainder of this chapter and also in the next chapter we will describe our work analysing the first possibility ; when there are two complementary regions of G in ∂N both if which are hexagons. The latter case when there are three more complementary regions is remained to be analysed.

From now on we assume ∂N has two complementary regions in G. Then both regions are hexagons. We have already denoted one such a region by B_1. We denote the other complementary region by by B_2. Each edge of B_2 is paired with an edge of B_1 to form ∂N. In this subsection, we try to classify all the possible edge labellings of B_2. To be precise, an edge labelling of B_2 should be so that the resulting quotient is a

- A surface
- Oriented
- Has two vertex quotients which are ● and ▲

In fact if there are only two vertex quotients matching vertex quotients which are ● and ▲ then the it ensure a link of each vertex class is a topological circle making the resultant quotient to be a surface. So we only need the edge labellings that satisfy last two conditions listed above. In figure 58 we include all the possible labellings that satisfy those two conditions.

The first three pairings belong to the case when $\tilde{\lambda}_2''$ is projected OP and the last one belongs to the case when $\tilde{\lambda}_2''$ is projected OR. While all of these labellings satisfy the conditions listed earlier hence produce a surface, it turns out not all of them produce a surface that are "compatible" with the projections of our $(1, 1, 1)$ hexagons. We will next properly explain what we meant by "compatibility" and show two of the edge labellings in figure 58 fail to be "compatible".

We will start with the first edge labelling in figure 58. Figure 59 shows how exterior edges are attached to the end points of λ_0. Now let's consider a small strip along $\tilde{\lambda}_1'$ that lies in
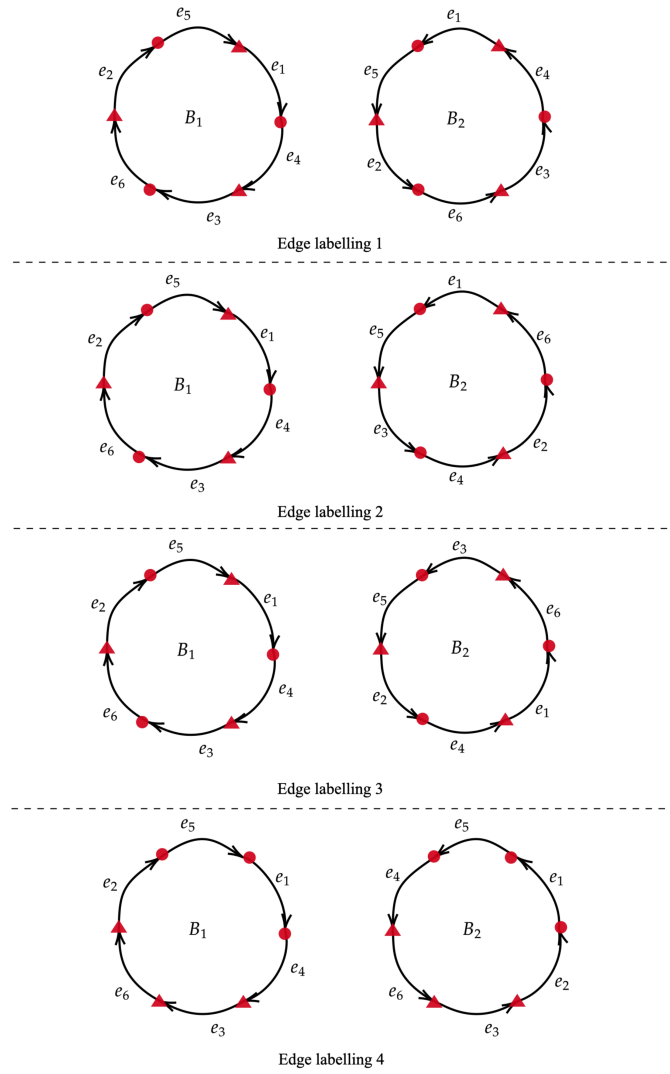
Figure 58: Edge labellings of B_1 and B_2 that can yield an oriented surface with two vertices
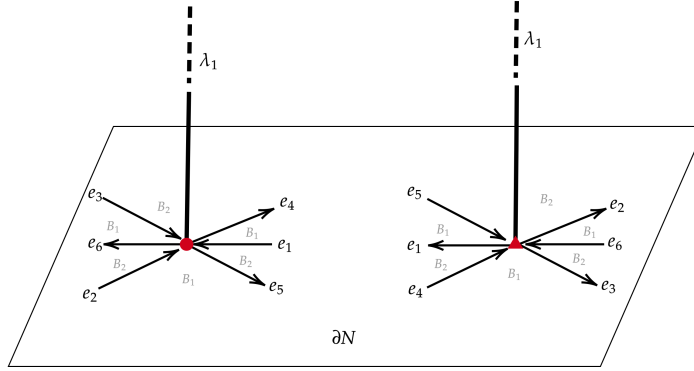
118

Figure 59: Edge labelling 1 : How external edges are attached to end points of λ_1

H_0 (figure 60 top). Then its projection will be attached along λ_1, e_1 near ● and e_2 near ▲ as shown in the bottom of the same figure.

Similarly we can consider strips along other 5 interior edges of H_0 and H_1 and their projections should be attached along λ_1 and corresponding exterior edges near ● and ▲. In figure 61 we show three such strips.

Now let's consider an arbitrary lift $\overline{\lambda_1}$ of λ_1. Then each of the six strips mentioned above determine a unique $(1, 1, 1)$ hexagon that intersect along $\overline{\lambda_1}$. In particular three strips shown in the bottom of figure 61 lifts to be contained in three different $(1, 1, 1)$ hexagons each of which now share $\overline{\lambda_1}$ as an interior edge. See figure 62. When we attach these $(1, 1, 1)$ hexagons to $\overline{\lambda_1}$, it should be done in a way so that adjacency is preserved. In particular if two $(1, 1, 1)$ hexagons are adjacent near one end point of $\overline{\lambda_1}$ then they must also be adjacent near the other end point. In the figure 38 blue and yellow strips (hence the hexagons that contain them) are adjacent near ● but they are separated by two exterior edges e_2 and e_5 near ▲. So in order for the yellow strip to be adjacent to the blue strip near near ▲ , the hexagon containing the yellow strip should go through the hexagons containing e_2 and e_5. This can not happen as $(1, 1, 1)$ hexagons can only intersect along an interior edge. Hence

119
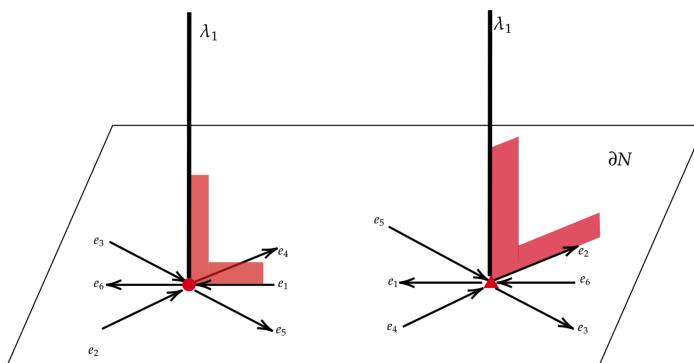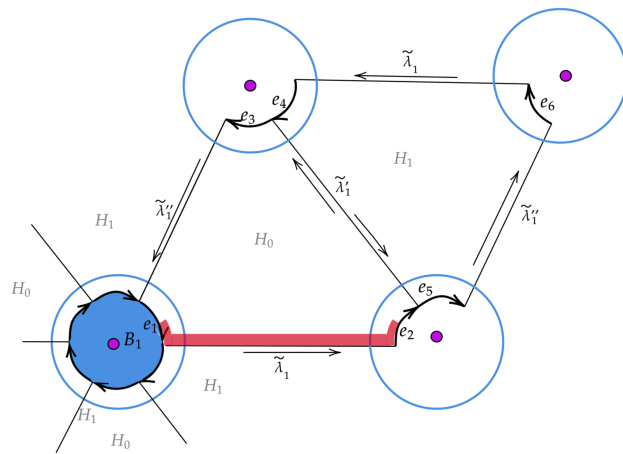
Figure 60: A strip along an internal edge
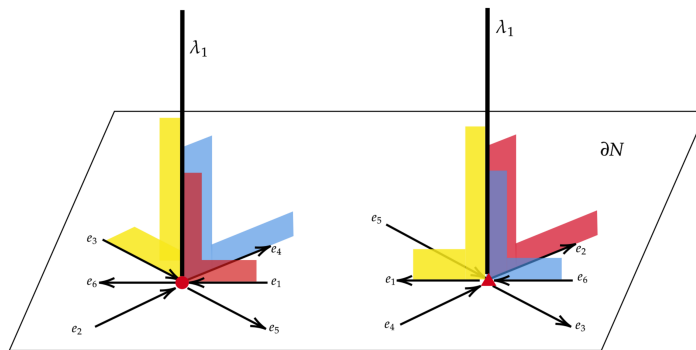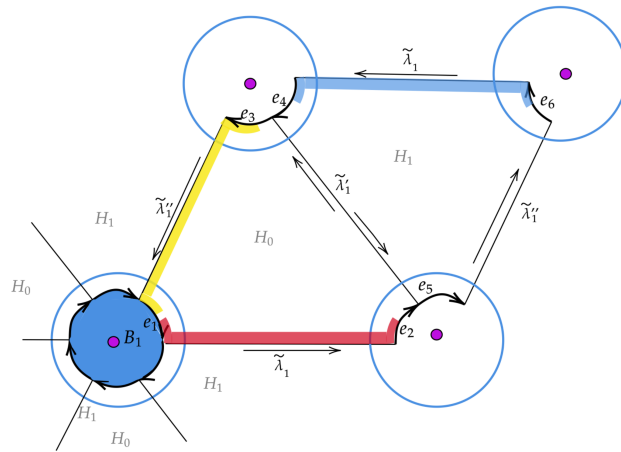
Figure 61: Small 'strips' inside H_0 and H_1 and their projections

the first edge labelling in figure 58 does not produce a surface to which we can attach our two $(1, 1, 1)$ hexagons along the labelled exterior edges in the proper order.
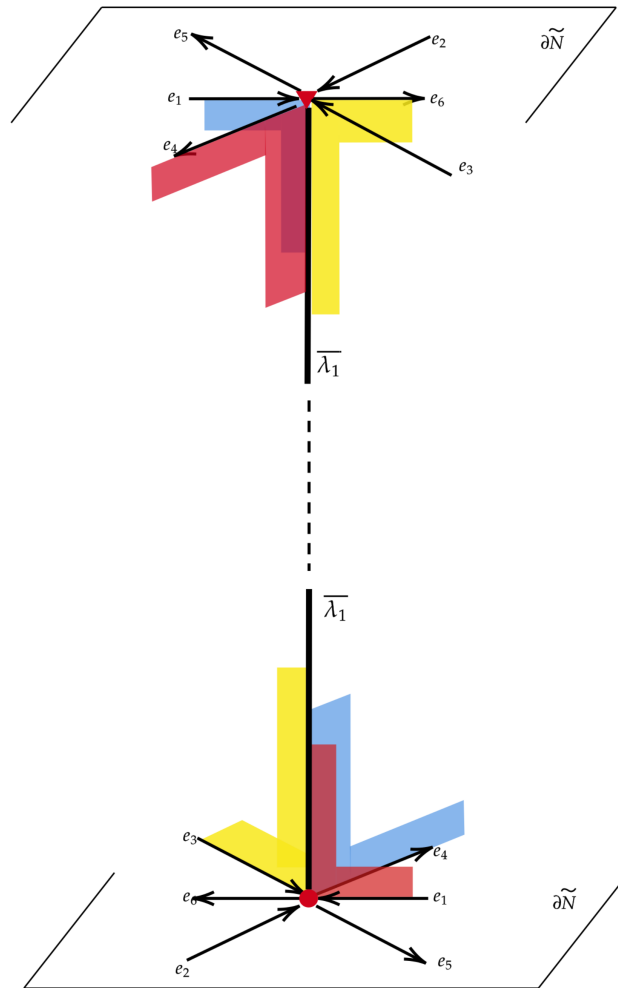
Figure 62: Strips of edge labelling 1 do not align properly along λ_1

We then performed the same analysis on other three labellings. Second and third labellings passes this test of adjacency. But the fourth edge labelling fails it as shown in figure 63
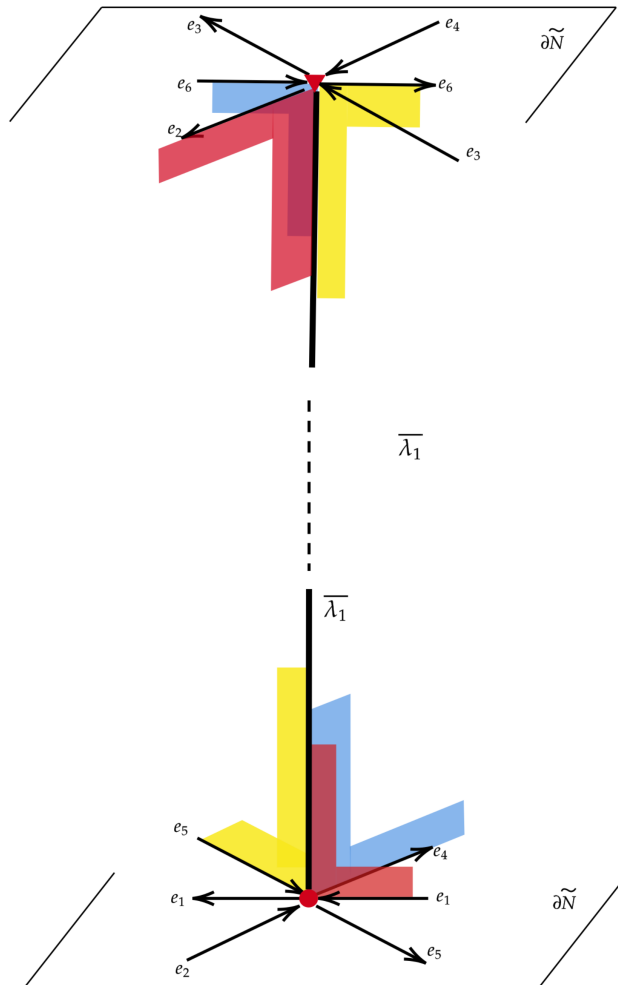
Figure 63: Same issue with the strips of edge labelling 4

Hence we are left with only two pairs of possible edge labellings (second and third labellings in figure 58) such that their resultant quotient produce ∂N. Next we will show both of them are actually the "same" meaning one can be obtained by a simple relabelling of the other. We show this by using a cellular map from one labelling to the other which we define below.

Notation : We denote B_1 and B_2 in the second edge labelling by B_1' and B_2' and B_1 and B_2 in the third edge labelling by B_1'' and B_2''.

To define a cellular map from from the second labelling to the third labelling, it's enough to specify how a single edge of B_1' or B_2' is mapped to an edge of B_1'' or B_2''. We start by mapping e_1 in B_1' to e_1 in B_1'' orientation reversingly. This determines how remaining edges of B_1' should be mapped into edges of B_1''. By traversing in along B_1 in the direction its oriented, we see edges of B_1' should be mapped as below.

- $e_1 \in B_1' \Rightarrow e_1 \in B_1''$ OR
- $e_4 \in B_1' \Rightarrow e_5 \in B_1''$ OR
- $e_3 \in B_1' \Rightarrow e_2 \in B_1''$ OR
- $e_6 \in B_1' \Rightarrow e_6 \in B_1''$ OR
- $e_2 \in B_1' \Rightarrow e_3 \in B_1''$ OR
- $e_5 \in B_1' \Rightarrow e_4 \in B_1''$ OR

We know $e_1 \in B_1'$ is glued to $e_1 \in B_2'$ in the second edge labelling. We also know $e_1 \in B_1'$ is mapped to $e_1 \in B_1''$ orientation reversingly under the cellular map we are constructing. Furthermore $e_1 \in B_1''$ is glued to $e_1 \in B_2''$ in the third edge labelling. Hence $e_1 \in B_2'$ should be mapped to $e_1 \in B_2''$. Now there are two ways to define the map on remaining edges of B_2'.

Method 1 : We can continue in the same way. This means if $e_i \in B_1'$ is mapped to $e_j \in B_2''$ then we map $e_i \in B_2'$ to $e_j \in B_2''$. This yield the following map on the edges of B_2'.

- $e_1 \in B_2' \Rightarrow e_1 \in B_2''$ OR
- $e_2 \in B_2' \Rightarrow e_3 \in B_2''$ OR
- $e_3 \in B_2' \Rightarrow e_2 \in B_2''$ OR

124

- $_{e4} \in B_2' \Rightarrow e_5 \in B_2''$ OR

- $_{e5} \in B_2' \Rightarrow e_4 \in B_2''$ OR

- $_{e6} \in B_2' \Rightarrow e_6 \in B_2''$ OR

Method 2 : Since we know how one edge of B_2' is mapped by traversing along B_1' in the direction it's oriented, we can define the cellular map on the remaining edges of B_2'. This method yields the following map.

- $_{e1} \in B_2' \Rightarrow e_1 \in B_2''$ OR

- $_{e4} \in B_2' \Rightarrow e_5 \in B_2''$ OR

- $_{e2} \in B_2' \Rightarrow e_3 \in B_2''$ OR

- $_{e5} \in B_2' \Rightarrow e_4 \in B_2''$ OR

- $_{e3} \in B_2' \Rightarrow e_2 \in B_2''$ OR

- $_{e6} \in B_2' \Rightarrow e_5 \in B_2''$ OR

Both methods yields the same map, hence the map determined by sending $_{e1} \in B_1'$ to $e_1 \in B_1''$ orientation reversingly is well defined. Hence the cell decomposition in the second edge pairing is simply an orientation reversing relabelling of the cell decomposition in the third edge pairing. Hence we will only analyse the cell decomposition in the third edge pairing going forward.

6.4   Thickening up of the two-complex

In the preceding sections, we analysed complementary regions of ∂N and possible ways of labelling their edges. To summarise the discussion so far : We assumed there are only two complementary regions in ∂N, both of which are hexagons. There were four possible ways of labelling the edges of these hexagons (figure 58) initially. We further reduced this to only two by showing the other two labellings are not "compatible" with the $(1, 1, 1)$ hexagons. Finally we showed remaining two edge labellings are actually the "same". Hence we only

have to analyse one of them which is shown in figure 64.
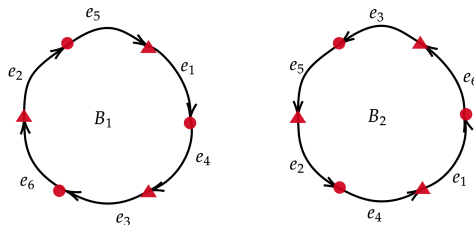
Figure 64: Edge labellings of B_1 and B_2 that can yield an oriented surface with two vertices

Now consider the $2-$ complex lying inside our manifold N which consists of the following.

- Union of cell decompositions B_1 and B_2 as shown in figure 64
- Shortest return path λ_1
- Projections of H_0 and H_1 under the covering map (which we also denote by H_0 and H_1 by slightly abusing the notation)

Our next task is to analyse the manifold obtained by thickening up this $2-$ complex. This thickened up $2-$ complex consists of the following.

- $(B_1 \times I) \cup (B_2 \times I)$
- $\lambda_1 \times D^2$
- $H_0^* \times I \cup H_1^* \times I$

where $I = [0, 1]$ and D^2 is the unit disk. H_i^* are obtained by removing a neighbourhood of λ_0 in H_i. We then attach $H_i^* \times I$ along the tube $\lambda_1 \times D^2$. We denote this thickened complex by X_N.

6.4.1   Boundary of X_N

$B_1 \cup B_2$ is a boundary component of this thickened complex X_N. We want to understand the other boundary components of X_N.

126

$H_i^* \times I$ are attached to this tube

$\lambda_1 \times D^2$

λ_1

e_2 B_2
B_1
e_5
B_2
e_3 B_1
e_4
B_1
e_1
e_6

e_5 B_2
B_1
e_1
B_2
e_4 B_1
e_2
B_1
e_6
B_2
e_3

$(B_1 \times I) \cup (B_2 \times I)$
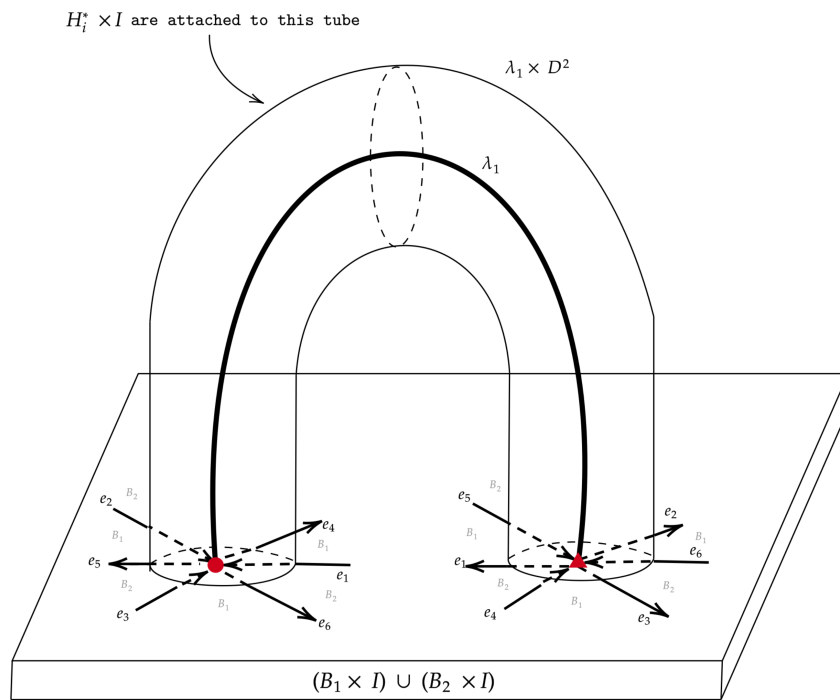
Figure 65: Thickened up $2-$ complex X_N

127

First we orient I such that $H_i^* \times 1$ face the cusp of N. Figure 66 shows $H_i^* \times 1$s seen from the ∞ in the universal cover.
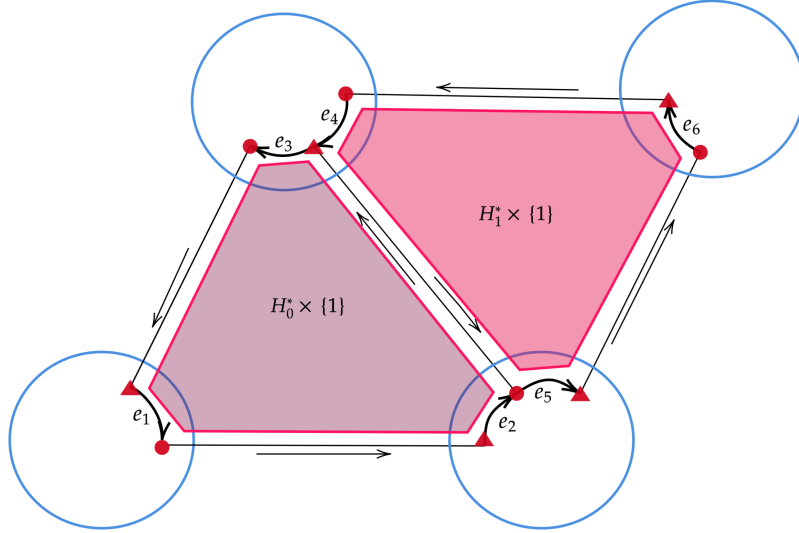
Figure 66: $H_i^* \times \{1\}$ seen from ∞

We orient $H_i^* \times 1$ using the orientation of H_i. Three edges in an $H_i^* \times 1$ are running parallel to exterior edges of H_i. If an edge of $H_i^* \times 1$ is parallel to e_j then we label that edge of $H_i^* \times 1$ by e_j^*. We give the same labelling to the end points of e_j^* as end points of e^j. Figure 67 shows orientations of $H_i^* \times 1$s with these labels.

$H_i^* \times 1$s are also part of the boundary of X_N. But the question is what are the other parts of the boundary component of X that contain them. To identify these remaining parts, we need to look at how $H_i^* \times 1$s are attached to the tube $\lambda_1 \times D^2$ closely. For the moment let's specifically focus on attaching $H_0^* \times 1$ and $H_1^* \times 1$ to the tube near ● and in the region between e_3 and e_6 as shown in figure 68. e_3 is running into ● while e_6 is running out of ●. Note that the region between these two edges on ∂N belongs to B_1. There is a strip on the boundary $\lambda_1 \times S^1$ of the tube $\lambda_1 \times D^2$ (colored in purple) that connects $H_0^* \times 1$ to $H_1^* \times 1$.
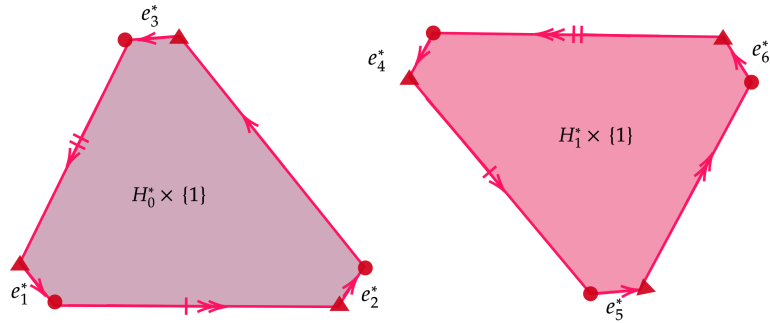
Figure 67: $H_i^* \times \{1\}$ oriented
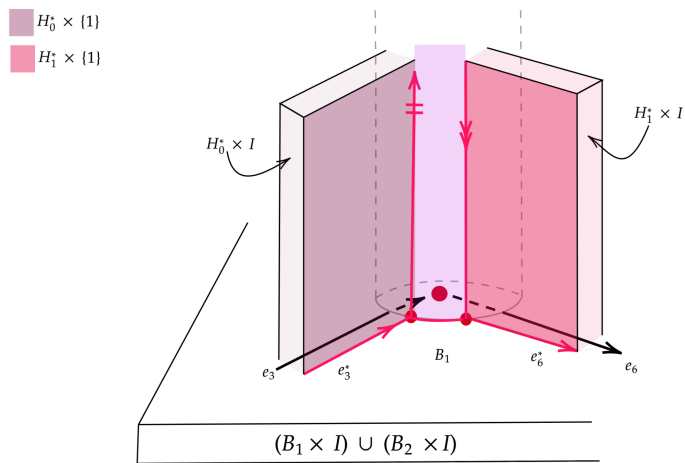
Figure 68: Strips on the tube that are a part of a boundary component of X_N

This strip runs along the $\lambda_1 \times S^1$ to the other end point of λ_1 ; ▲. Note that the interior edge in H_0 that connects to e_3 at ● connects to e_1 at ▲. The interior edge in H_1 that connects to e_6 ● connects to e_5 at ▲. Hence we should see the other end of this strip near ▲ in the region between e_1 and e_5 as shown in figure 69. As shown in figure 68 and 69, two
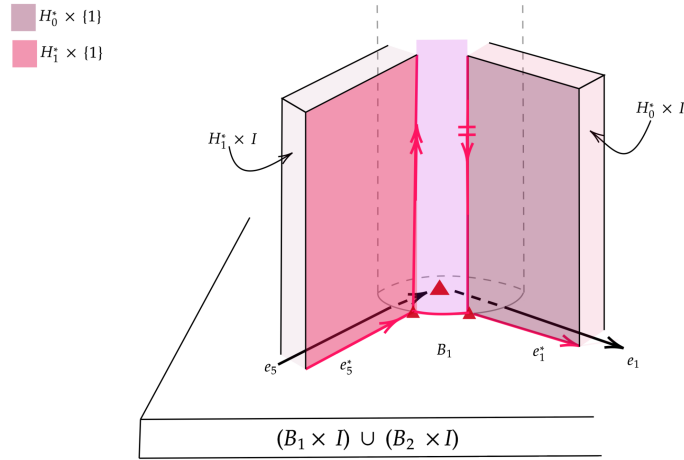
Figure 69: Strips that are part of the other boundary component of X_N

edges of this strip are glued to "interior" edges of $H_i^* \times 1$. Other two edges bound $B_1 \backslash$ an open neighbourhood of its edges.

There are two more similar strips on $\lambda_1 \times S^1$ that connects $H_0^* \times 1$ to $H_1^* \times 1$. Similar to the strip in figure 68 and 69, these two strips also has two of their edges glued to "interior" edges of $H_i^* \times 1$ and bound $B_1 \backslash$ an open neighbourhood of its edges by remaining two edges. So the boundary component of X_N that contains $H_1^* \times 1$s can be describe as the union of following things glued along their edges.

- $H_i^* \times 1$
- Three strips of $\lambda_1 \times S^1$
- $B_1 \backslash$ an open neighbourhood of its edges

The gluing pattern of this boundary component is shown in figure 70. This boundary component has 12 vertices (6 ●s and 6 ▲s) , 12 edges and 6 faces. So its Euler characteristic
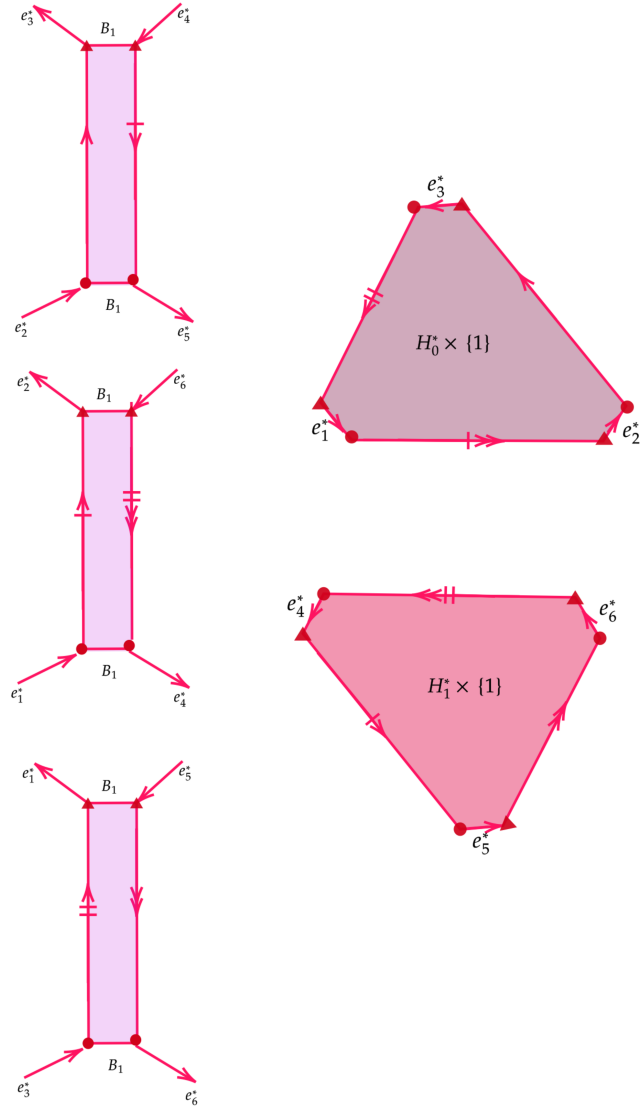
Figure 70: The boundary component of X_N that can be seen from cusp of N

is 0. Hence this boundary component is a torus and it cuts off the cusp of N. Let's call this boundary component by T_0

Now we focus on the other end of $H_i^* \times I$; $H_0^* \times 0$ and $H_1^* \times 0$. Because of the way we oriented I earlier, these can not be seen from cusp at ∞ in $\tilde{N}$. Similar to $H_i^* \times 1$s, we orient $H_i^* \times 0$ using the orientation of H_i. We also label their edges parallel to e_is and their vertices similarly. Right hand side of figure 71 shows $H_i^* \times 0$ with these orientations and labels.

Again there are three different strips on $\lambda_1 \times S^1$ that connects $H_0^* \times 0$ to $H_1^* \times 0$. So two edges of each of these strips are glued to interior edges of $H_i^* \times 1$s. Other two edges bound $B_2 \backslash$ an open neighbourhood of its edges. So we have another boundary component of X_N which is consisted of the following.

- $H_i^* \times 0$
- Three (different from earlier) strips of $\lambda_1 \times S^1$
- $B_2 \backslash$ an open neighbourhood of its edges

The gluing pattern of this boundary component is shown in figure 71. This boundary component also has 12 vertices , 12 edges and 6 faces yielding an Euler characteristic of 0. Hence this boundary component is also a torus. Let's call it T_1

Hence the manifold X_N obtained by thickening up the two complex inside N has 3 boundary components which are listed below.

- $B_1 \cup B_2$ which is ∂N
- A torus T_0 that cuts off the cusp of N
- Another torus T_1 that does not cut off the cusp of N
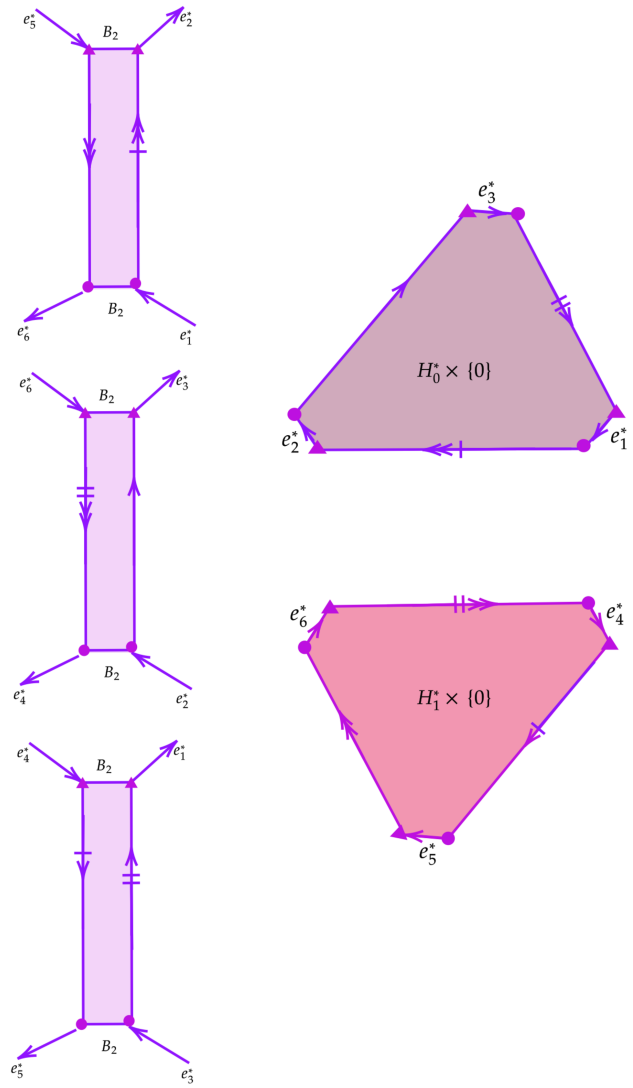
Figure 71: Boundary component of X_N that is hidden from cusp of N

133

6.5 Topological realization of X_N

In this section we construct a triangulation for the manifold X_N using partially truncated tetrahedra. Consider a partially truncated tetrahedron with one ideal vertex. (We can think of it as a tetrahedron with small open neighbourhoods of 3 vertices and the remaining vertex removed). Boundary of the removed open neighbourhoods are called as truncated faces and the remaining faces are called as internal faces. 3 of the interior faces of this partially truncated tetrahedra are non compact while the other interior face is a compact hexagon. All 3 truncated triangles are also compact. An edge of a truncated face is called as an external edge. Other edges are called as internal. (see figure 72).
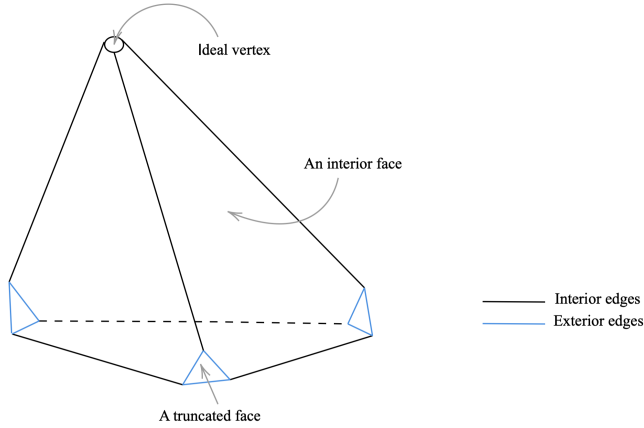
Figure 72: A partially truncated tetrahedron with one ideal vertex

Now let's take two copies of such a partially truncated tetrahedron. We will first glue non compact faces A, B and C of these two tetrahedra in the way specified in figure 73 top. If we look from the ideal vertex of these two tetrahedra we will see a torus. Two edges of each truncated triangle of these tetrahedra are also edges in non compact internal faces. Hence the identification of non compact faces as above, force each truncated triangle to be glued to two other truncated triangles along these pairs of external edges. Remaining edge of each truncated triangle is currently not glued to anything. We label them by $e_1 \ldots e_6$ and

orient them in the direction specified in the same figure. We label compact faces of these two tetrahedra by H_0 and H_1. For now we also leave them without gluing to anything. Note that e_1, e_2, e_3 and e_4, e_5, e_6 are alternating edges of these two compact hexagons.
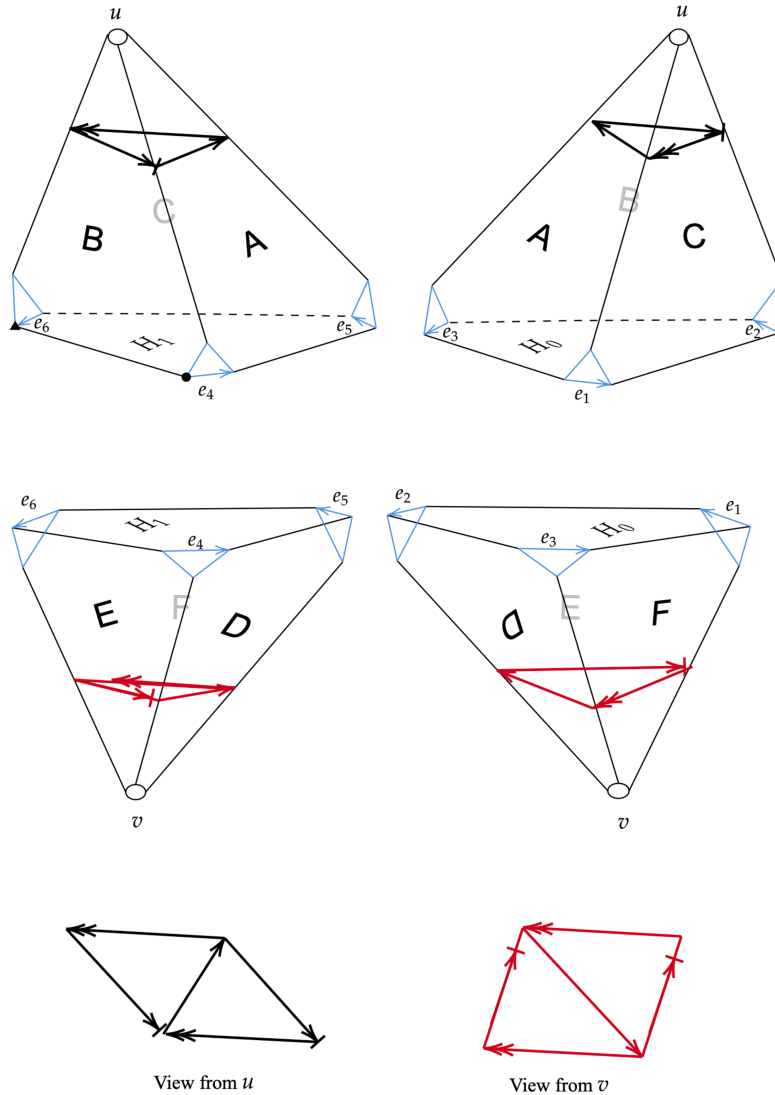
Figure 73: Identification of interior faces

Now we take another two copies of our partially truncated tetrahedron. We again glue their non compact faces D, E and F as specified in 73. By looking from the ideal vertex of these two tetrahedra we can see another torus. Similar to the first pair of tetrahedra, these

gluings of non compact internal faces determines a gluing of truncated triangles. We again label compact faces of these two tetrahedra by H_0 and H_1. We also label their external edges by $e_1 \dots e_6$ and orient them as shown.

Finally we glue the pair of compact faces labelled as H_0 by matching labels of e_1, e_2 and e_3 and their orientations. We do the same for the other pair of compact faces which we labelled as H_1.

This completes the face identification of the four partially truncated tetrahedra. Each internal face of each partially truncated tetrahedra is glued to another internal face. This face gluings yield 3 different edge classes of internal edges.

- Edge class 1 = {All 6 non compact internal edges of first two tetrahedra}
- Edge class 2 = {All 6 non compact internal edges of last two tetrahedra}
- Edge class 3 = {All 12 compact internal edges of the four tetrahedra}

We claim that the resultant quotient of the face identifications yield a complex homeomorphic to X_N. First we will see how we can recover the boundary components of X_N through this quotient. As mentioned earlier, by looking through ideal vertices we already see two torus components. Face identifications force interior edges in compact faces to be identified to a single edge class. We denote the end points of this edge class by $\bullet$ and $\blacktriangle$. Now let's look at the gluing of truncated triangles by the identification of interior faces. These are shown in figure 74. The hexagon in right is consists of all 6 truncated triangles of the first two partially truncated tetrahedra and the one in left is made of the 6 truncated triangles of the other two. We can now compare these two hexagons made from truncated triangles with complementary regions B_1 and B_2 pf ∂N. We observe they are actually the same.

Furthermore, the edge class of all the interior edges of compact faces can be identified to λ_1 of N and the compact faces labelled by H_i s are in fact the projections of their namesake $(1, 1, 1)$ hexagons in $\tilde{N}$.
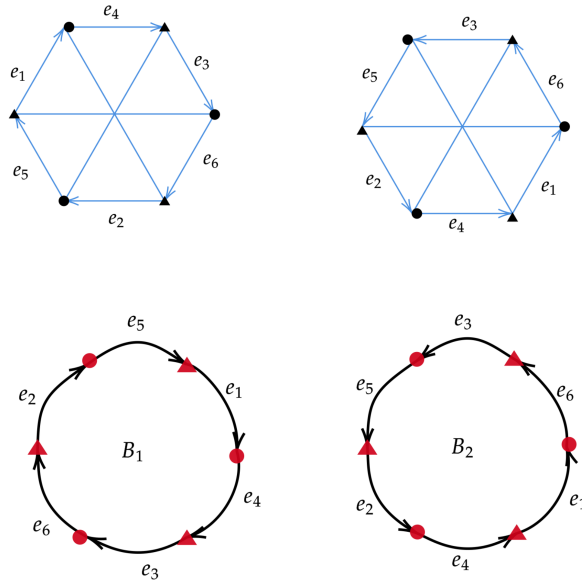
Figure 74: Gluing of truncated triangles (above) yields the complementary components of B_1 and B_2 of ∂N (below)

To see why the resultant quotient is in fact homeomorphic to X_N, we first consider the collection of all the compact faces of the four partially truncated tetrahedra. A collar neighbourhood $\mathcal{C}$ of these faces (after face identifications) is then homeomorphic to the thickened up $2-$ complex X_N. On the other hand the resultant quotient of the four partially truncated tetrahedra can also be deformation retracted to $\mathcal{C} \backslash$ its frontier. The deformation retraction can be constructed by first fixing a sub collar $\mathcal{S}$ of $\mathcal{C}$ and then rescaling each line from $\mathcal{S}$ to an ideal vertex to a line from $\mathcal{S}$ to frontier of $\mathcal{C}$. Figure 75 shows how this deformation retract acts on a non compact face of a partially truncated tetrahedra.
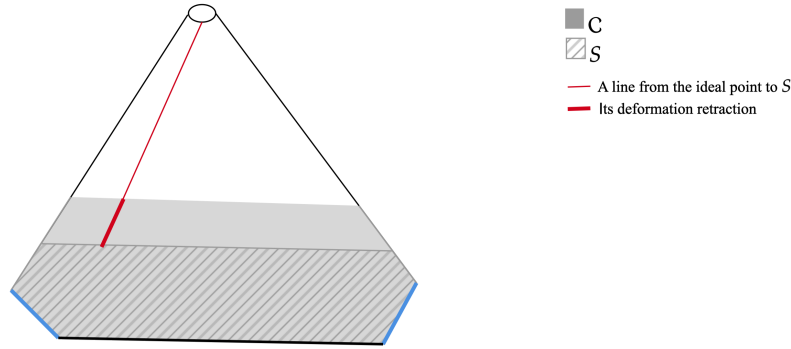
Figure 75: Topological realization of X_N

6.6 Geometric realization of X_N

Now that we have realised the thickened up $2-$ complex X_N topologically as a quotient of partially truncated tetrahedra with internal faces identified, the next step is to see if we can give this quotient a geometric structure. We will show that these tetrahedra can be embedded in $\mathbb{H}^3$ in a way that gives X_N a hyperbolic structure under which it becomes a two cusped manifold with totally geodesic boundary of genus 2

First we want to embed the four partially truncated tetrahedra in $\mathbb{H}^3$ so that their ideal vertices are ideal points in $\mathbb{H}^3$, their truncated triangles and internal faces are geodesic polygons in $\mathcal{H}^3$ and are perpendicular to each other whenever they share an external edge.

In order to embed such a partially truncated tetrahedron in $\mathbb{H}^3$, all we need to do is to assign dihedral angles to each of its internal edge satisfying the following.

- Sum of dihedral angle at an ideal vertex is π
- Sum of dihedral angle at any other vertex is less than π

We assign a dihedral angle of $\pi/3$ to non compact internal edges and a dihedral angle of $\pi/6$ to compact internal edges to each of the four partially truncated tetrahedra. This assignment of dihedral angles satisfies the above condition hence embedding our partially truncated tetrahedra in $\mathbb{H}^3$. We then glue their internal faces using the same face identification used in the topological realization. The assignment of dihedral angles as above also makes sure the following.

- Any two edges glued together under face identifications has same hyperbolic length
- Sum of dihedral angles of all 3 edge classes 2π

The last point follows because edge classes 1 and 2 have 6 edges each with a dihedral angle of $\pi/3$ and the edge class 3 has 12 edges each with a dihedral angle of $\pi/6$.

These two are sufficient conditions to provide the quotient obtained by face identifications a hyperbolic structure with a totally geodesic boundary of genus 2 and two cusps. Let's denote this manifold by X. Truncated triangles will be glued to form the genus 2 boundary surface of X_N. X can be realized geometrically by simply truncating the two cusps of X.

Now that we have realized X_N geometrically, a standard argument in hyperbolic $3-$ manifolds can be used to relate it back to N

Proposition 6.6.1. *N can be obtained by a Dehn filling of X.*

Proof. We know X has two torus boundary components ; T_0 that cuts off the cusp of N and T_1 that does not. Let U_1 be the component of $N \setminus X$ that has T_1 as the frontier and $V_1 = U_1 \cup T_1$. It's enough to show V_1 is a solid torus.

T_1 is compressible in N. Hence there is a disk D embedded in N such that $D \cap T_1 = \partial D$ and ∂D does not bound a disk in T_1. On the other hand T_1 is a cusp cross section of X and

hence incompressible in X. Hence $D \cap X = \partial N$ and $D \subset V_1$.

$\exists$ a collar neighbourhood $\eta(D)_1$ of D which is homeomorphic to $D \times I$. Let's denote $D \times \{0\} \cup D\{1\}$ by ∂_{hor} and $\partial D \times I$ by ∂_{ver}. So $\partial \eta(D) = \partial_{\text{hor}} \cup \partial_{\text{ver}}$. Note that $\eta(D) \cup T_1 = \partial_{\text{ver}}$. Then $S = (T_1 \setminus \partial_{\text{ver}}) \cup \partial_{\text{hor}}$ is homeomorphic to S^2.

Every hyperbolic $3-$ manifold is irreducible ; every S^2 contains a ball B^3 such that $\partial B^3 = S^2$. Let B $subsetN$ be the ball contained in S. Then $int B \cup (\eta(D) \setminus \partial_{\text{ver}}$ is a complementary component of T_1 in N. It has to be U_1 because the other complementary component of T_1 in N contains ∂N. Hence $V_1 = B \cup \eta(D)$.

If $\eta(D) \cup B = \partial_{\text{hor}}$ then $V_1 = B \cup \eta(D)$ will be a solid torus. Note that $(X_{N1}) \cup \eta(D) \setminus \partial_{\text{hor}}$ is connected and hence contained in a single component of $N \setminus S$. Therefore $int B \cap \eta = \emptyset$. Hence $\eta(D) \cup B$ is indeed equal to ∂_{hor} and it follows V_1 is a solid torus. $\quad\square$
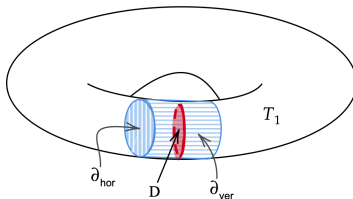
Figure 76: N can be obtained by a Dehn filling of X

6.7 Dehn fillings of X

We showed that N can be obtained by a Dehn filling of a $2-$ cusped hyperbolic manifold with

a totally geodesic boundary. We named this manifold as X and described a triangulation of it by 4 partially truncated tetrahedra. Our next step is to understand the possible Dehn fillings of X that can yield N. A basic first step in that regard is to compute the volume of X. For this we use the volume formula proved by Ushijima for generalized hyperbolic tetrahedra.[19]

Consider a generalized hyperbolic tetrahedra T with dihedral angles as shown in 77.Define the following.
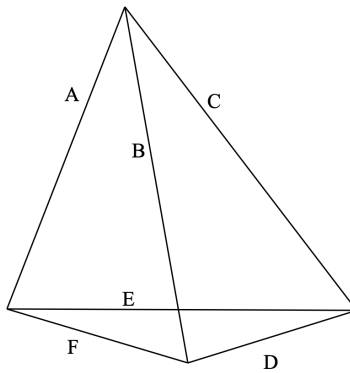
Figure 77: Dihedral angles of a generalised tetrahedra

$$
G=
\begin{pmatrix}
1 & -cos(A) & -cos(B) & -cos(F) \\
-cos(A) & 1 & -cos(C) & -cos(E) \\
-cos(B) & -cos(C) & 1 & -cos(D) \\
-cos(F) & -cos(E) & -cos(D) & 1
\end{pmatrix}
$$

$a = e^{iA}, b = e^{iB}, c = e^{iC}, d = e^{iD}, e = e^{iE}, f = e^{iF}$

$$\mathcal{U}(z,T) = \frac{1}{2}\Big\{ Li_2(z) + Li_2(abdez) + Li_2(acdfz) + Li_2(bcefz)$$
$$- Li_2(-abcz) - Li_2(-aefz) - Li_2(-bdfz) - Li_2(-cdezz) \Big\}$$

where $Li_2(x) = -\int_0^x \frac{log(1-t)}{t} dt$

$$z_\pm = -2 \frac{sin(A)sin(D) + sin(B)sin(E) + sin(C)sin(F) \pm \sqrt{det(G)}}{ad + be + cf + abf + ace + bcd + def + abcdef}$$

Lemma 6.7.1. *(Theorem 1.1 , [19]) The volume of the generalize hyperbolic tetrahedra with dihedral angles shown in figure 77 is given by*

$$\frac{1}{2} Im((U(z_+, T) - U(z_-, T))$$

where $\mathcal{U}, z_+$ and z_- are defined as above.

Lemma 6.7.2. *Volume of X is 9.13447*

Proof. Take one of the partially truncated tetrahedra in the triangulation of X. We can take dihedral angles as $A = B = C = \Pi/3$ and $D = E = F = \pi/6$. Then we computed the following.

$det(G) = -9/2 \quad z_+ = 1 \quad z_- = e^{\frac{2\pi i}{3}}$

$Im(U(z_+, T)) = 3\Lambda(\pi/2) - 3\Lambda(-\pi/6)$

$Im(U(z_-, T)) = -3\Lambda(5\pi/6) - \Lambda(\pi/6)$

where $\Lambda(x)$ is the Lobachevsky function given by $\Lambda(x) = 2 \int_0^x log(|2sin(t)|)dt$.
Λ at following values are computed to

- $\Lambda(\pi/2) = 0$

- $\Lambda(-\pi/6) = -0.507471$

- $\Lambda(5\pi/6) = -0.507471$

- $\Lambda(\pi/6) = 0.507471$

Hence we compute the volume of one of the partially truncated tetrahedra to be $\frac{9}{2} * 0.507471 = 2.2836$. Each of the four partially truncated tetrahedra has this volume. Hence the volume of X which is four times the volume of a single tetrahedra is 9.13447 $\qquad \Box$

A slope of a torus boundary component of a manifold is an isotopy class of a simple closed curves. A length of a slope is defined to be the length of its representative on the largest horoball cusp cross section. Dehn fillings of a manifold can be parameterized by slopes. We know the manifold X has two tours boundary components T_0 and T_1. What we want to do is to analyse Dehn fillings of X on T_1. Let γ be a slope on T_1. Then we define by $X(\gamma)$, the manifold obtained by filling T_1 with a solid torus along the slope γ. A Dehn filling of X reduce the volume by a fraction depending on the length of the slope along which T_1 was filled. The following result in [9] provides us with the lengths of the slopes that could possibly yield N.

Lemma 6.7.3. *(Theorem 1.1 [9])*

$$Vol(X(\gamma)) \geq \left(1 - \left(\frac{2\pi}{l}\right)^2\right)^{3/2} Vol(X) \text{ where } l \text{ is the length of the slope } \gamma.$$

If $Vol(X(\gamma) > vol(N_0)$ then we obtain $l < \dfrac{2\pi}{\sqrt{1 - \left(\frac{Vol(N_0)}{Vol(X)}\right)^{2/3}}} = 19.8576$.

Hence the Dehn fillings that could possibly yield a manifold that does not exceed the volume of N_0 are the ones along slopes with at most this length. There are only finitely many slopes with such lengths. Our final task is to find a way to list them and to compute volumes of the manifolds obtained by Dehn fillings of X along them.

As mentioned above, length of a slope is defined using its representative on at the largest

horoball cross section. We now describe such a cross section of X for the cusp corresponding to T_1.

Lemma 6.7.4. *The Euclidean horizontal plane $z = \sqrt{2}$ considered as a subset of $\mathbb{H}^3$ is a lift of the largest horoball cross section of T_1 in $\tilde{N}$. There are slopes α and β which generates $\pi_1(T_1)$ each with hyperbolic length $3/\sqrt{2}$.*

Proof. Again we start with one of the partially truncated tetrahedra T in the triangulation of X and assume ∞ is the ideal point of T. Let P be the geodesic plane in $\mathbb{H}^3$ that contains the compact face of T and P_1, P_2 and P_3 be the geodesic planes containing truncated triangles of T. These geodesic planes are hemispheres perpendicular to $\mathbb{R}^2$. Without loss of generality take the radius of P to be 1 and radii of P_is to be r. We would like to know whether a cross section of T_1 first touches the boundary triangles or the compact face of T; i.e., whether $r > 1$. Let A be the center of P on $\mathbb{R}^2$ and B, C and D be the centers of P_i s.

Note that the lengths of all compact internal edges of T are the same and the lengths of external edges of T are also the same. Hence the triangle BCD on $\mathbb{R}^2$ is equilateral and $BAE\angle$ is $\pi/3$. Since external and internal faces are perpendicular, the hemispheres P and P_1 intersect perpendicularly. Hence the Euclidean length between their centers on $\mathbb{R}^2$ is $\sqrt{1+r^2}$ and $AE = \frac{1}{2}\sqrt{1+r^2}$. On the other hand the dihedral angle between non compact internal faces and the compact internal face is $\pi/6$. Hence we have $sin(\pi/3) = \frac{AE}{1} \Rightarrow r = \sqrt{2}$. So the radii of P_is are bigger than the radius of P and the maximal cusp cross section of T_1 is at a Euclidean height of $\sqrt{2}$ from $\mathbb{R}^2$.

Sides of the equilateral triangles on the cusp cross section are simple closed curves intersecting only once and they generate $\pi_1(T_1)$. (see figure 79) Let's label their isotopy classes by α and β. Euclidean side lengths of these curves are same as the distance between centers of P_is which is equal to $2 * sin(\pi/3) * \sqrt{1+r^2} = 3$. At height $\sqrt{2}$, these sides have lengths of $3/\sqrt{2}$ under the inherited Euclidean metric. $\square$

View from ∞

Side views

$\mathbb{R}^2$
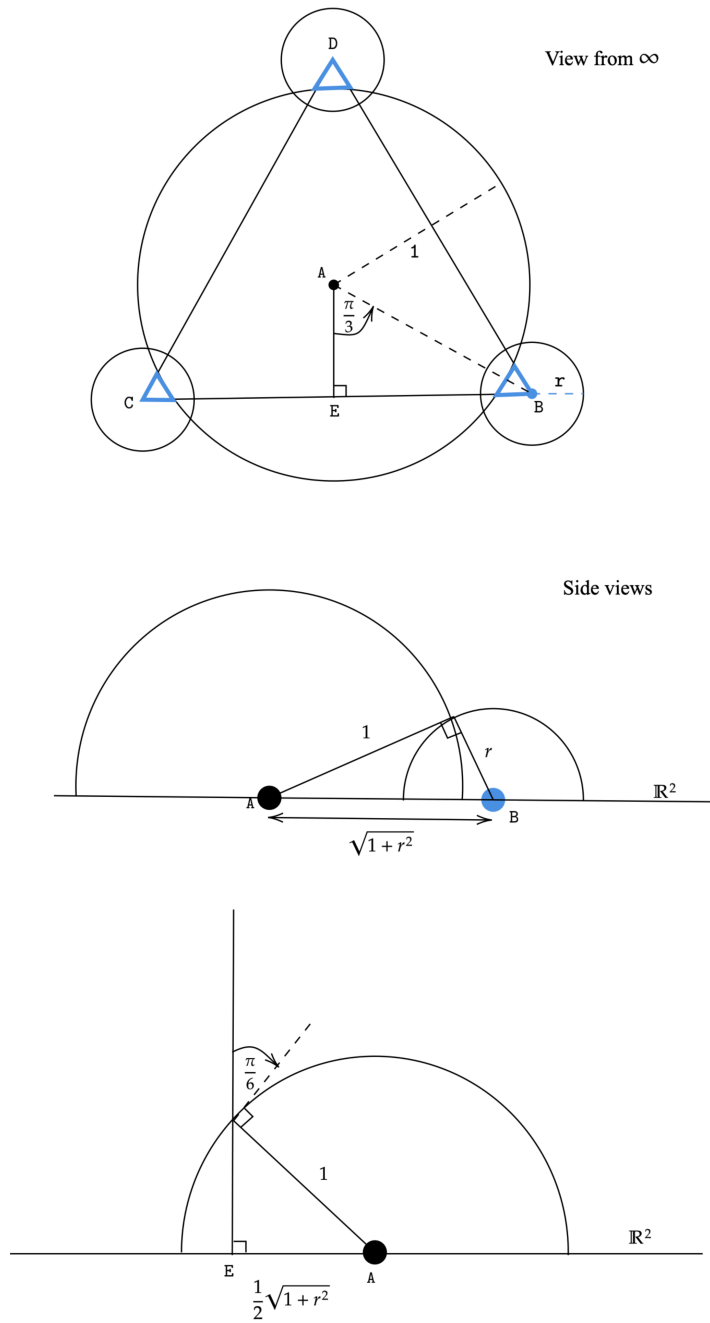
Figure 78: Computing the height of the largest horoball cusp cross section

145
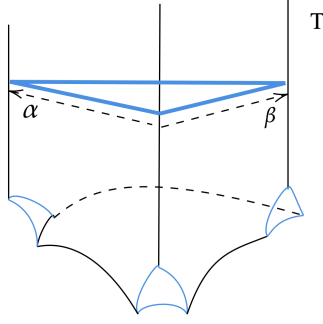
Figure 79: Slopes that generate $\pi_1(T_1)$

Then for any slope γ on T_1 there exists coprime integers p and q such that $\gamma = p\alpha + q\beta$. We represent the slope γ in $\mathbb{Q} \cup \{\infty\}$ by p/q. We draw the lattice on the largest horoball cusp neighbourhood discussed in the last lemma (figure 80)with each lattice point represent a slope on T_1 by a rational number p/q where p and q are coprime. Each triangle in the lattice has hyperbolic side length $3/\sqrt{2}$ which are the lengths of α and β. We can compute the length of any slope on T_1 using this lattice. In particular we can list the ones with a length than 19.8576. These are the ones corresponding to Dehn fillings that could possibly yield N. For an example, the Euclidean length of the line segment from the origin to the lattice point 2 is $\sqrt{(3\sqrt{3})^2 + 6^2} = \sqrt{63}$. Hence the slope given by 2α has the length $\sqrt{63}/\sqrt{2} = 5.6125$. In the table 2 we list all the slopes with length less than 19.8576. There are 89 such slopes in total.
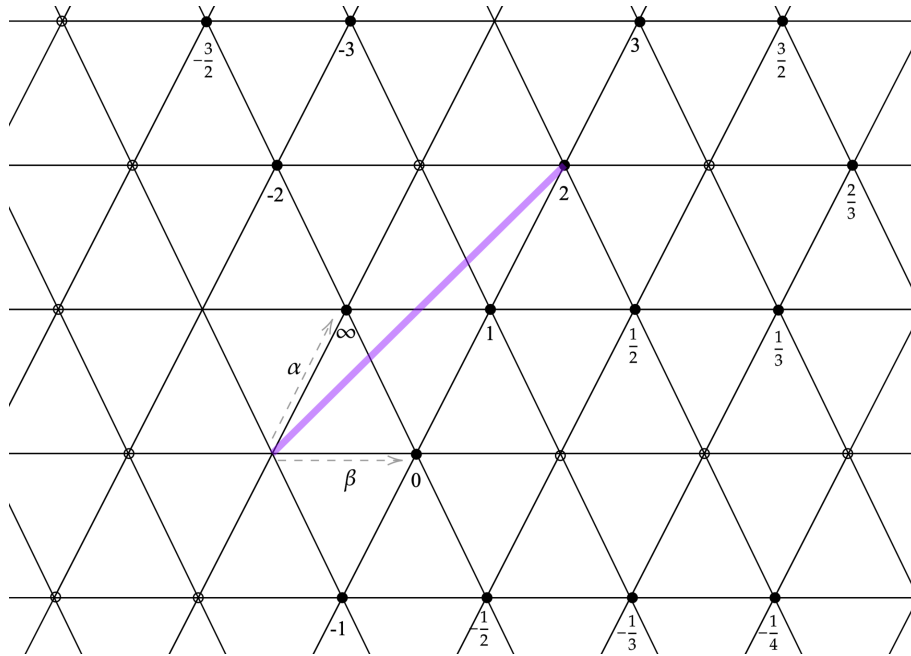
Figure 80: Lattice on the largest horoball cusp cross section. Each lattice point represent a slope

6.8 Computing the volumes of Dehn fillings of X using its double

The software package *SnapPy* is a one of the most frequently used programs to study the hyperbolic structures of $3-$manifolds. In particular it can provide various information about Dehn fillings of a given finite volume hyperbolic manifolds (without a boundary). *SnapPy* takes a description of such a manifold as the input and compute this information.

While what we wanted to compute is volumes of Dehn fillings of a manifold with a totally geodesic boundary, a description of such a manifold can not be fed into *SnapPy*. On the other hand, the double of X along its boundary which is defined below is a finite hyperbolic manifold without a boundary.

$$DX = X \times \{0,1\}/ \sim$$

where the quotient $\sim$ is the identification of points $x \times \{0\}$ and $x \times \{1\}$ for $x \in \partial X$. DX defined as above is a hyperbolic $3-$manifold with 4 cusps and no boundary. The boundary of X is embedded inside DX as a genus 2 surface.

DX has an obvious orientation reversing isometry which is the reflection across the boundary of X. Let's call this isometry by Ψ. It acts on DX as follows.

$$\Psi(x,i) = (x, 1-i)$$

for $i = 0, 1$. Now let γ be a slope on the torus component T_1 of X. Then Ψ takes γ to a slope $\Psi(\gamma)$ on the torus component $\Psi(T_1)$ of DX. Let $DX(\gamma, T_1, \Psi(\gamma), \Psi(T_1))$ be the manifold obtained by filling T_1 and $\Psi(T_1)$ along γ and $\Psi(\gamma)$ respectively. Then we have

$$DX(\gamma, T_1, \Psi(\gamma), \Psi(T_1)) = D\big(X(\gamma)\big)$$

where $D\big(X(\gamma)\big)$ is the double of the Dehn filling $X(\gamma)$ of X. Hence the volume of $X(\gamma)$ is one half of the volume of $DX(\gamma, T_1, \Psi(\gamma), \Psi(T_1))$.

If we can compute a triangulation or some other form of description of DX that can be

fed into *SnapPy* then we can obtain the volumes of its Dehn fillings, in particular volumes of the Dehn fillings of form $DX(\gamma, \psi(\gamma))$ and hence the volumes of $X(\gamma)$ for any slope γ on T_1. Therefore our next goal is to construct a description of DX that can be read by *SnapPy*.

6.9 Frigerio, Martelli, Petronio census

In [3] Frigerio, Martelli and Petronio classified all the hyperbolic $3-$manifolds with nonempty compact totally geodesic boundary that admits a triangulation with at most four tetrahedra. They defined $\mathcal{M}_{g,k}$ to be all such manifolds with k cusps and a geodesic boundary of genus g and admits a triangulation of $g + k$ tetrahedra.

The unique member in $\mathcal{M}_{2,1}$ in their classification is our candidate N_0 for the minimal volume manifold of $\mathcal{N}_{c,c}$. Furthermore the class $\mathcal{M}_{2,2}$ in their census also has a unique member. We showed that X has a hyperbolic structure and admits a triangulation of 4 partially truncated tetrahedra and hence must also belong to $\mathcal{M}_{2,2}$. So it has to be the unique member in $\mathcal{M}_{2,2}$. Hence we can restate the proposition 6.6.1 as below.

Theorem 3. *Let N be a manifold in $\mathcal{N}'_{c,c}$ and contain a $(1,1,1)$ hexagon visible from the cusp in its universal cover. If ∂N has two hexagonal complementary regions in G then N can be obtained by a Dehn filling of X where X is the unique two cusped manifold with a totally geodesic boundary of genus 2.*

Going forward, we will adapt their notation for the face gluings of partially truncated tetrahedra that produce X. We describe it below.

First denote the vertices of a tetrahedron by $0, 1, 2$ and 3. Some of the vertices may be ideal or truncated. Then label the face of the tetrahedron by i if it is opposite to the vertex

i. So face 0 consists of vertices $1, 2$ and 3 and face 1 consists of vertices $0, 2$ and 3 and so on. We label the four tetrahedra in the triangulation of X by Tet 0, Tet 1 , Tet 2 and Tet 3. The gluing data of their faces to produce X is given in table 3.

Table 1: Only slopes, along which a Dehn filling could possibly yield N

Slope	Length	Slope	Length
0	2.1213	∞	2.1213
(1,1)	3.6742	(1,2)	5.6124
(1,3)	7.64852	(1,4)	9.7211
(1,5)	11.8110	(1,6)	13.9104
(1,7)	16.0156	(1,8)	18.1245
(2,1)	5.6124	(2,3)	9.2466
(2,5)	13.2476	(2,7)	17.3637
(3,1)	7.6485	(3,2)	9.2466
(3,4)	12.9034	(3,5)	14.8492
(3,7)	18.8547	(4,1)	9.7211
(4,3)	12.9034	(4,5)	16.5680
(5,1)	11.8110	(5,2)	13.2476
(5,3)	14.8492	(5,4)	16.5680
(6,1)	13.9104	(7,1)	16.0156
(7,2)	17.3637	(7,3)	18.8547
(8,1)	18.1245	(-1,1)	2.1213
(-1,2)	3.6742	(-1,3)	5.6124
(-1,4)	7.6485	(-1,5)	9.7211
(-1,6)	11.8110	(-1,7)	13.9104
(-1,8)	16.0156	(-1,9)	18.1245
(-2,1)	3.6742	(-2,3)	5.6124
(-2,5)	9.2466	(-2,7)	13.2476
(-2,9)	17.3637	(-3,1)	5.6124
(-3,2)	5.6124	(-3,4)	7.6485

151

Table 2: Only slopes, along which a Dehn filling could possibly yield N contd..

Slope	Length	Slope	Length
(-3,5)	9.2466	(-3,7)	12.9034
(-3,8)	14.8492	(-4,1)	7.6485
(-4,3)	7.6485	(-4,5)	9.7211
(-4,7)	12.9034	(-4,9)	16.5680
(-5,1)	9.7211	(-5,2)	9.2466
(-5,3)	9.2466	(-5,4)	9.7211
(-5,6)	11.8110	(-5,7)	13.2476
(-5,8)	14.8492	(-5,9)	16.5680
(-6,1)	11.8110	(-6,5)	11.8110
(-6,7)	13.9104	(-7,1)	13.9104
(-7,2)	13.2476	(-7,3)	12.9034
(-7,4)	12.9034	(-7,5)	7.6485
(-7,6)	14.8492	(-7,8)	16.0156
(-7,9)	17.3637	(-7,10)	18.8547
(-8,1)	16.0156	(-8,3)	14.8492
(-8,5)	14.8492	(-8,7)	16.0156
(-8,9)	18.1245	(-9,1)	18.1245
(-9,2)	17.3637	(-9,4)	16.5680
(-9,5)	16.5680	(-9,7)	7.6485
(-9,8)	18.1245	(-10,3)	18.8547
(-10,7)	18.8547		

Table 3: Face gluings of X in the notation used in Frigerio, Martelli, Petronio census

	Face 0 (123)	Face 1 (023)	Face 2 (013)	Face 3 (012)
Tet 0	1	1	1	2
	213	203	103	123
Tet 1	0	0	0	1
	213	203	103	312
Tet 2	0	3	3	3
	012	032	031	021
Tet 3	1	2	2	2
	120	032	031	021

We conclude this chapter with the following version of the theorem 1.6 from [8] adapted to our situation.

Proposition 6.9.1. *(Theorem 1.6 , [8]) There are at least six slopes on T_1, along which X can be Dehn filled to obtain N_0*

7.0 Construction of an ideal triangulation for DX

Under the notaion in table3, Tet 0 and Tet 1 has their ideal points at vertex 3 and Tet 2 and Tet 3 has their ideal points at vertex 0.

All of the compact edges in the four tetrahedra are identified to a single edge class under face gluings. The end points of this edge class is denoted by ● and ●. (See figure 81.)
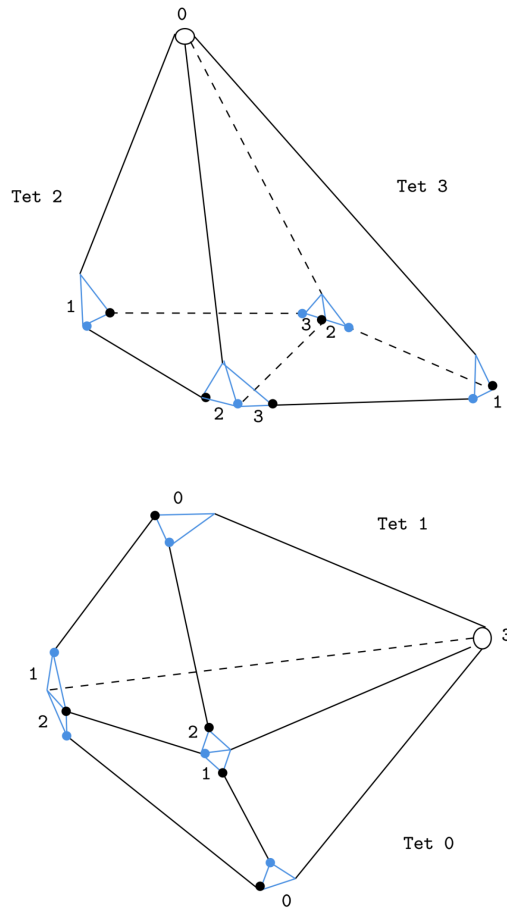

Figure 81: Vertex classes of X

7.1 An inventory of edges

We now define several classes of geodesic lines along the four partially truncated tetrahedra.

Type 1

An edge from the ideal point of the tetrahedron to the center of its compact face.

There is a one such edge for each tetrahedra. Compact faces of Tet 0 and Tet 2 are glued, hence the type 1 edge of Tet 0 is connected to the type 1 edge of Tet 2 at the center of the compact face, creating a line segment between their ideal points. Same is true for the type 1 edges of Tet 1 and Tet 3. Type 1 edges of all 4 tetrahedra are shown in figure 82 top.

Color code : Blue (for Tet 0 and Tet 2) and Purple (for Tet 1, 3)
(rounded ends are the centers of compact faces)

Type 2

An edge lying on a non compact internal face of a tetrahedra that connects its ideal point to the center of one of its compact internal edges.

Each tetrahedron has 3 type 2 edges, one along each non compact internal face. Each type 2 edge is glued to a type 2 edge of a different tetrahedra respecting face gluings. In fact type 2 edges of Tet 0 are glued to edges of the same type in Tet 1 because all non compact internal faces of Tet 0 are glued to those of Tet 1. Type 2 edges of Tet 2 are glued to edges of the same type in Tet 3 for the same reason. Type 2 edges of Tet 2 are shown in figure 82 middle left.

Color code : Orange

Type 3

An edge connecting the center of the compact face of a tetrahedron to the center of the one of the compact internal edges. Each tetrahedra has 3 type 3 edges.

Type 3 edges of Tet 0 are glued to edges of the same type in Tet 2 as the their compact faces are glued. Type 3 edges of Tet 1 are glued to edges of the same type in Tet 3 for the same reason. Type 3 edges Tet 2 are shown in figure 82 middle right.

Color code : Green

Type 4

An edge connecting the center of the compact face of a tetrahedron to the center of an external edge that lie on the same compact face.
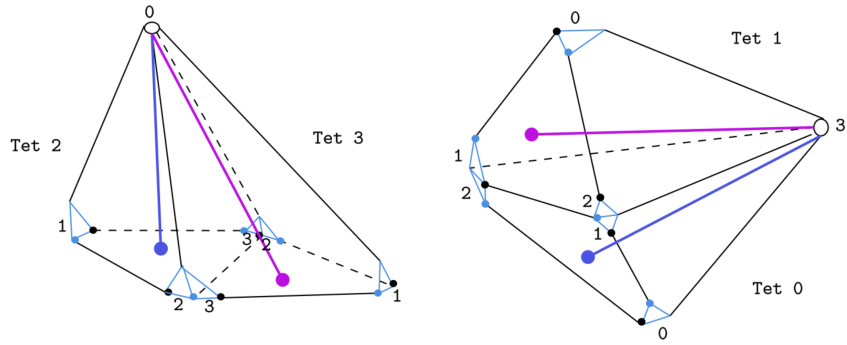
Each tetrahedra has 3 type 4 edges. Type 4 edges of Tet 0 are glued to edges of the same type in Tet 2 and type 3 edges of Tet 1 are glued to edges of the same type in Tet 3. Type 4 edges Tet 2 are shown in figure 82 bottom.

Color code : Red

Spinal hexagons

Consider a triangle inside a partially truncated tetrahedra that is bounded by one of each type 1, type 2 and type 3 edges. We call such a triangle by a spinal triangle. A spinal triangle can be viewed from two sides ; from ● and from ●. For an example, the spinal triangle of Tet 2 showed in figure 83 can be seen from ● at vertex 1 and from ● at vertex 2.

If a spinal triangle in Tet i can be seen from ● at vertex j we assign it the label i_j. If the same triangle can be seen from ● at vertex k, then we give it a second label by i_k. Hence the two labels assigned to the spinal triangle seen in figure 83 are 2_1 and 2_2. There are 12 spinal triangles in total. The pair of labels assigned to each of them is listed below.

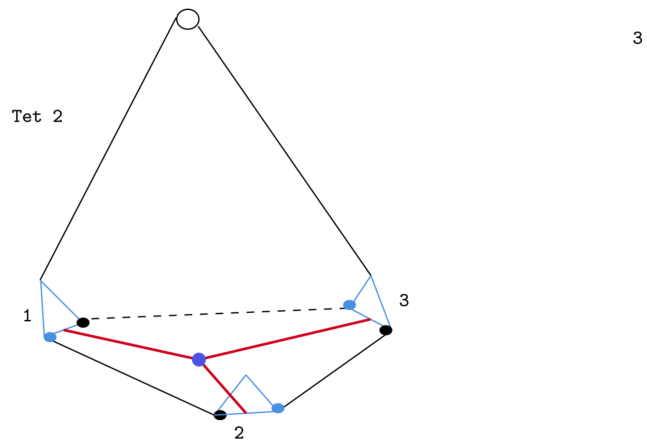Type 1 edges of the four tetrahedra
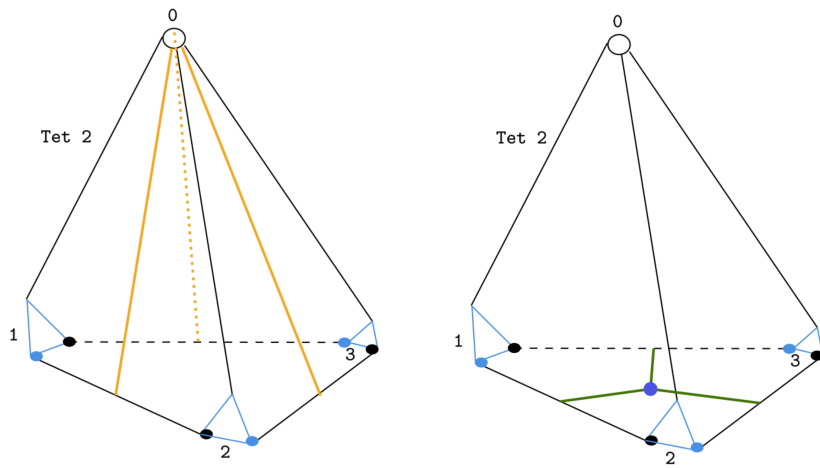
Type 2 edges of Tet 2

Type 3 edges of Tet 2

Type 4 edges of Tet 2

Figure 82: Inventory of edges

Tet 2

Type 2 edge

Type 1 edge

$2_1 = 2_2$

Type 3 edge

A spinal triangle

Labelling of spinal triangles

3_2 2_1 0_0

3_1 2_2 0_1

Gluing of spinal triangles as viewed from ● (left) and as viewed from ● (right)
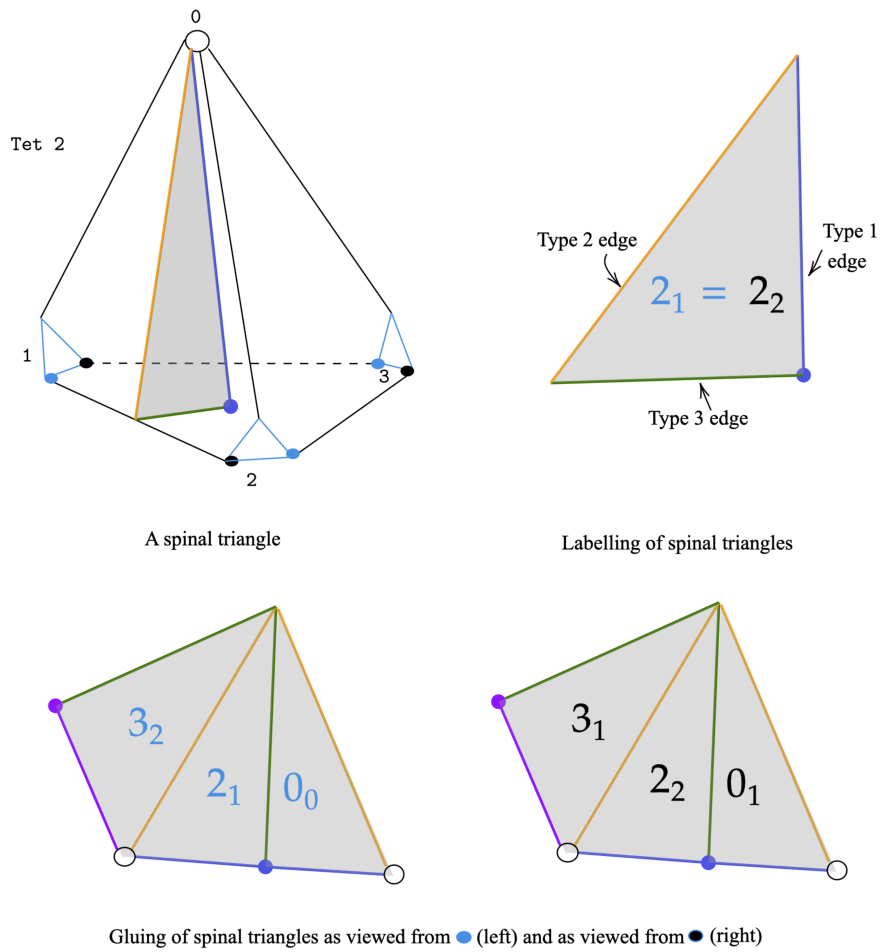
Figure 83: Spinal triangles

7.2 Labelling of spinal triangles

Spinal triangles in Tet 0 are

1. $0_0 = 0_1$
2. $0_1 = 0_2$
3. $0_2 = 0_0$

Spinal triangles in Tet 0 are

1. $1_0 = 1_2$
2. $1_1 = 0_0$
3. $1_2 = 1_1$

Spinal triangles in Tet 0 are

1. $2_1 = 2_2$
2. $2_2 = 2_3$
3. $2_3 = 2_1$

Spinal triangles in Tet 0 are

1. $3_1 = 3_3$
2. $3_2 = 3_1$
3. $3_3 = 3_2$

Then we glue these spinal triangles along their type 2 and type 3 edges. Again, looking at the spinal triangle 2_1, its type 2 edge is glued to the type 2 edge of 3_2. Type 3 edge of 2_1 is glued to the type 3 edge of 0_0. (figure 83 bottom left). The gluings can also be viewed from ● in which case 2_2 is glued to 3_1 along the type 2 edge and to 0_1 along type 3 edge. (figure 83 bottom right).

By completing these gluings we can obtain two hexagons as shown in figure 84 ; one is when spinal triangles are viewed from ● and other when they are viewed from ●. We call

these hexagons as **spinal hexagons of X**. The spinal triangles that form these two hexagons are identified by the labelling given in 7.2. As sketched in figure 84 this identification can also be done by simply reflecting one of the hexagons along the dotted line.
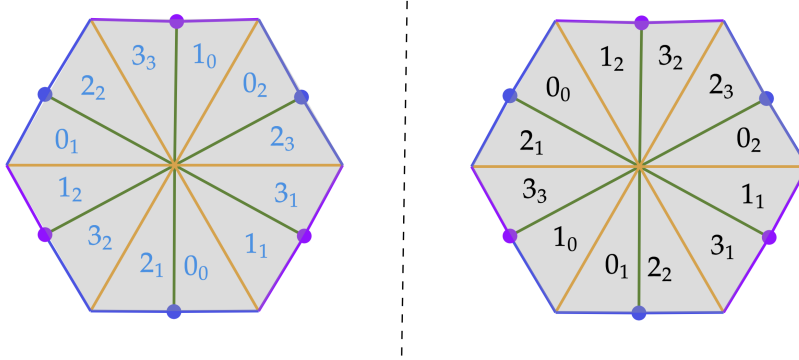

Figure 84: Two spinal hexagons of X ; viewed from ⬤ (left) and ⬤ (right)

Similarly $\overline{X}$ also has two spinal hexagons. If the partially truncated tetrahedra that forms $\overline{X}$ are labelled by Tet $\overline{0}$, Tet $\overline{1}$, Tet $\overline{2}$ and Tet $\overline{3}$ then the triangles that form the two spinal hexagons of $\overline{X}$ has labellings of the form $\overline{i}_j$ and $\overline{i}_k$.
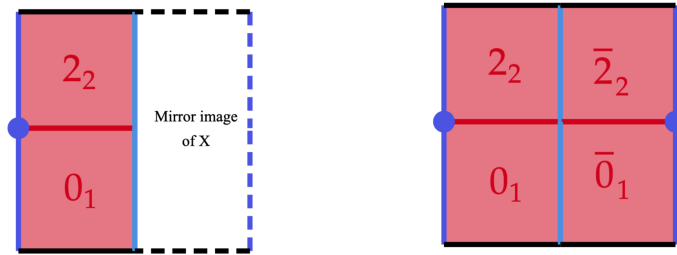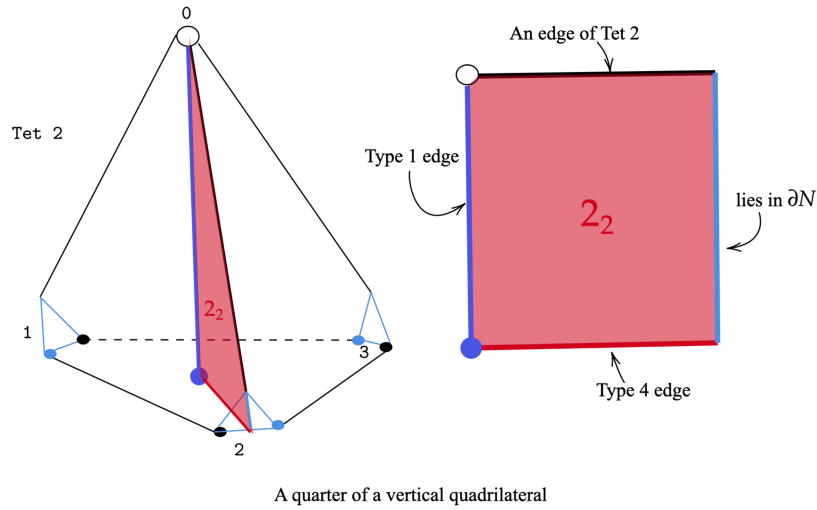
7.3   Vertical quadrilaterals

Consider the region inside a tetrahedron bounded by the following.

- A non compact interior edge
- A line in a truncated triangle that connects the edge above to the center of the opposite external edge.
- A type 4 edge that connects the center of the compact face to the center of the same external edge

160

- Type 1 edge of the tetrahedron

We call this region as "a quarter of a vertical quadrilateral". If such a region that lies in the tetrahedra i has an edge goes through the truncated triangle at vertex j we label it as i_j. The quarter of a vertical quadrilateral 2_2 is shown in figure 86.

A quarter of a vertical quadrilateral

Gluing of "quarterss" to form a vertical quadrilateral

Figure 85: Vertical quadrilaterals

The reason we call these regions as quarters is we can glue four such regions and form what we call as a **vertical quadrilateral**. First we glue two "quarters" along their type 4 edge. For the quarter 2_2 the one that glued to its type 4 edge would be 0_1. Next we consider the mirror images of the partially truncated tetrahedra that forms $\overline{X}$. These four tetrahedra can be glued to the original four tetrahedra along truncated triangles. We labelled these

161

tetrahedra by Tet $\bar{i}$. Hence each "quarter" in Tet i can be glued to a "quarter" in Tet $\bar{i}$ along its edge that lies on the truncated triangle. For an example, 2_2 in figure 86 can be glued to $\overline{2}_2$ along the edge lying on the truncated triangle. Similarly 0_1 can be glued to $\overline{0}_1$. The four "quarters" glued this way is then form a "vertical quadrilateral". There are 6 vertical quadrilaterals as shown in figure 38
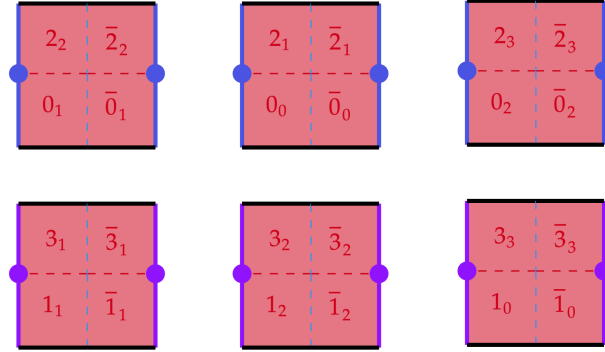
Figure 86: Six vertical quadrilaterals in X and $\overline{X}$

7.4   Gluing of spinal triangles to vertical quadrilaterals

Note that type 1 edges form boundaries of spinal hexagons. Each vertical quadrilateral also has a pair of edges of type 1. We glue vertical quadrilaterals to spinal hexagons along these edges.

For an example when we view the quarter of the vertical quad 2_2 from ●, we see the quarter is glued to spinal triangle 2_2. So this quarter should be glued to 2_2 in the spinal hexagon corresponding to ●. On the other hand when we view the quarter of the vertical

quad 2_2 from ●, we see the quarter is glued to spinal triangle 2_2. Hence 2_2 should be glued to 2_2 in the spinal hexagon corresponding to ● (See figure 87)
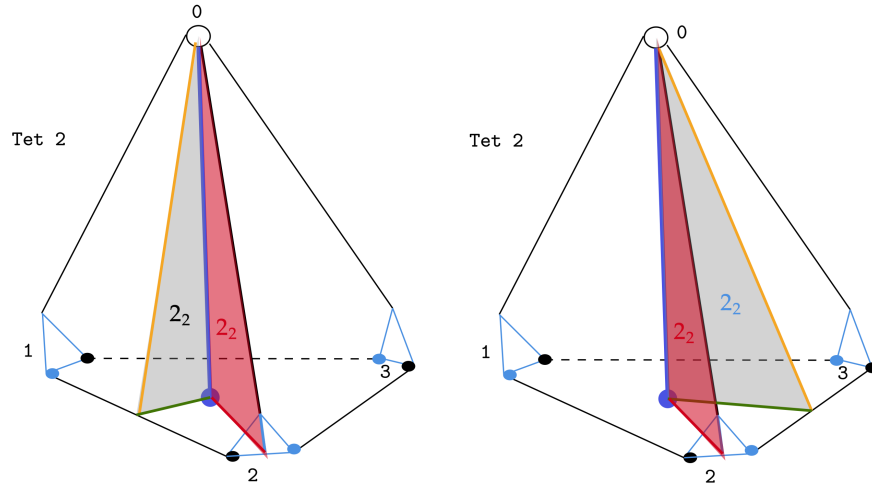
Figure 87: Gluing of vertical quads to spinal triangles as seen from ● (left) and ● (right)

This creates two 'drums', each of which connects a spinal hexagon in X to a spinal hexagon in $\overline{X}$ via vertical quadrilaterals as shown in figure 88.

Note that these two drums are ideal polyhedra as their vertices are ideal end points of type 1 edges. Surface of each drum consists two spinal hexagons and six vertical quadrilaterals. Triangles that made spinal hexagons are identified as shown in figure 84. Vertical quads in the two 'drums are identified if they simply have the same labelling. The quotient of the two drums under these identifications is then isometric to DX. Hence we have a decomposition of DX by two ideal polyhedra.
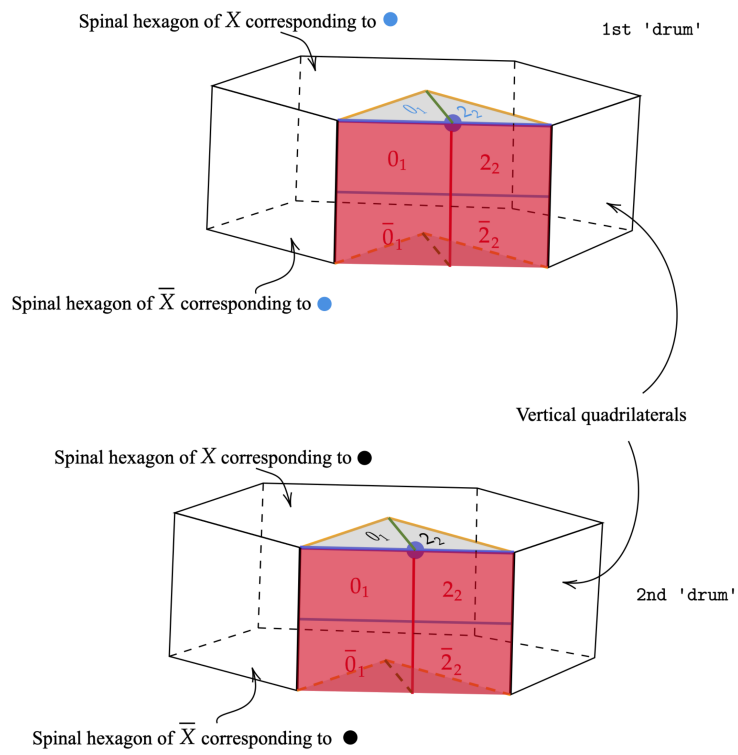
Figure 88: DX can be decomposed into two ideal polyhedra ('drums')

7.5 Division of drums in to ideal tetrahedra

The next step is to divide these two polyhedra into smaller ideal tetrahedra. There are several ways to do that. Below we describe the method we used.

Step 1

Consider the two pairs of spinal hexagons of X. Place them in the way shown in figure 84. This means their identification can be done by simply reflecting across the dotted line in that figure. Now we forget about the labels of the spinal triangles that make these hexagons. Instead we label the ideal vertices of these hexagon by a, b, c, p, q, r as shown in figure 89. This labelling still preserve the identification of the spinal hexagons, meaning two hexagons will be glued by identifying the vertices with the same label. Now do the same for the spinal hexagons of $\overline{X}$ as shown in the bottom of the same figure. We label the ideal vertices of those hexagons by d, e, f, s, t, u.
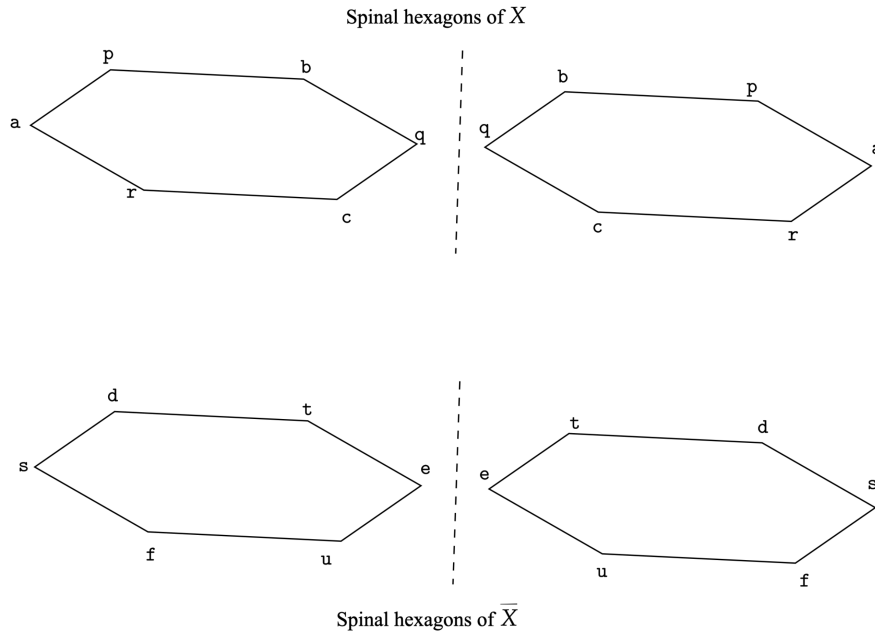
Figure 89: Triangulation of drums : Step 1

Step 2

Now divide each spinal hexagon into four triangles as shown in figure 90. These triangles still preserve the identifications of the spinal hexagons, meaning a triangle on one spinal hexagon of X (or $\overline{X}$) will be mapped to the triangle with same labelling of vertices on the other spinal hexagon of X (or $\overline{X}$). For an example the triangle apr in the spinal hexagon of X in the left will be identified to the triangle apr in the spinal hexagon of X in the right.
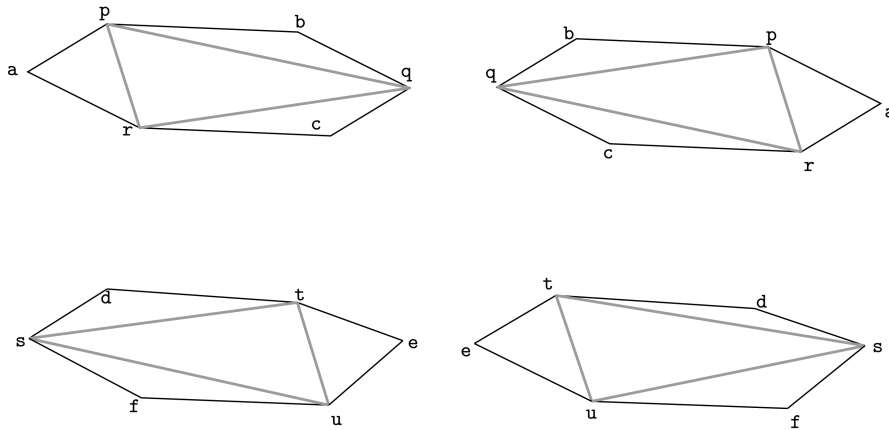
Figure 90: Triangulation of drums : Step 2

Step 3

Now create the following six tetrahedra inside the first drum by adding new edges inside the drum as necessary.

$aprs$, $rqcu$, $pbqt$, $dstp$, $etuq$, $fsur$

Do the same for the second drum ; create six more tetrahedra inside the second drum which has the same vertices.

Now each of these tetrahedra has a face that is a triangle from step 2. In the face pairing, we will identify them as explained there. Also another face of each of these 12 tetrahedra

166
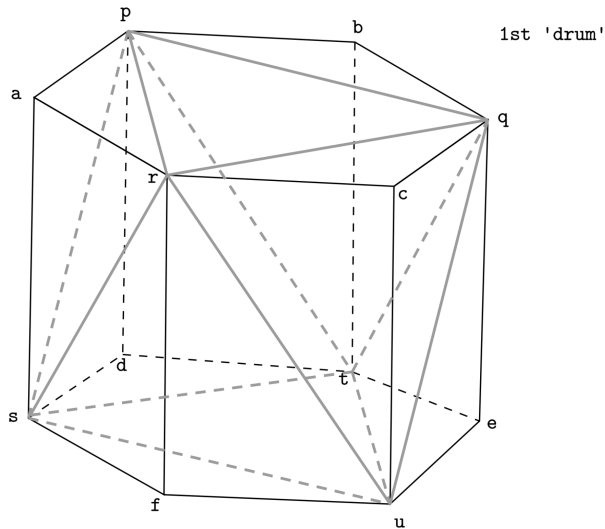
Figure 91: Dividing a drum into 6 tetrahedra leaving an octahedron in the middle

cut a vertical quads diagonally. Such a face must also be identified with a face in the other drum that also cuts a vertical quad diagonally in a way it respects the pairing of vertical quads.

Step 4

The creating of six tetrahedra in the last step leaves an octahedron inside each drum. Six of the faces of each of these octahedra are shared with tetrahedrons created in step 3. Other two faces of the octahedra are the triangles pqr and stu. We finally divide each of this octahedra into 4 tetrahedra by adding one more additional edge (in red) as shown in figure 92.

This division of drums into tetrahedra creates no new vertices, hence all the tetrahedra are also ideal. Each drum is divided into 10 tetrahedra and we have a triangulation of DX by 20 ideal tetrahedra. Faces of these tetrahedra that lie on the surface of drums are identified as explained in step 2 and step 3.
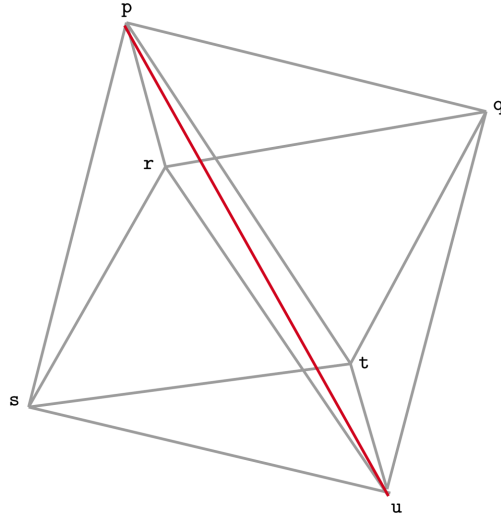
Figure 92: Triangulation of drums : Step 4 - Dividing the remaining octahedron into 4 tetrahedra

7.6 Computations using software packages

The ideal triangulation of DX by 20 tetrahedra we constructed in the previous section is described by how their faces should be glued together in pairs. This description can be fed into the low dimensional topology software package *Regina*.[20]

Regina can determine whether a given triangulation represent a manifold with hyperbolic structure and if so it can compute information about the manifold such as its hyperbolic volume. It determined the triangulation of DX described earlier represent a hyperbolic manifold with a volume of 18.2689. This was expected as we computed the volume of X to be 9.13447 earlier.

Given a triangulation, *Regina* can also compute its isomorphism signature ; a string of characters that identifies the triangulation up to a relabelling the tetrahedra in the triangu-

lation and their vertices. The isomorphism signature for the triangulation we described in 7.5 is

$$tLwvLLLwAMPQQkbbhhjilkmmmsporqqrsspuappuoowsfpabuuvvbb$$

This isomorphism signature can be used as the input to *SnapPy*.[10]

In : DX=Manifold('tLwvLLLwAMPQQkbbhhjilkmmmsporqqrsspuappuoowsfpabuuvvbb')

SnapPy can compute the group of self isometries of a manifold.

In : DX.symmetry_group
Out : $\mathbb{Z}/2 \times D6$

where $D6$ is the dihedra grpup of order 12. Hence DX has 24 self isometries. They are listed below with their action on cusps.

In : S=DX.symmetry_group()
In : isoms=S.isometries()

The array *isoms* contains all the self isometries of DX . An element of *isoms* is a description of cusp transformations under the isometry. It specifies destinations of the meridian and longitude of each cusp under the isometry. Let's consider an example.

In : isoms[19]
Out :

 $0 \to 3$ $1 \to 2$ $2 \to 1$ $3 \to 0$

 [0 -1]   [0 -1]   [1 -1]   [1 -1]

 [-1 -1]   [-1 -1]   [-1 0]   [-1 0]

First row describes the destination of each cusp. isoms[19] takes cusp 0 to 3 , 1 to 2 , 2 to 1 and 3 to 0. First columns of each matrix describe the image of the meridian of each cusp and the second column does the same for the longitude of the cusp. If α_0, β_0 and α_3, β_3

169

are the meridians and longitudes of cusp 0 and cusp 3 respectively then isoms[19] takes α_0 to $-\beta_3$ and β_0 to $-\alpha_3 - \beta_3$.

Recall that Ψ, the reflection along the boundary of X is also a self isometry of DX. and satisfies following properties.

- is an involution that exchanges cusps in pairs
- orientation reversing
- is in the center of the self isometry group

The *SnapPy* command *multiply_elements(i, j)* produce the composition of ith and jth element of the group *isoms*. We use this command to identify all the elements in *isoms* that satisfy the properties above. There are two self isometries of DX that satisfy all three of them. The first self isometry is *isoms*[19]. Its description was given earlier. The second self isometry that satisfies above three properties is *isoms*[22]. Its *SnapPy* description is given below.

In : isoms[22]

Out :

$0 \to 1$	$1 \to 0$	$2 \to 3$	$3 \to 2$
[-1 0]	[-1 0]	[0 1]	[0 1]
[1 1]	[1 1]	[1 0]	[1 0]

One of these two self isometries should be Ψ , the reflection along the boundary of X. For simplicity let's label *isoms*[19] by Ψ_1 and *isoms*[22] by Ψ_2. We need to identify which of these two is actually the isometry Ψ and which two of the four cusps are T_1 and $\Psi(T_1)$. We have four possibilities.

- $\Psi = \Psi_1$ and $\{T_1, \Psi(T_1)\} = \{C_0, C_3\}$
- $\Psi = \Psi_1$ and $\{T_1, \Psi(T_1)\} = \{C_1, C_2\}$
- $\Psi = \Psi_2$ and $\{T_1, \Psi(T_1)\} = \{C_0, C_1\}$
- $\Psi = \Psi_2$ and $\{T_1, \Psi(T_1)\} = \{C_2, C_3\}$

The property of Ψ that we can use to distinguish Ψ_1 and Ψ_2 comes from proposition 6.9.1. It says there are 6 slopes of T_1 Dehn fillings along which can yield N_0. These slopes should be among the ones in the table 2 as Dehn filling along any other slope can not produce a manifold with volume less than or equal to the volume of N_0. Let γ be any of those six slopes. Then the manifold $DX(\gamma, \Psi(\gamma))$ obtained by filling T_1 and $\Psi(T_1)$ should be the double of N_0 along its boundary and hence should have two times the volume of N_0.

The *SnapPy* command *P.dehn_fill((a,b),i)* fill the ith cusp of P along the slope (a, b). Using this command multiple times, we can fill different cusps of P along slopes we want. The volume of the manifold produced by the Dehn fillings we specified can then be computed using the command *P.volume()*. An example is given belo.w

In : P.dehn_fill((2,3),2)
In : P.dehn_fill((3,2),3)
In :P.volume()
Out : 15.5952737606

Hence the volume of the manifold obtained by filling C_2 of P along the slope $(2, 3)$ and C_3 along the slope $(3, 2)$ is equal to 15.5952737606.

Now we compute the volumes of all the Dehn fillings of DX of the form $DX(\gamma, C_i, \Psi_k(\gamma), \Psi_j(C_j))$ where

- γ is a slope in table 2
- The triple (Ψ_k, C_i, C_j) represent one of the four possibilities above.

The triples (Ψ_1, C_0, C_3) and (Ψ_1, C_1, C_2) yield no manifolds with twice the volume of N_0. On the hand (Ψ_2, C_0, C_1) and (Ψ_2, C_2, C_3) yield exactly six manifolds with that volume. Hence we conclude $\Psi = \Psi_2$. The table 5 lists all the volumes of Dehn fillings of DX of the form $DX(\gamma, C_2, \Psi_2(\gamma), C_3)$ for all the slopes γ in table 2

Volumes in the second (fourth) columns of table 5 are the volumes of Dehn fillings of DX obtained by filling C_2 along the slope γ in column one (three) and C_3 along the slope $\Psi(\gamma)$. We observe that six of the slopes yield non hyperbolic manifolds. These slopes are $0, 1, \infty, -1, 1/2$ and 2.

Smallest volume in the table 2 is 15.5952 which is twice the volume of N_0. Exactly six slopes yield this volume. They are $-2, -1/2, 1/3, 2/3, 3/2$ and 3. Comparing this observation with proposition 6.9.1 we conclude that the manifold obtained by X from filling T_1 along these six slopes is N_0.

All the remaining volumes in table 5 are greater than twice the volume of N_0. Hence no slope in table 5 except for the 12 mentioned above can produce a manifold with a smaller volume than N_0. With these observations we can finally conclude

Theorem 4. *Let N be a manifold in $\mathcal{N}'_{c,c}$ which satisfy the following conditions.*

1) N has a $(1,1,1)$ hexagon visible from the cusp
2) ∂N has two complementary components in G
where G is the graph on ∂N which has the feet of λ_1 as vertices and projections of external edges of the two $(1,1,1)$ hexagons as edges.

$$\text{Then volume of } N \geq \text{volume of } N_0$$

Furthermore if the volume of N is equal to the volume of N_0 then $N = N_0$

Proof. Only the last statement is remained to be proved. From proposition 6.9.1, we know there at least 6 slopes that yield N_0. From table 5 we see there are only 6 slopes that yield manifolds with same volumes as N_0. Hence the manifolds yield by these 6 slopes should be N_0. $\qquad\square$

We summarise all of our results in chapters 3 -7 below.

Theorem 5. *If N is the smallest volume manifold in $\mathcal{N}_{c,c}$ then one of the following must be true.*

- $N = N_0$

- $\tilde{N}$ *has no* $(1,1,1)$ *hexagons visible from the cusp but has a* $(1,1,k)$ *hexagon visible from the cusp for some $k > 1$. Furthermore volume of N is greater than* 7.78 *and x_1 of N is between* 1.208 *and* 1.2091

- $\tilde{N}$ *has* $(1,1,1)$ *hexagons. N has two complementary components of G in ∂N*

Table 4: Volumes of Dehn fillings of DX

Slope	Volume	Slope	Volume
0	Non hyperbolic	∞	Non hyperbolic
(1,1)	Non hyperbolic	(1,2)	Non hyperbolic
(1,3)	15.5952	(1,4)	16.8933
(1,5)	17.4325	(1,6)	17.5992
(1,7)	17.8662	(1,8)	17.9661
(2,1)	Non hyperbolic	(2,3)	15.5952
(2,5)	17.3415	(2,7)	17.8242
(3,1)	15.5952	(3,2)	15.595
(3,4)	16.8933	(3,5)	17.3415
(3,7)	17.7998	(4,1)	16.8933
(4,3)	16.8933	(4,5)	17.4325
(5,1)	17.4325	(5,2)	17.3415
(5,3)	17.3415	(5,4)	17.4325
(6,1)	17.7074	(7,1)	17.8662
(7,2)	17.8242	(7,3)	17.7998
(8,1)	18.1245	(-1,1)	Non hyperbolic
(-1,2)	15.5952	(-1,3)	16.8933
(-1,4)	17.4325	(-1,5)	17.7074
(-1,6)	17.8662	(-1,7)	17.966
(-1,8)	18.0329	(-1,9)	18.0799
(-2,1)	15.5952	(-2,3)	17.3415
(-2,5)	17.8242	(-2,7)	18.0116
(-2,9)	18.1020	(-3,1)	16.8933
(-3,2)	17.3415	(-3,4)	17.7998

Table 5: Volumes of Dehn fillings of DX contd..

Slope	Volume	Slope	Volume
(-3,5)	17.9160	(-3,7)	18.0510
(-3,8)	18.0917	(-4,1)	17.4325
(-4,3)	17.7998	(-4,5)	17.9861
(-4,7)	18.0840	(-4,9)	18.1398
(-5,1)	17.7074	(-5,2)	17.8242
(-5,3)	17.9160	(-5,4)	17.9861
(-5,6)	18.0799	(-5,7)	18.1113
(-5,8)	18.1358	(-5,9)	18.1553
(-6,1)	17.8662	(-6,5)	18.0799
(-6,7)	18.1337	(-7,1)	7.9661
(-7,2)	18.0116	(-7,3)	18.0510
(-7,4)	18.0840	(-7,5)	18.1113
(-7,6)	18.1337	(-7,8)	18.1674
(-7,9)	18.1801	(-7,10)	18.1906
(-8,1)	18.0329	(-8,3)	18.0917
(-8,5)	18.1358	(-8,7)	18.1675
(-8,9)	18.1245	(-9,1)	18.0800
(-9,2)	18.1021	(-9,4)	18.1399
(-9,5)	18.1553	(-9,7)	18.1801
(-9,8)	18.1900	(-10,3)	18.1455
(-10,7)	18.1907		

Bibliography

[1] William P Thurston and John Willard Milnor. The geometry and topology of three-manifolds, 1979.

[2] Sadayoshi Kojima and Yosuke Miyamoto. The smallest hyperbolic 3-manifolds with totally geodesic boundary. *Journal of Differential Geometry*, 34(1):175–192, 1991.

[3] Roberto Frigerio, Bruno Martelli, and Carlo Petronio. Small hyperbolic 3-manifolds with geodesic boundary. *Experimental Mathematics*, 13(2):171–184, 2004.

[4] Jason DeBlois and Peter B. Shalen. Volume and topology of bounded and closed hyperbolic 3-manifolds. *Comm. Anal. Geom.*, 17(5):797–849, 2009.

[5] Jason DeBlois and Peter B. Shalen. Volume and topology of bounded and closed hyperbolic 3-manifolds, II. Preprint in preparation. Available on request.

[6] Jason DeBlois. Some trigonometric results for partially truncated triangles and tetrahedra with ideal vertices. preprint on webpage at `https://sites.pitt.edu/~jdeblois/`.

[7] Jason DeBlois. The centered dual and the maximal injectivity radius of hyperbolic surfaces. *Geometry & Topology*, 19(2):953–1014, 2015.

[8] Roberto Frigerio, Bruno Martelli, and Carlo Petronio. Dehn filling of cusped hyperbolic 3-manifolds with geodesic boundary. *Journal of Differential Geometry*, 64(3):425–455, 2003.

[9] David Futer, Efstratia Kalfagianni, and J Purcel. Dehn filling, volume, and the jones polynomial. *Journal of Differential Geometry*, 78(3):429–464, 2008.

[10] Marc Culler, Nathan M. Dunfield, Matthias Goerner, and Jeffrey R. Weeks. SnapPy, a computer program for studying the geometry and topology of 3-manifolds. Available at `http://snappy.computop.org` (DD/MM/YYYY).

[11] Yosuke Miyamoto. Volumes of hyperbolic manifolds with geodesic boundary. *Topology*, 33(4):613–629, 1994.

[12] Werner Fenchel. Elementary geometry in hyperbolic space. In *Elementary Geometry in Hyperbolic Space*. de Gruyter, 2011.

[13] Bruno Martelli. An introduction to geometric topology. 2016.

[14] John G Ratcliffe, S Axler, and KA Ribet. *Foundations of hyperbolic manifolds*, volume 149. Springer, 1994.

[15] Jason DeBlois. Bounding the area of a centered dual two-cell below, given lower bounds on its side lengths. *New York J. Math.*, 23:315–349, 2017.

[16] Jason DeBlois. The geometry of cyclic hyperbolic polygons. *The Rocky Mountain Journal of Mathematics*, 46(3):801–862, 2016.

[17] Stanko Bilinski. Zur Begründung der elementaren Inhaltslehre in der hyperbolishchen Ebene. *Math. Ann.*, 180:256–268, 1969.

[18] Jason DeBlois. Tessellations of hyperbolic surfaces. *arXiv preprint arXiv:1103.4604*, 2011.

[19] Akira Ushijima. A volume formula for generalised hyperbolic tetrahedra. *Non-Euclidean Geometries: János Bolyai Memorial Volume*, pages 249–265, 2006.

[20] Benjamin A. Burton, Ryan Budney, William Pettersson, et al. Regina: Software for low-dimensional topology. `http://regina-normal.github.io/`, 1999–2023.